Cape Peninsula
University of Technology

COMPARATIVE STRATEGIES FOR EFFICIENT CONTROL AND STORAGE OF RENEWABLE ENERGY IN A MICROGRID

by

HENRI DU PLOOY

Thesis submitted in fulfilment of the requirements for the degree

Master of Engineering: Electrical Engineering

in the Faculty of Electrical Engineering

at the Cape Peninsula University of Technology

Supervisor: Dr M.A. Adonis
Co-supervisor: Dr A.K Raji

Bellville Campus
September 2016

DECLARATION

I, Hendrik Petrus Du Plooy, declare that the contents of this dissertation/thesis represent my own unaided work, and that the dissertation/thesis has not previously been submitted for academic examination towards any qualification. Furthermore, it represents my own opinions and not necessarily those of the Cape Peninsula University of Technology.

ABSTRACT

Power fluctuations in a microgrid are caused by disturbances due to the connection and disconnection of Distributed Generators (DG's), as well as the irregular input of the sun and wind renewable energy.

Renewable penetration such as the sun, wind and tidal energy causes intermittency which directly affects the input and resultant output power of a microgrid. Control systems have to be implemented on three different levels to ensure the stability and reliability of the power supplied to the load.

This can be achieved by implementing the following: 1) Primary control with mechanical valves and actuators to translate feedback signals through droop control.
2) Secondary control with power electronics to facilitate maximum power point tracking, phase lock loops and switch mode inverters to manipulate the electrical signals to a desired set points including PID control. 3) Tertiary control with software program management to monitor the power flow as well as to evaluate congregated logic and implement decision making.

Energy storage systems like super capacitors can compensate for power imbalance by providing excess stored energy to the microgrid for short periods of time. The added advantage of capacitor banks is that it can facilitate power factor correction where inductive loads like rotating motors form large part of the total load. Battery banks can compensate for energy shortage for longer periods of time. The duration of the compensation can be determined by the size, topology and the type of batteries used.

The objectives of this study is to improve the unstable power output responses of a renewable energy microgrid by designing and analysing control strategies intended at power wavering compensation which also includes energy storage. Sub control systems is created and simulated in Matlab/Simulink for analytical comparative observations. Results of the simulated model are discussed and recommendations are given for future works.

Keywords: Renewable Energy, Microgrid, Control, Distributed Generators, Inverters, Energy Storage, Simulink.

ACKNOWLEDGEMENTS

I wish to thank:

- God for giving me the ability to study.
- Dr Adonis, for his guidance, mentorship and input.
- Dr Raji, for his expertise and time given to me.
- My family, especially my wife, for your moral & emotional support.
- My friends for encouraging me all the way.
- TTA Consulting Engineers, for their financial contribution, expertise and support.
- The financial assistance of the National Research Foundation towards this research is acknowledged. Opinions expressed in this thesis and the conclusions arrived at, are those of the author, and are not necessarily to be attributed to the National Research Foundation.

DEDICATION

I dedicate this thesis to my Father Philip du Plooy and my 3 brothers, Drikus, Phil & Ruan who share my interest in Engineering.

TABLE OF CONTENTS

LIST OF FIGURES

LIST OF TABLES

ACRONYMS

AC	Alternating current
CCA	Cold Cranking Amps
CEAS	Compressed Air Energy Storage
CESS	Composite Energy Storage System
CPV	Concentrating photo voltaic
CSI	Current source inverters
CSP	Concentrated Solar Power
DC	Direct current
DESS	Distributed energy storage systems
DFIG	Doubly fed induction generator
DG	Distributed Generator
DNI	Direct Normal Irradiation
DOD	Depth of discharge
DSSC	Dye sensitized solar cells
DSSCs	Dye sensitized solar cells
ESS	Energy storage systems
FDI	Fault detection and isolation
FESS	Flywheel Energy Storage System
GSC	Grid Side Converter
HAWT	Horizontal-axis wind turbines
HAWT	Horizontal Axis Wind Turbines
IEEE	Institute of Electrical and Electronics Engineers
IGBT	Insulated Gated Bipolar Transistor
KESS	Kinetic Energy Storage System
LAES	Liquid air energy storage
LC	Inductive capacitive
LCOE	Levelized Cost of Electricity
LEC	Levelized Energy Cost
LED	Light emitting diode
MEA	Membrane Electrode Assembly
MFC	Microbial Fuel Cell
MOSFET	Metal–oxide–semiconductor field-effect transistor
MPPT	Maximum Power Point tracking
NREL	National Renewable Energy Laboratory

PID	Proportional Integral derivative
PLL	Phase Lock Loop
PV	Photo Voltaic
PWM	Pulse Width Modulation
RES	Renewable Energy System
RMS	Root mean square
SC	Switched capacitive
SCADA	Supervisory Control and Data Acquisition
SCO	Synchronous condensing operation
SFCL	Superconducting fault current limiters
SMES	Super Magnetic Electric Storage
SOC	State of Charge
SOFC	Solid Oxide Fuel Cells
UNEP	United Nations Environment Programme
UPS	Uninterruptible power supplies
UTP	Unshielded twisted pair
VAWT	Vertical-axis wind turbines
VAWT	Vertical Axis Wind Turbines
VCO	Voltage Controlled Oscillator
VRB	Vanadium Redox battery
VSI	Voltage source inverters

GLOSSARY

Anode	Releasing electrons
Cathode	Collecting electrons
Deep cycle battery	Less instant delivery, greater long term energy Discharges 60-70% of capacity
Droop	output frequency, voltage or power loss
Electrochemistry	Chemical reaction taking place involving an electrode
Electrode	Conductor of electric charge
Eskom	South African electricity utility
Feedback	Returning a part of the output of a control system to the input of the system
Grid-Tied system	Connected to main grid, powered by renewable energy
Hybrid system	Grid tied system including a battery back-up system
Inertia	State of mass to resist acceleration
Inverter	Converts DC to AC
Irradiance	Intensity of light
Load	Consumer of electrical power
Matlab	Matrix Laboratory programming developed by Mathworks
MicroGrid	Independent power network including DG sources, loads & storage devices

Off-Grid system	Self-powered System, disconnected from the main grid
Per unit system	Representing an actual quantity
Primary battery	Discharge once
Psim	Specialized electrical simulation and design software
Renewable Energy	Natural energy produced by sun, wind, water, tides ext.
Secondary battery	Rechargeable battery, accumulator
Simulink	Graphical Software Simulation created by Mathworks
Single line diagram	Representing a 3 phase system as a single phase system
Starter battery	Max power, short duration Discharges 1-3% of capacity

CHAPTER 1: INTRODUCTION

1.1 Problem statement

The intermittent nature of renewable energy sources causes unwanted power fluctuations in a microgrid. The switching between grid and island mode of DG's also causes power fluctuations including the connection and disconnection of DG's and related loads.

1.2 Background

During the past decade, terminology like 'carbon footprint', 'renewable energy' and 'sustainability' are being used. Renewable energy can almost be compared to computers, it's been around for the last half a century but as it exponentially grows and knowledge increases, greater awareness gets triggered. Growing interests reduce purchased prices which lures the sceptic consumer to participate in this energy revolution. The questions however are whether renewable energy systems are firstly sustainable and secondly affordable?

There are areas in South Africa and in the world that hasn't got a constant supply of energy via the main national grid/s. Eskom's load shedding in 2008 and 2015 also encouraged smaller independent microgrids which consists of various distributed generators (DG's) as a viable option for constant electricity supply. These microgrids can supply a constant power output hence at higher financial costs, especially when fossil or natural gas fuelled generators are utilized as back-up power.

A microgrid consists of distributed generators with a lower voltage output. In the Islanded mode the microgrid frequency needs to be regulated, and the power balance needs to be sustained for system stability. Electric energy became a basic need in the modern world (Scherer, et al., March 2016). A smart grid can also be described as a flexible, open-access, intelligent and sustainable system (Arboleya , et al., Feb 2015).

A difference between dispatchable and non-dispacthable as well as the difference between inertial and non-inertial distributed generators can be distinguished in the following matter; Dispatchable - The output power can be controlled to maintain the frequency and voltage; examples would be micro turbines, fuel cells and bio-diesel generators. Non-dispatchable - Photo Voltaic (PV) panels & wind turbines, the output power depends on external environmental factors that cannot be controlled.

Control systems has to be implemented to compensate for the droop that is imposed on the microgrid output. The control of the power in the microgrid can be solved with power electronics technology. Effective electricity storage is an important key to mitigate the intermittent supply of renewable generated electricity as well as a control method employed.

When non-dispatchable DG's run simultaneously the result will be an excess of power that goes wasted when it can't be stored. The demand will be less than the supply and energy will be wasted. Conventional rechargeable batteries are effective but comprises of limitations such as size, durability and costing.

Electricity can be stored in other forms of potential energy like in a hydro-pumping, compressed air, super capacitors or custom designed flywheels called kinetic energy-storage systems (KESS). Micro pumped storage is very cost effective when two established dams are connected with flow piping. Power storage devices helps to meet the energy demand by storing unused or low cost off-peak electricity (Wei, et al., Aug 2014).

Hybrid PV systems supplements the usage of the national utility and also reduces the carbon footprint. Other first world country like Australia allows any household to feed back to the main grid with good incentives that reduces the investor's payback period. Microgrid control lies at various levels, from field instrumentation to supervisory control and data acquisition (SCADA) systems, programming software, communication via networks and various communication protocols.

The popular four renewable distributed generator technologies are mainly; bio-diesel generators, photo voltaic cells, wind turbines, and a bio-fuel cells in microgrids. The compliance of the different DG's technologies to an Islanded microgrid required control techniques. The resultant electrical power will supply the load in that specific microgrid. Energy storage methods contributes to practical and sufficient microgrid stability through composite energy storage systems (CESS).

1.3 Aims & Objectives

- The main aim of the research project is to investigate renewable energy technologies and storage methods in order to analyse different control strategies to ensure proper dynamic operation of the microgrid.
- Control concepts are developed, including progressive simulated results in order to improve compensation for power fluctuations in microgrids.
- The objective is to design and model sub control elements that regulates a steady electrical power output when loads are connected in a microgrid.
- These control methods have to mitigate, reduce and eliminate power fluctuations caused by disturbances when connecting dispatchable, non-dispatchable, inertial and non-inertial distributed generators interchangeably.
- Further investigation of control concepts will be conducted which includes bio-diesel generators, microbial fuel cells photovoltaic cells and wind turbines.

1.4 Thesis Outline

1) Chapter one contains the introduction, background, aims and objectives and the outline of this thesis.
2) Chapter two consists of a thorough literature review on renewable energy systems including distributed generators with its control methods as well as energy storage systems and its control implications.
3) Chapter three experiments on the implementation and development of the sub control concepts as a basis for microgrid control in operation.
4) Chapter four establishes the control parameters for renewable energy sources and an energy storage system through formulae derivations.
5) Chapter five demonstrates the simulation results of the control sub systems designed for microgrids. Energy storage methods are evaluated. Previous case studies are summarised and the results are analysed and replicated upon.
6) Chapter six discusses the conclusions, knowledge gained as well as the related future works.

CHAPTER 2: ENERGY SOURCES & STORAGE

2.1 Overview

This chapter focusses on the literature review of renewable energy sources and its related control approaches. Key aspects of renewable energy sources relating to microgrids are summarized which explains the nature of its operation. Technologies such as bio-fuel and wind generators, as well as microbial fuel cells and photo voltaic cells will be investigated and presented.

Secondly, electrical energy needs to be stored in order to maximise the energy produced by renewable sources, utilizing energy storage for additional efficient control in a microgrid system. Four types of storage technologies are analysed including chemical batteries, gravitational pumped storage systems, compressed pressurised air storage and mechanical flywheels.

2.2 Renewable energy background

2.2.1 Global and Local Energy Sectors

Globally, renewable energy systems are growing at a fast pace. The Renewables Global Status Report is a sister publication to the Global Trends in Renewable Energy Investment Report produced by Frankfurt School - United Nations Environment Programme (UNEP) Collaborating Centre for Climate & Sustainable Energy Finance. The most recent edition of the report was launched on the 1st of June 2016.

The two tables represented in Figure 2.1 and figure 2.2 below were adapted from the original data and indicate that the estimated world consumption of fossil fuel as well as nuclear is decreasing slightly. The pie chart in figure 2.3 illustrates that there is still much room for the deployment of renewable energy systems (Sawin, L., 2015).

The renewable electric energy demand has grown the past 20 years with an average of 30% as the cost to implement such systems decreased over the years (Singh, et al., July 2011). Microgrids play a key role in the advancement of renewable energy technology. Electric energy became a basic need in the modern world (Scherer, et al., March 2016).

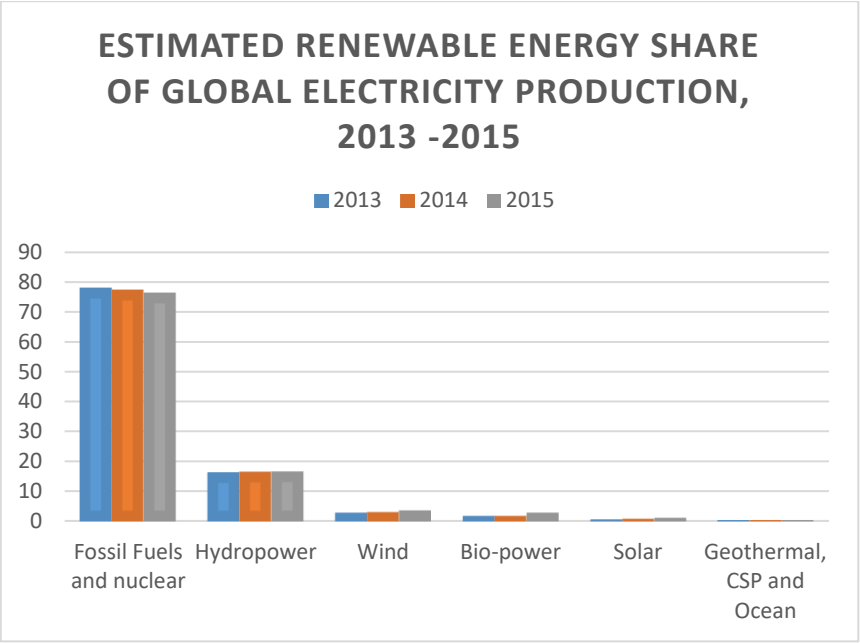

Figure 2.1: World Energy Consumption

(Sawin, L., 2015)

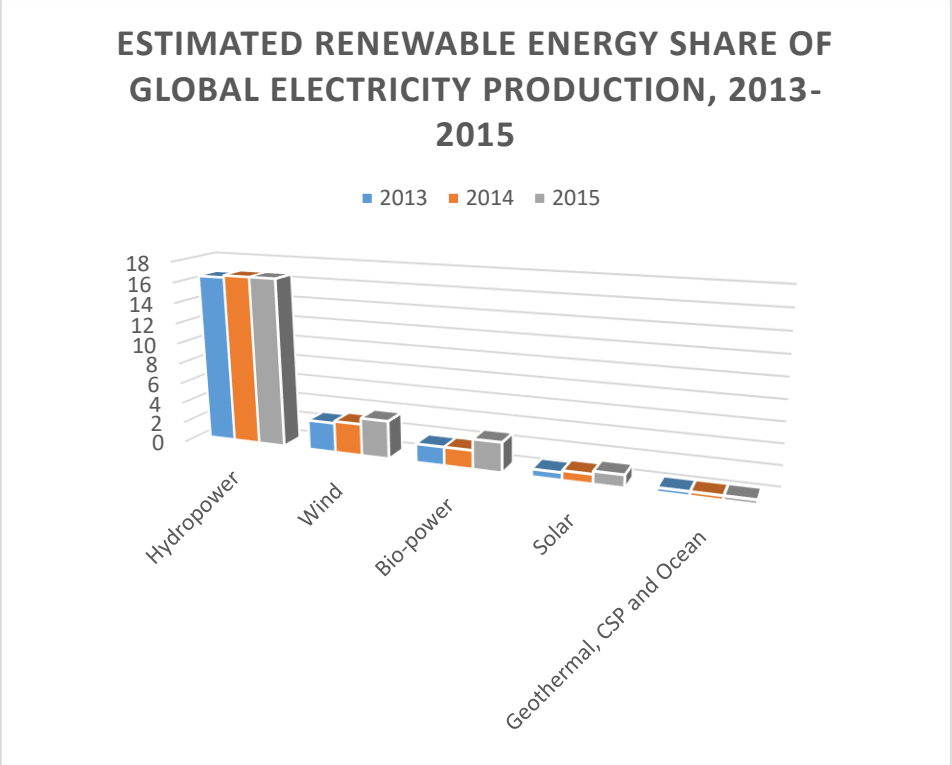

Figure 2.2: Global Renewable Energy Usage

(Sawin, L., 2015)

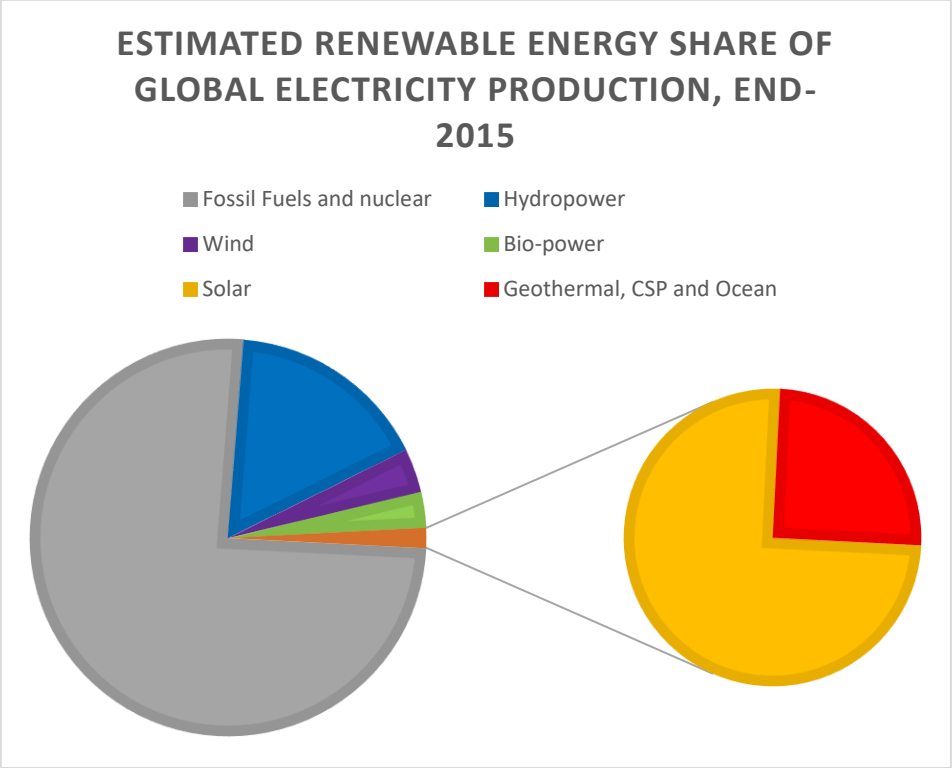

Figure 2.3: Global Energy Usage for 2015

(Sawin, L., 2015)

British Petroleum (BP) indicates that renewable energy is worldwide the fastest growing technology measured and estimated over a period of 25 years (Centre for Energy Economics Research and Policy, Heriot-Watt University, 2015). This fast development reduces the dependence on fossil fuels with the challenge of consistent operation and control strategies (Wei, et al., Dec 2015).

According to Eskom represented at the CSP solar augmentation conference (Sudarkasa, 2013), the energy demand in South Africa, especially the residential sector will grow rapidly by 400% till 2050 – Estimated at 6000 peta-joules. The transport sector was estimated at approximately 300%. The commercial sector was projected at 200% till 2050.

This indication shows us that the residential sector is the fastest growing energy sector thus the opportunity for microgrid expansion is very promising. According to Eskom, the other sectors are projected not to grow more 100% in the next 15 years. These sectors include manufacturing, mining and agriculture (Sudarkasa, 2013).

South Africa is rich in non-depletable renewable energy sources such as wind and solar. According to the South Africa's department of energy, South Africa is in the top three countries in the world with suitable irradiance provided by the sun (The Department of Energy, 2015).

2.2.2 Distributed Generators

Distributed generation is progressively a competitive option compared to conventional centralized systems. Distributed generator's configured in terms of a microgrid solution offers favourable attraction due to flexibility and reliability in the power system (Kim, et al., Nov 2010).

The difference between dispatchable and non-dispacthable distribution generators needs to be distinguished. Dispatchable: The output power can be controlled to maintain the frequency and voltage magnitude; examples would be micro turbines, fuel cells and bio-diesel generators. Non-dispatchable: Photo Voltaic (PV) panels & wind turbines, the output power depends on external environmental factors that cannot be controlled.

DG's can also further be classified into two categories: The distinction can be made between Inertial and non-inertial. Inertial distributed generators generate power by means of rotational mechanical forces that induce electrical voltage into the stator windings. These mechanical forces are driven by pressure and/or forces, like micro-turbines, wind generators, reciprocating engines, combined cycle turbines.

Non-inertial DG's are mechanically static and generate electricity as a result of chemical and/or biological reactions. To model a microgrid system, it must accommodate both the transient and steady-state characteristics which includes the following models; wind turbines, diesel generator, batteries and inverters (Yubing, et al., Oct 2008).

When non-dipatchable DG's run alone the result will be an excess or shortage of power.in the case of excess generated power, the demand will be less than the supply and energy will be wasted. Electricity storage systems should be implemented to 'save' that wasted energy. A microgrid should appear as a single load that can be controlled to respond to changes in the distribution system (Majumber, et al., Jan 2009).

The advantages of distributed generators are less electrical losses due to shorter distance travelled by electricity, increased capacity for more connections, constant power to the consumer when a failure in the network voltage occurs as well as reduced cost to reinforce network systems (Shang & Redfern, 1-4 Sept. 2009).

2.3 Microgrid

A microgrid is a local group of electrical loads and generation sources that is connected in a close proximity that functions independently, an integration of various distributed generators, controllable loads and/or storage devices. This improves the power supply reliability and power quality as well as enhancing the safety of the power grid (Jing, et al., Sept 2012). Microgrid control consists of three components which is the static switch, micro sources and loads (Lasseter, et al., 23 Dec 2010).

A microgrid can operate in both islanded or grid connected mode (Jaehong, et al., May 2011). One of the reasons for a microgrids implementation is that it produces independent self-sufficient power, which could also feed into a large-scale grid. These microgrid systems can lead to the mitigation of power loss in long transmission lines and the reduced cost of electricity with the replacement of renewable alternatives.

The formation of an autonomous grid is due to the islanding process when an electrical region capable of independent operation is isolated or islanded from the remainder of the grid (Dou , et al., July 2011). In an autonomous (islanded) mode all the DG's are contributing to the system voltage and frequency while sharing the same active and reactive power demand (Divshali, et al., Oct 2012). The microgrid's frequency needs to be regulated, and the power balance needs to be sustained for stability.

Distributed generators need to be controlled first in order to be connected to the microgrid. Power electronics optimizes the regulation and control of the DG's. Grid side converters (GSC) enables grid synchronisation, thus meeting the specifications of interconnection of applicable DG's to that relevant power bus or grid (Hadjidemetriou, et al., Nov 2013). Energy storage systems in microgrids is imperative to optimize the energy efficiency of the total input energy. The storage component also increases the independence of the microgrid up to a point of self-sustainability.

A smart grid can also be described as an intelligent bi-directional electricity network (Beshr, Oct 2013). The variables in a microgrid is the energy source, storage availability as well as the changing load. See the figure 2.4 below which illustrates a basic microgrid.

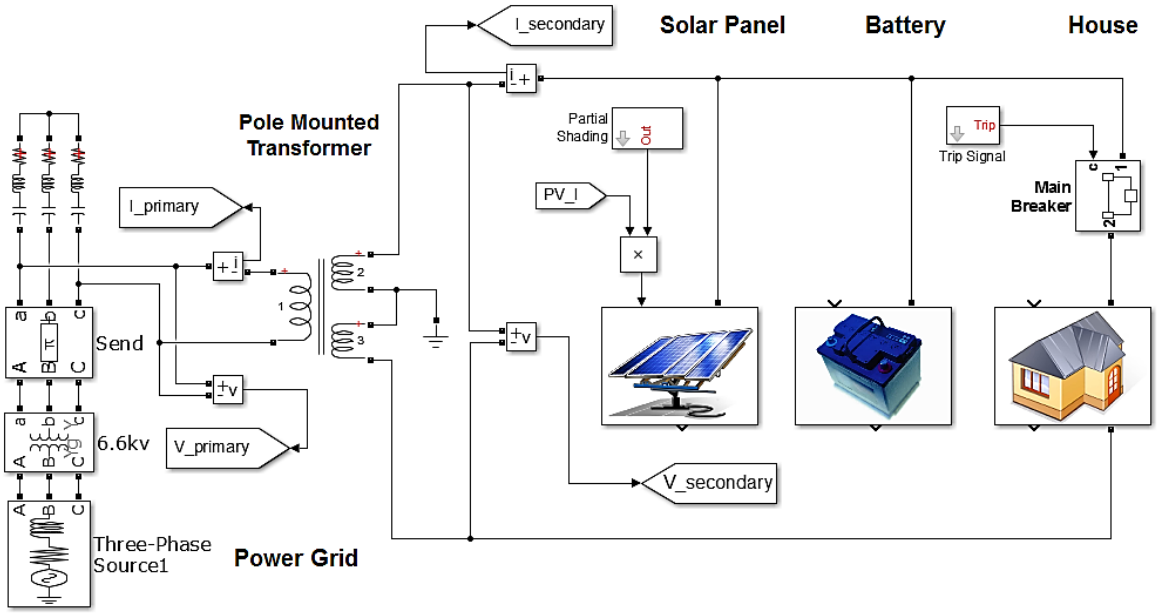

Figure 2.4: Microgrid Connected to Power Grid

(Matlab, 2016)

The increasing use of renewable distributed generation and improved energy storage technology qualifies microgrids as a better solution due to reliability, sustainability, resilience and energy efficiency (Zubieta, May 2016). A smart microgrid can be described as a low voltage grid incorporating local generators with real time control (Falvo, et al., Sept 2014).

The conventional droop control method is used in a microgrid to realize power sharing. The droop control is applied to set the magnitude and the frequency of the voltage output based on active and reactive power (Kohansal, et al., March 2012). The DG's should be connected in parallel, operating in an islanded mode and its advantages are in terms of power flexibility and the absence of critical communications systems (Planas, et al., Aug 2013).

2.4 Standards and guidelines

2.4.1 Grid codes

Technical and organizational requirements of a grid have to be met by distributed generators in order to connect. A DG needs to stay connected during a fault. The continuous operating frequency range is 0.95-1.03 pu (per unit). Automatic grid disconnection relay without delay should activate once the frequency and voltage ranges are violated. The necessary protection devices should be in place as stipulated (Syed, et al., March 2014).

Connection of micro sources to the main grid in most cases would include an isolation transformer and an energy storage unit as required by authorities (De Souza, et al., Aug 2015) to help stabilize the grid and for safety purposes.

2.4.2 IEEE 1547 Standard

On June 25, 1998, the Institute of Electrical and Electronics Engineers (IEEE) standards board expanded the responsibilities of IEEE standards coordinating committee 21 (SCC21) to include all distributed generation and energy storage. The scope of this standard establishes criteria and requirements for the interconnection of distributed resources within electrical power systems.

This standard endeavours to unify technical requirements and specifications that can then be globally acknowledged. This standard involves industries and institutions like utilities, manufacturers, energy companies, regulators and standards organisations (IEEE Standards Coordinating Committee 21, April 2009). Grid codes stipulates certain technical and organizational requirements for connecting generating units (Alobeidli , et al., April 2015).

2.4.3 Levelized cost of electricity standard

The cost of electricity can be determined by the following factors: Initial capital cost, utility and municipal selling price, operation and maintenance cost, fuel/source as well as the life span of the various power plants.

The levelized cost of electricity (LCOE) is a method of measuring and comparing different energy generation technologies by providing the price at which energy has to be sold to break even with the value of the total life cycle of the plant (Hallam & Contreras, March 2015). This method is also known as levelized energy cost (LEC).

The LCOE can also be seen as the financial break-even point: In essence the sum of accumulated costs for building and operating a plant is compared to the total sum of the annual power generation. The result is measured in capital per kWh. The LCOE method is ideal for comparing various kinds of generation plants and not necessarily for one isolated specific power plant.

The cash values of all expenditure are divided by the cash value of the power produced in its entire life span. The profit of the energy sold is compared to the set up costs as well as the production costs of the plant (Kost, et al., Nov 2013).

LCOE in Euro/kWh:

I_0	Investment expenditures in Euro
A_t	Annual total costs in Euro in year t
$M_{t,el}$	Produced quantity of electricity in the respective year in kWh
i	Real interest rate in %
n	Economic operational lifetime in years
t	Year of lifetime (1, 2, ...n)

Annual total costs A_t = Fixed operating costs + Variable operating costs + (residual value/disposal of the plant)

$$\text{LCOE} = \frac{I_0 + \sum_{t=1}^{n} \frac{A_t}{(1+r)^t}}{\sum_{t=1}^{n} \frac{M_{t,el}}{(1+i)^t}} \qquad 2\text{-}1$$

Learning curve models can also be used to predict future developments of plant prices. This concept proposes a relationship between the market size and the production cost of a product. The relationship between the quantities X_t produced at time t, the costs C(X_t) compared to the output quantity at reference point X_0, the corresponding costs C(X_0) and the learning parameter b can be presented in the following equation below. See Appendix B for the derivation.

$$\mathrm{C}(X_t) = \mathrm{C}(X_0)\,\frac{X_t}{X_0}^{-b} \qquad 2\text{-}2$$

A comparison for the capital costs, operating costs and uncertainty in terms of unavailability for different technologies is summarised in table 2.1 below.

Table 2.1: LCOE Comparison for different technologies

(The SUSTAINABLE ENERGY RESOURCE HANDBOOK South Africa Volume 6, 2015)

Generation Technology	**Capital Costs**	**Operating Costs**	**uncertainty**
Renewable Energy			
Solar PV	High	Very Low	Yes
Wind	High	Very Low	Yes
Solar CSP	Very High	Very Low	Yes
Tidal/Wave Power	Very High	Very Low	Yes
Biomass	Very High	High	No
Traditional Generation			
Gas	Low	High	No
Coal	Medium	High	No
Nuclear	Very High	Low	No

2.5 Renewable Energy Sources and control considered in this study

2.5.1 Bio-Fuel Generators

Biofuel generators function on the same principle as normal diesel/petrol generators, except that it runs on environmental friendly biofuel energy like biogas, biodiesel and even vegetable oil. The control method of the conventional fuel generator can be applied to the bio-fuel generator. Diesel gen-sets are regularly used in peak shaving applications as well as back-up or standby power and even as prime movers in remote areas (Best, et al., Dec 2010) .

Induction generators are some of the most popular generators used. These generators are small scale and robust without a dc excitation supply thus brushless due to the squirrel cage induction effect. The maintenance cost is lower with improved transient responses compared to other conventional generators (Wang & Lin, Feb 2009).

The diesel engine speed and voltage control is a complete conventional droop control method that consists of two components: The governor and the excitation system. The governor uses the feedback signal from the generator output speed and compares it with the reference of 1 p.u (wref) as shown in figure 2.5 below.

The Pm output signal provides the mechanical power reference for the generator. The excitation control uses the ABC three-phase voltage and the DQ multiplexer breaks the power line signal up into the Vd and Vq components to compare that with the reference of 1 p.u (Vref). The Vf signal feeds into the input of the voltage reference of the generator.

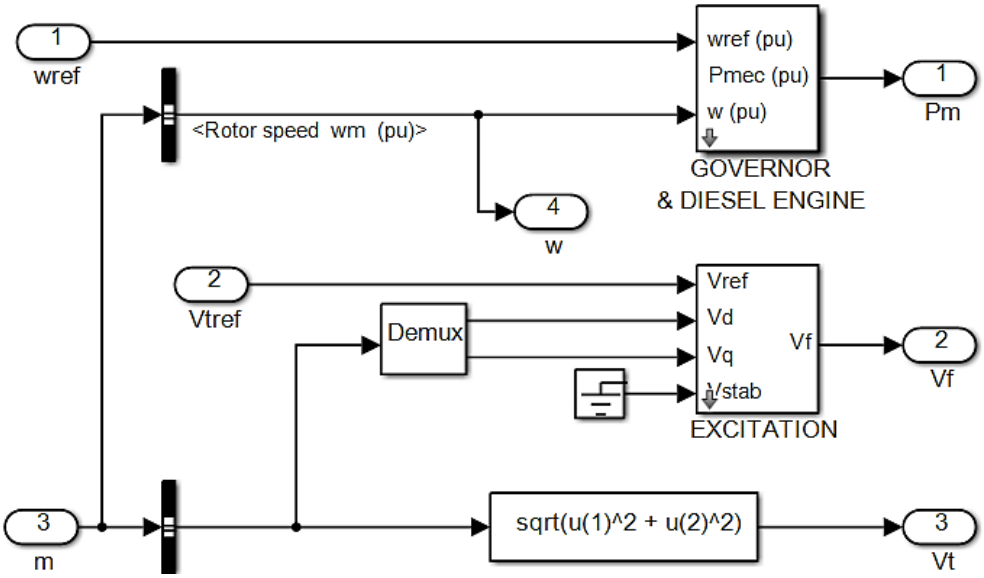

Figure 2.5: Diesel Engine Speed & Voltage Control

(Matlab, 2013)

The following block diagram is equipped with a speed governor, as shown in figure 2.6 below. The difference between the speed reference and the rotational speed reference is processed by a control box. The output of the control box activates the actuator which drives the engine (Wang & Lin, Feb 2009).

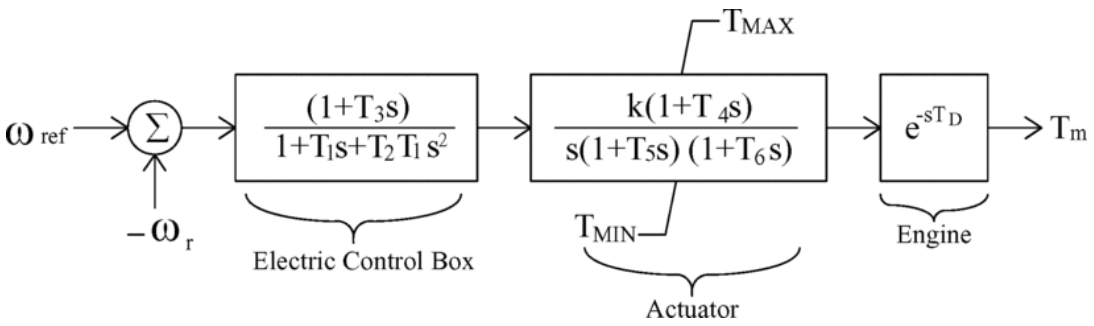

Figure 2.6: Block diagram of gas engine

(Wang & Lin, Feb 2009)

If the governor set point for one generator is increased and the total load active power demand remains constant, the system frequency increases. The active power contributed by that generator increases, while the active power contributed by the other generator decreases as illustrated in the figure 2.7 below.

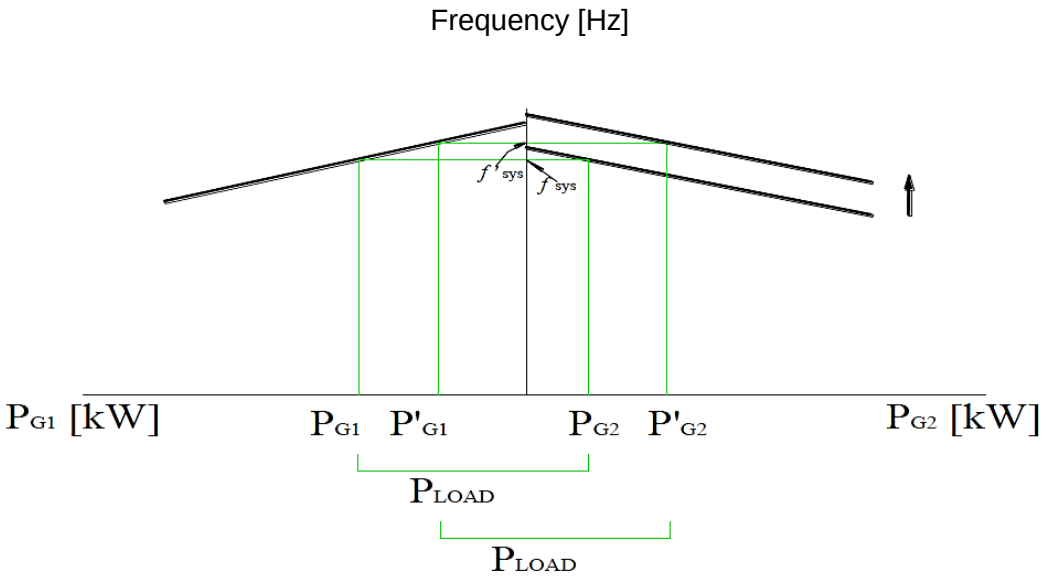

Figure 2.7: Changing the Governor set point for one generator

(Fish, 2014)

If the field current of one generator is increased and the total load reactive power demand remains constant, the system terminal voltage increases. The reactive power contributed by that generator also increases, while the reactive power contributed by the other generator decreases as illustrated by figure 2.8.

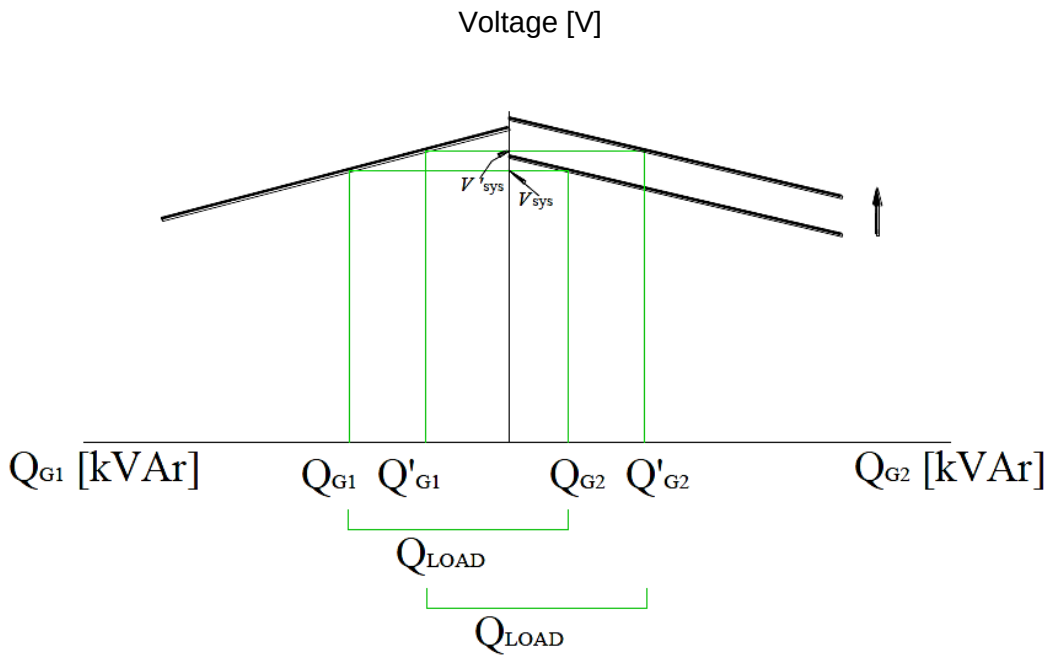

Figure 2.8: Changing the Field Current for one Generator

(Fish, 2014)

Acceleration control limits the rotor from accelerating out of control when a sudden load loss occurs. A temperature controller monitors the exhaust gases to prevent over temperature that can cause damages (Grillo, et al., Aug 2010). Four inputs to a seamless control would be the rotor actual speed, generated power, the turbine exhaust temperature and compressor outlet pressure (Enalou & Soreshjani, April 2015).

2.5.1.1 Synchronous versus Asynchronous Machines

In a common alternating current (AC) motor, a rotating magnetic field is produced in the air gap between the stator and the rotor – The speed of this rotating magnetic field is called the synchronous speed. With a synchronous motor, the rotor rotates at the same speed as the rotating magnetic field in the gap. The operating speed of a synchronous rotor is directly proportional to the frequency of the electrical grid.

Other research has shown that permanent-magnet synchronous motors are widely used for industrial purposes due to their high efficiency, high power density and wide constant power region (Filipescu & Filipescu, Oct 2014). A synchronous diesel generator is used in some simulations presented in this work because of the constant frequency it maintains and a synchronous machine is more commonly used as a generator rather than in a motor application.

The rotor is capable of running at constant speed irrespective of the load acting on them. The pull out torque also needs to be considered otherwise the motor will slip out of synchronism. It is a high efficient machine and very durable and cost effective. They are also used in high precision applications.

The desired frequency for a microgrid is 50Hz in South Africa and 60 Hz in some countries elsewhere. The frequency of the voltages induced by the synchronous generators are determined by the following calculations.

$$n = \frac{120f}{p} \quad \text{where } n = \text{rotor speed} \qquad 2\text{-}3$$

$$f = \frac{np}{120} \quad \text{where } p = \text{number of poles} \qquad 2\text{-}4$$

Asynchronous motors are also called induction motors and are commonly used as velocity controlled actuators such as household appliances, elevators and trains (Bascetta , et al., April 2010).

The rotor consists of an additional winding in the form of a squirrel cage (also called a damper). The applied stator current induces an opposing current thus creating magnetic flux which turns the rotor without the help of an external direct current (DC) excitation field current.

The rotor of the asynchronous motor rotates at a slower speed than the synchronous speed – The opposite applies to induction generators; the rotor is mechanically forced to speed faster than that of the synchronous speed in order to produce active power. The operating speed therefore is less (motor) or more (generator) than the synchronous speed, that is where the term asynchronous comes from (meaning non-synchronous).

2.5.1.2 Governor Control

A diesel generator consists of an internal combustion engine and a synchronous generator connected to the same shaft. Diesel generators are usually used for back-up generators or in remote places. The diesel generator is controlled by the conventional frequency droop control.

The frequency is directly proportional to the speed of the prime mover. An increasing load demands results into a decrease in the speed of the prime mover, thus the frequency of the voltage supply. The prime mover then needs to turn faster to catch up with the frequency set point reference.

The speed of the prime mover compensates for the disturbance, by the increase in mechanical input power to the prime mover. The governor system maintains the speed of the output frequency by moving the prime mover in response to shaft speed due to various load changes or disturbances.

The conventional engine speed of a diesel generator is regulated by implementing a fixed droop mechanical governor or an analogue Proportional-Integral-derivative (PID) control circuit (McGowan , et al., June 2006). The governor consists of three control loops: turbine gate opening control loop, unit speed control loop, and power output control loop. Each control loop has its own set point that is maintained after disturbances (Van Vuuren, 2006). See figure the following 2.9.

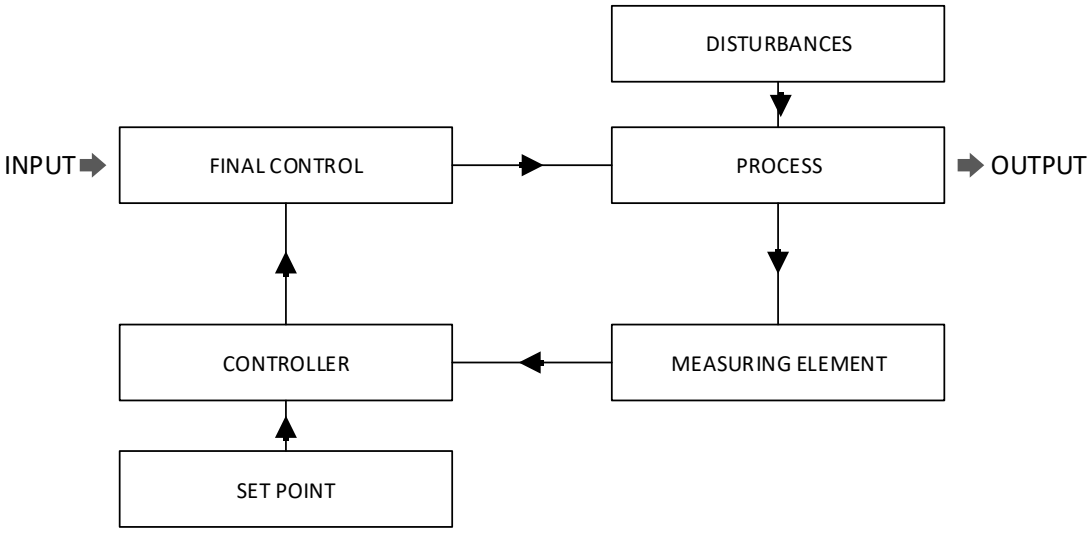

Figure 2.9: Basic Governor Control

(Van Vuuren, 2006)

The speed of synchronous machines is controlled by changing the supply frequency thus at a fixed frequency the speed remains constant. There are two types of speed control namely direct controlled and self-controlled. With direct control, the output voltage and frequency of an inverter is changed to obtain the required speed (*Open-loop control*) (Fish, 2014). See figure 2.10.

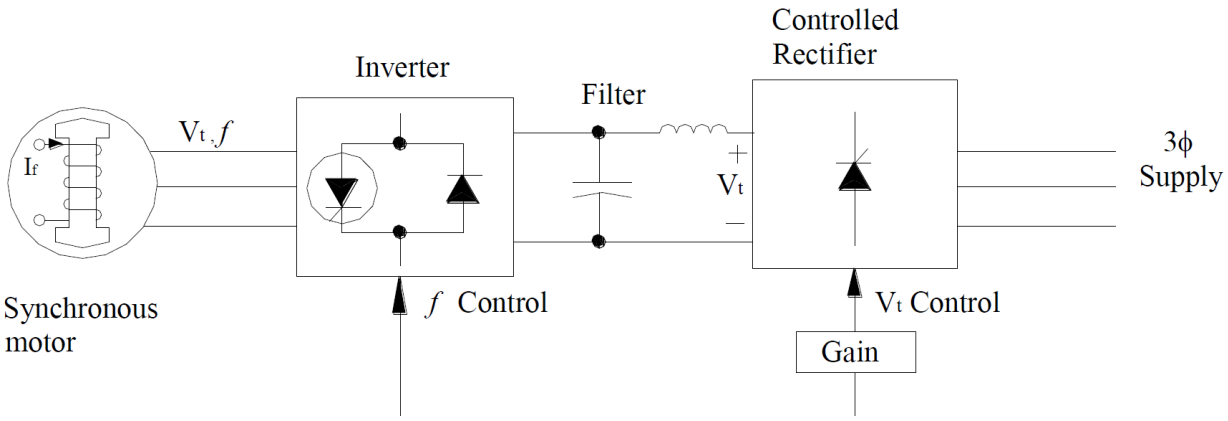

Figure 2.10: Open-loop frequency Control

(Fish, 2014)

With self-control, the variations in the rotor speed due to sudden load changes is fed back in a closed-loop control circuit so that the necessary frequency compensation is automatically made to return to the required speed (*closed-loop control*) (Fish, 2014). See figure 2.11 below.

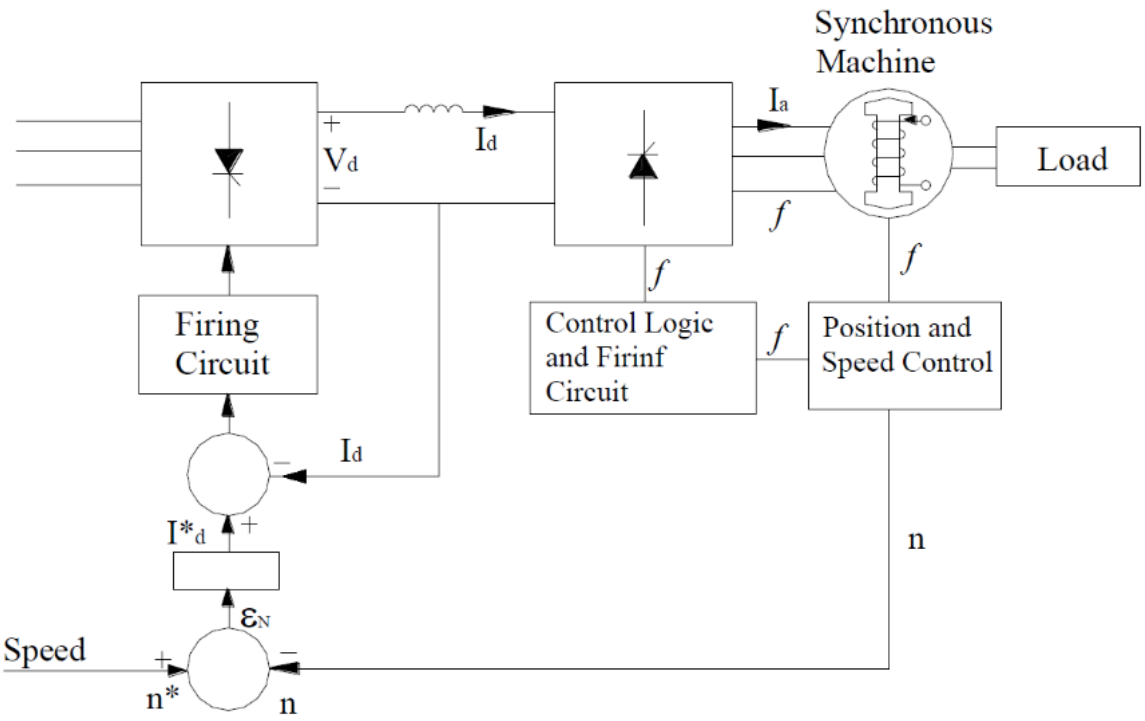

Figure 2.11: Closed-loop frequency Control

(Fish, 2014)

2.5.1.3 Bio-diesel generator fuel

One of the first commercially viable biogas projects in South Africa is the BMW Bio2Watt renewable energy project. Cattle manure and organic waste is directed into a digester where biogas is produced. With a vegetable oil generator, 100% pure vegetable oil is extracted from various plants without requiring chemicals. One can also produce own organic home grow oil. The oil extracts vary from peanut, coconut, soybean, sunflower, safflower, linseed rapeseed to palm oil extracts (Hasan, et al., Dec 2013).

Vegetable oil is thicker and must be diluted to be used by the appropriate engine. This generator would typically consist of two fuel systems. The secondary system will consume normal diesel to start the generator.
After a few minutes an automatic transfer switch will connect the vegetable oil as it is thinned by a rise in temperature. During the shutdown process an alarm will remind you to purge the fuel to enable a smooth start, especially in cold climates.

2.5.2 Wind Turbine Generators

2.5.2.1 Operation

Wind turbines is directly affected by the strength of the wind and indirectly affected by the sun, because the sun's heat create low pressure air vacuums which is filled by higher pressured air to create moving air, thus wind. The important elements of a wind generator are wind, blades, shaft rotor, stator and a resulting electromotive force (EMF).

See the figure 2.12 below to establish the mechanical process from the blades right through to the generator. Wind turbines are classified as non-dispacthable DG's due to the inconsistent wind speed fluctuations as well as the seldom match between the maximum wind power produced and the maximum wind power available (Abdullah, et al., June 2015).

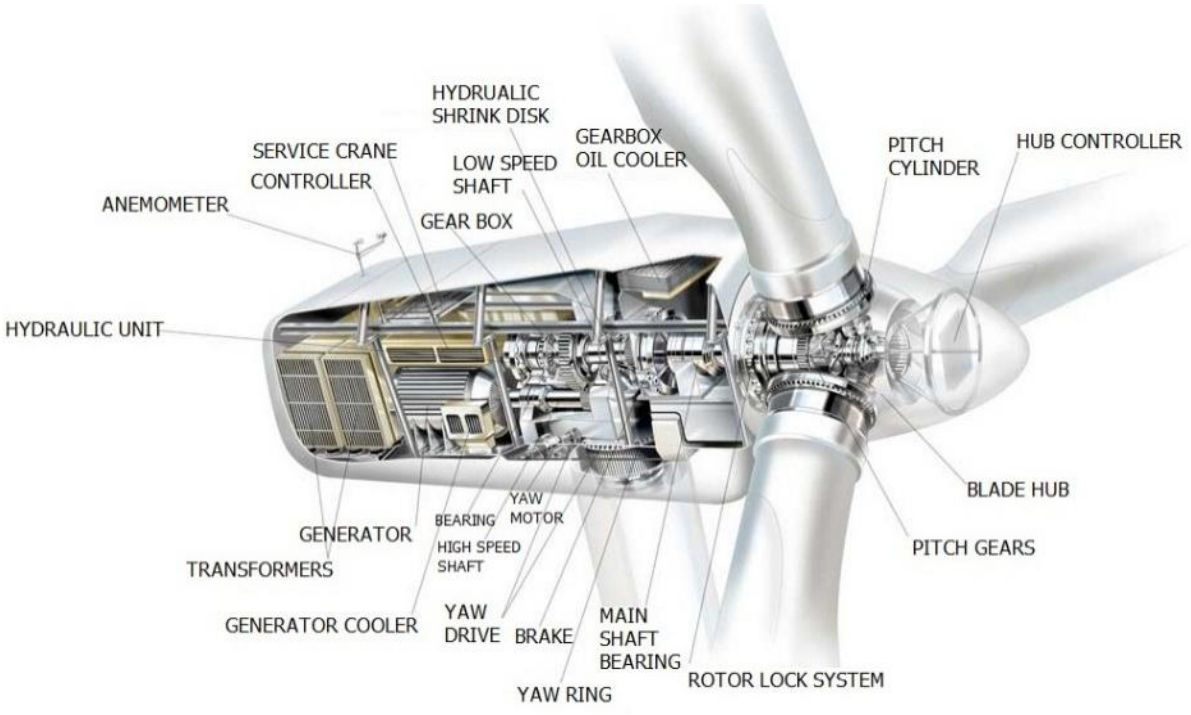

Figure 2.12: Detailed Wind Turbine Generator

(Daniels & Daniels, n.d.)

Wind power is generated by the rotation of the blades caused by the flow of air due to the force of the wind. Offshore islands where fuel is costly are highly favourable for wind energy (Kang, May 2007). The blades are connected to a shaft which is connected to a rotor that is housed inside a stator. The rotor induces an EMF into the stator by

converting mechanical energy into electrical energy. Once the torque exerted by the wind turbine exceeds the maximum generator drive, the mechanical brake is activated (Lumbreras, et al., May 2016).

There are mainly two types of wind generators: Horizontal-axis wind turbines (HAWT) and vertical-axis wind turbines (VAWT) respectively. The horizontal axis generator is the most common type and consists of three or five blades and operates like the reverse process of a fan. The vertical-axis generator looks like an eggbeater which could produce potentially larger off shore turbines thus reducing energy costs (Parker, et al., April 2016).

Regarding wind turbine efficiency, not all the energy of the wind can be harvested and utilized. According to Betz's law, the theoretical maximum efficiency that the blade rotor of a wind turbine can operate at, is 59.3%. The factor 16/27 is also known as Betz's coefficient.

Three types of wind speed limits were compared with each other as indicated in figure 2.13 below. For example, if a wind blows at 13m per seconds, the measured power would be 1300W/sq.m. The theoretical maximum power is limited to 800w/sq.m and the actual maximum power the generator could produce would be 500w/sq.m. This indicates a blade rotor efficiency of 38.4%.

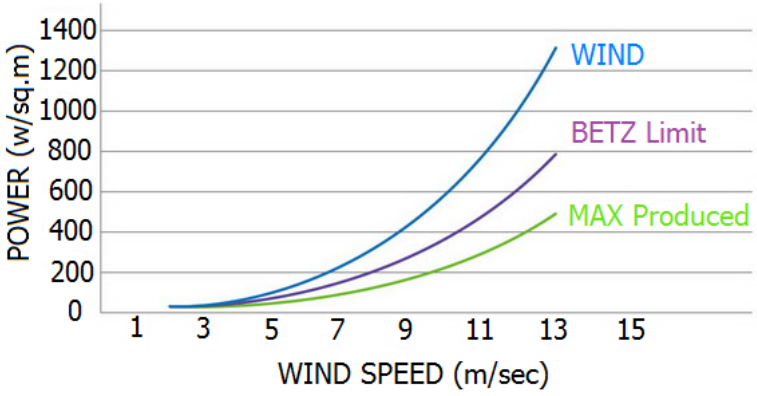

Figure 2.13: Power versus Wind Speed

(Guangzhou HY Energy Technology Limited Corp, 2008-2016)

The five-blade turbine produces good power at lower wind speeds, the extra two blades creates more resistance thus harvesting more wind power. See figure 2.14 for illustrative purposes. With its smart brake, aerodynamic breaking the rotor speed can be limited at higher wind speeds. The three-blade wind turbine is not as efficient as the five-blade turbine because of the mechanical furling braking system.

Larger blade spans increase the total energy production however the aerodynamic loads on the blades increases as well, causing the blades to be more at risk of damage. Research has proposed blade form monitoring that uses optical sensors connected to a wireless network (Oh, et al., May 2015). The fault detection and isolation (FDI) mode protects the turbine from severe damage and enables repair and maintenance operations (Odgaard & Stoustrup, April 2015).

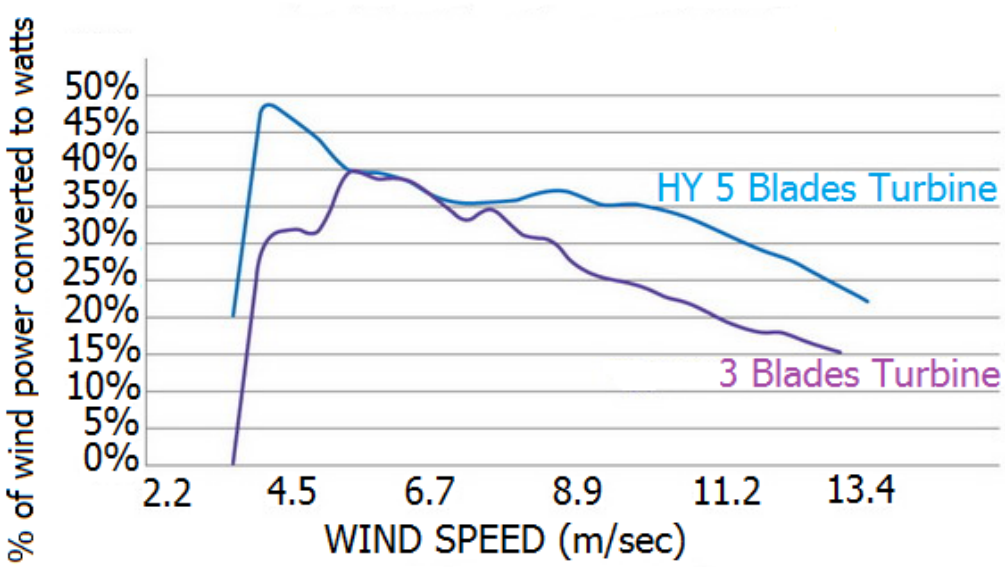

Figure 2.14: 5-Blade versus 3-Blade Efficiency Comparison

(Guangzhou HY Energy Technology Limited Corp, 2008-2016)

The efficiency of a wind turbine is simply calculated according to the output power versus its input power:

$$\text{Efficiency} = \frac{Shaft\ power\ out\ of\ turbine\ into\ gear\ box}{Wind\ power\ into\ turbine\ blades} \qquad 2\text{-}5$$

2.5.2.2 Wind Turbine Control

The wind turbine generator assembly can be controlled via the methods stated in table 2.2 below. A combination of all five strategies would be highly beneficial.

Table 2.2: Wind Turbine Control Aspects

Method	Description
Passive and Active stall	Adjust blades to regulate wind attack
Generator torque	Variable speed drive
Yawing	Guiding turbine into/out of the wind direction
Electric braking	Using resistance (heat) to dissipate energy
Mechanical breaking	Disc or Drum breaks

Mathworks' Matlab/Simulink software program also offers the option to model a wind turbine in the mechanical and hydrologic domain with its respective toolboxes. The figure 2.15 illustrates an overview of a wind turbine and its mechanical components as well as its electrical control system.

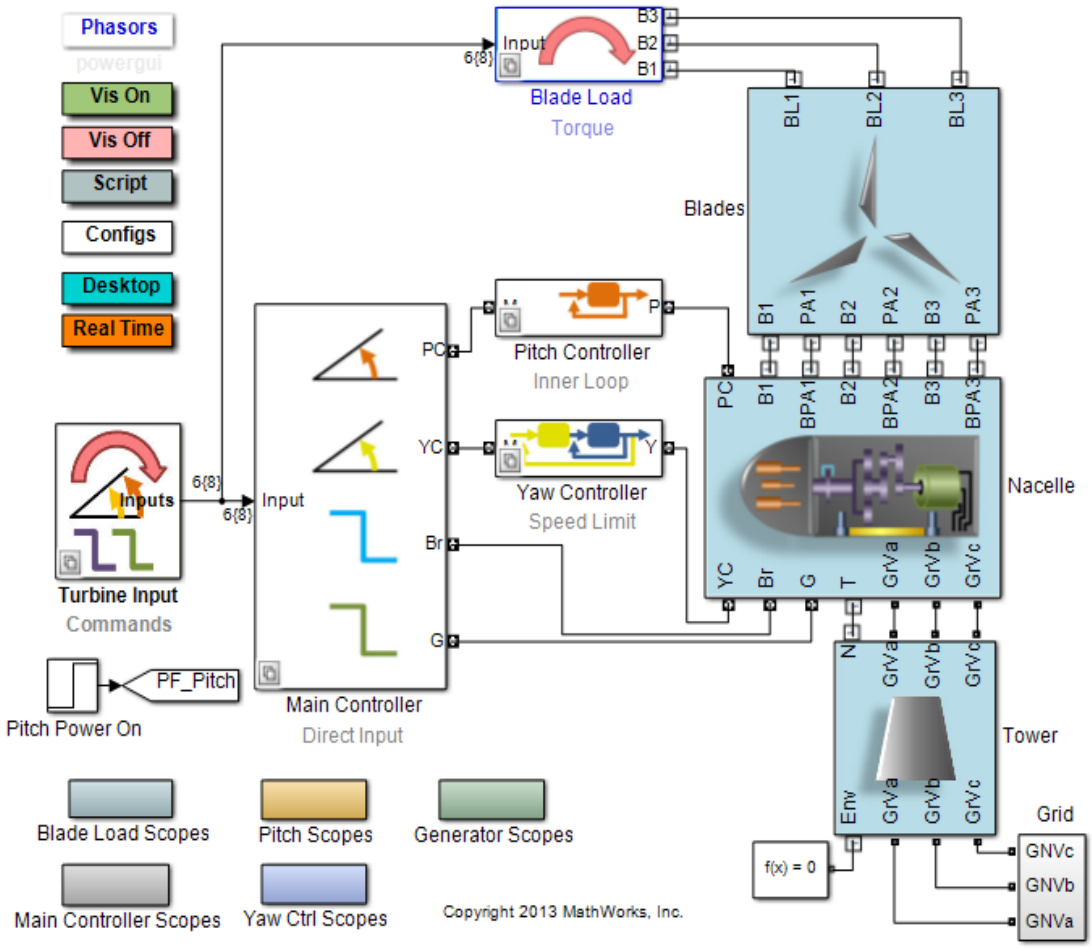

Figure 2.15: Mechanical Turbine control

(Matlab, 2012)

The nacelle is the main house that host every turbine component except the blade rotors. See figure 2.16 below.

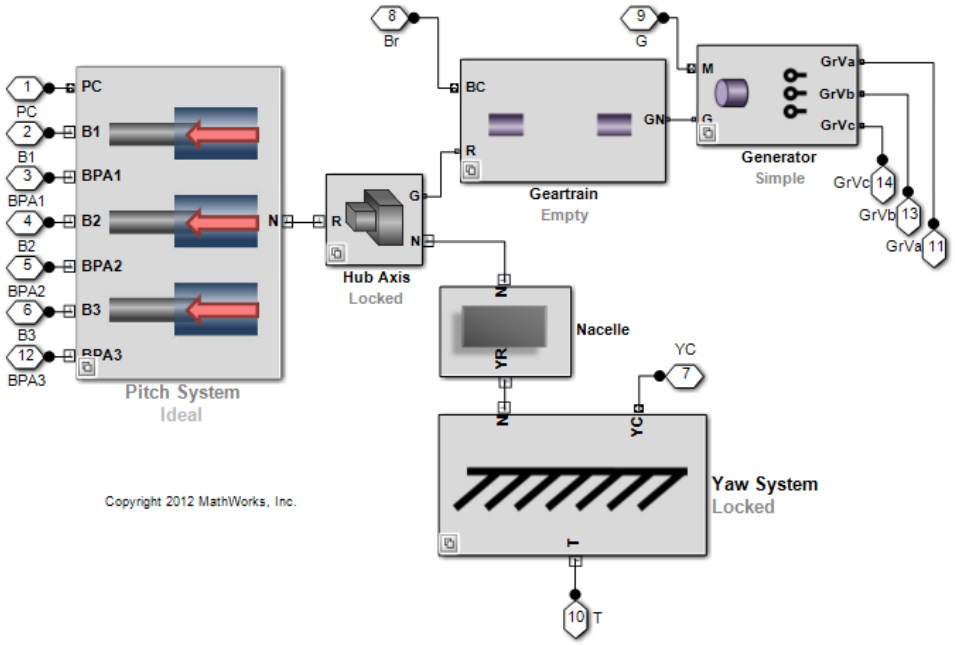

Figure 2.16: Mechanical Nacelle

(Matlab, 2012)

2.5.2.3 The Doubly Fed Induction Generator

There is a growing interest particularly in wind power conversion system technologies (Suwan, et al., July 2012). Doubly fed induction generators (DFIG) has been become the most popular choice for megawatt wind turbines due to their better control topologies and cost competitive arrangement (Shu, et al., March 2009). The generator's rotor must be able to operate in various wind speeds.

The rotor in this system operates at both sub- and super synchronous modes around the synchronous speed of the stator. Wind generators can be exposed to over-voltages that occur during unbalanced faults, loss of large loads and switching transients. Long transmission lines also cause over-voltages due to the Ferranti effect (Cai & Erlich, June 2015).

The stator is directly connected to the grid while the rotor is connected to a three-phase inverter via slip rings. The rotor side circuit is connected to an AC-DC-AC converter linking back through inductors to the main grid. The power converters reduce power losses because it only needs 30% of the total power nominal generator power.

Both the rotor and stator are connected to electrical sources and that is where the term 'doubly fed' existed from (double feed). The rotor three-phase windings are energised by the three-phase grid current and establishes the rotor magnetic field. The rotor magnetic field induces current in the stator three-phase windings and the induced stator current also develops a magnetic field.

The interaction between the rotor and stator magnetic field develops torque. The DC-linked capacitor is place in between the converters acting as an energy storage and to minimise voltage fluctuations (ripples) (Fletcher & Yang, 2010).

A doubly-fed induction generator can automatically control the active & apparent power, frequency and voltage. Both the rotor-side converter C_{rotor} and grid-side converter C_{grid} consists of power electronic devices to amalgamate an AC voltage from a DC source. The capacitor on the DC side acts as a DC power source. The C_{grid} converter is connected to the grid with coupling inductors.

The three phase rotor is connected to C_{rotor} via slip rings and brushes, the stator is directly connected to the grid. The wind power is converted to electrical power by the induction generator and fed into the grid by the stator as well as the rotor windings.
The controller sends the pitch angle command as well as the voltage command signals V_r to C_{rotor} and V_{gc} to C_{grid} in order to control the wind turbine, DC bus voltage and the voltage at the grid terminals (reactive power).

With a double-fed induction generator, the stator is directly connected to the grid side while the rotor side is fed with an AC/DC/AC insulated-gate bipolar transistor (IGBT) - based Pulse Width Modulation (PWM) converter modelled by a voltage source as shown in figure 2.17.

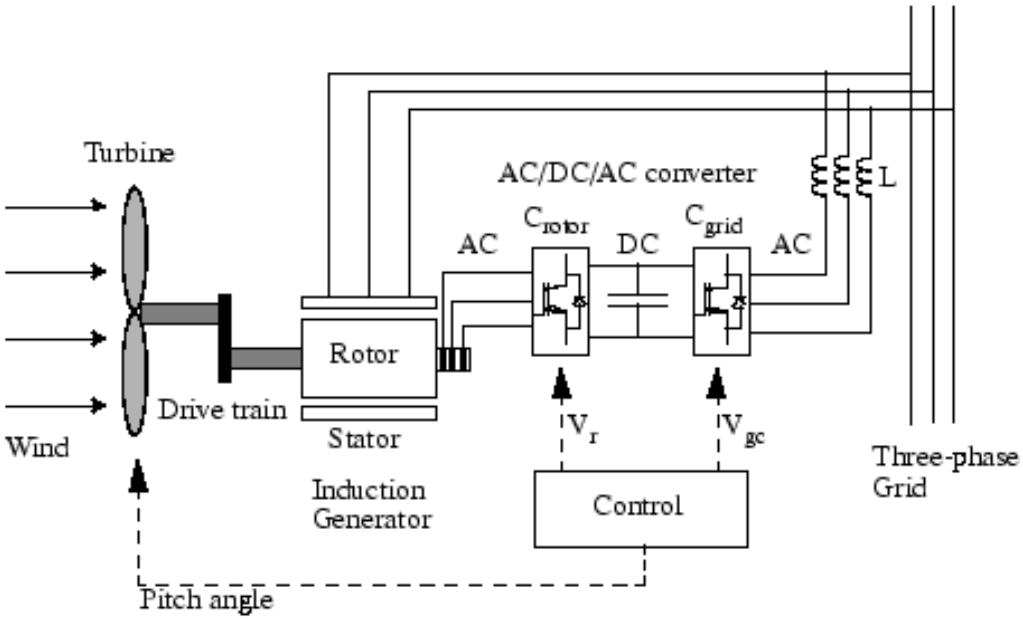

Figure 2.17: DFIG Control

(Matlab, 2013)

The diagram in figure 2.18 below represents the per phase equivalent circuit of the DFIG

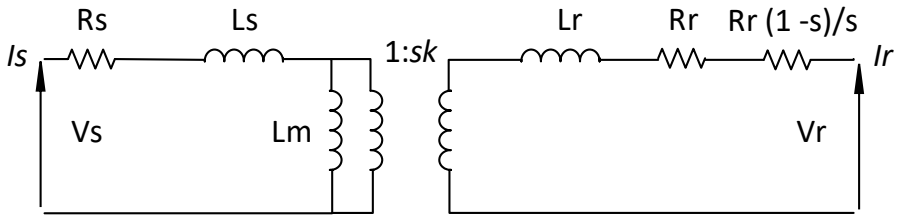

Figure 2.18: Induction Circuit

(Fletcher, 2010) (Fletcher & Yang, 2010)

The stator side of the DFIG diagram includes the resistance of the stator winding (Rs) and the leakage inductance of the phase winding (Ls). The stator resistance depends on the type of material that was used to fabricate the winding.

The leakage inductance represents all the generated flux in the stator that doesn't cross the air-gap of the machine, thus not useful for the creation of torque. The magnetism branch (Lm) represents the useful flux that crosses the air-gap for the contribution to the torque. The rotor side of the DFIG diagram also includes the rotor leakage reactance (Lr) and the rotor resistance (Rr).

The rotor circuit models the generated mechanical power by including and adding the rotor resistance component, Rr (1 – s)/s. A transformer is used to link the rotor and stator circuits, the turns ratio (*N*) depends on the actual turns ratio between the stator and rotor (1: k), including the machine slip (s).

$$s = \frac{N_s - N_r}{N_s} \qquad 2\text{-}6$$

2.5.3 Fuel Cells

Advancement in solid oxide fuel cell (SOFC) technology have increased in attentiveness in their use towards distributed electricity generation. SOFC converts chemical fuel to electricity having some advantages over conventional generation methods, as well as the use of the exhaust heat recovered that improves the system energy efficiency (Colson & Nehrir, Feb 2011).

The operation on fuel cells depicts the conversion of chemical energy into electrical energy. The current flow is a direct result of a chemical reaction between positively charged ions (hydrogen) with an oxidizing agent (oxygen) which generates an EMF. A basic single fuel cell consists of a membrane electrode assembly (MEA), gas diffusion layers (GDL), bipolar plates, current collectors and compression plates.

Portable fuel cell technology is available for the required applications but faces challenges due to the complex control system as well as the balance of plant systems requirements (Benavides & Chapman, May 2008). DC portable Fuel cell systems are developed with a silent operation including a portable hydrogen cylinder can that can supply a small load for up to a month. There will also be no resulting carbon emissions.

The general advantages of a fuel cell above a battery (car) are that there will be no emissions, noise or vibrations. The fuel cell also shows increased performance and on board power, higher reliability and flexibility in terms of design.

2.5.3.2 Microbial Renewable Fuel Cell

A microbial fuel cell (MFC) is a bio-electrochemical device that produces a current by utilizing the interactions of microbes. The microbes can be described as living organisms that can't be seen with the naked eye. Theses microbes breaks down organic matter and releases electrons that flows through a cathode to an external load as it combines with protons and oxygen to complete an electrical circuit (Carreon-Bautista , et al., Oct 2015).

The difference between MFC's and normal Fuel Cells is that their catalysts facilitates the redox processes. MFC's uses biocatalysts (microbes) while fuel cells use traditional chemical catalysts. The microbes grow on electrodes that are oxygen free. These cells can act as small scale power sources for sensors when other sources are not accessible (Finarelli, et al., Sept 2012).

The unconfined electrons are then guided through an external conductor where it can combine with oxygen thus electrical current can be extracted from the conductor. This redox reaction causes electrons to move around, a potential difference always exists among moving electrons. See the applicable figure 2.19.

There are two types of MFC's: Those that use a mediator and those that are mediator-less. Most of the biological fuel cell systems are electrochemically inactive, thus the electron transfer from the microbial cells to the respective electrode needs to be facilitated by a mediator like thione and methyl viologen or natural red. These mediators radically increase the current.

Electron are extracted from the oxidation proses of a naturally occurring fuel like a carbohydrate. The organisms inside the electrochemical cell act as a source of electrons. The transfer of these electrons are effected by a redox mediator directing the electrons via the anode to the external circuit, completed by the cathode. The anode reaction for the oxidation of glucose is as follow:

$$C_6H_{12}O_6 + 6H_2O \rightarrow 6CO_2 + 24e^- + 24H^+ \qquad 2\text{-}7$$

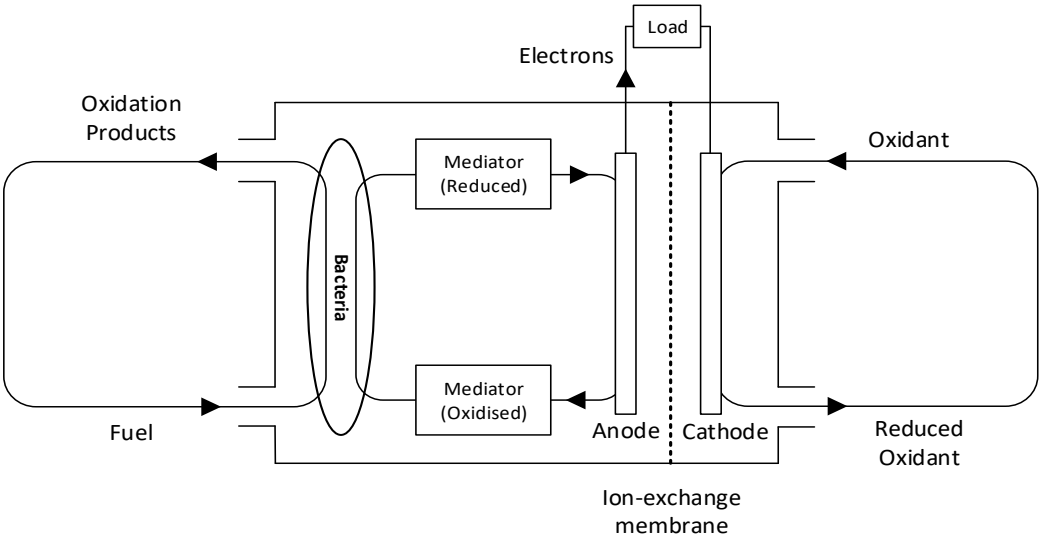

Figure 2.19: Diagram of Microbial principle

Mediator free MFC'S produces power directly to the electrode without a mediator/facilitator. Electrochemically active bacteria is used to transfer these electrons. Mediator-less MFC's can run on waste water and can also derive energy directly from plants like cord grass, rice, tomatoes and algae.

A Third group of microbes that transfer electrons extra-cellularly directly onto solid conductors are called exo-electrogens. The electrical output of MFC's can power small applications such as a distributed wireless sensor network for environmental monitoring at waste water plants, especially when no other power sources is available.

Individual microbial fuel cells produce a very low power output, the power profile of a MFC varies with Ph level, temperature and the amount as well as the type of substrate in the anode compartment. The low density and wide range MFC parameters over time creates complications. Another researcher introduced an inductor less dc-dc converter that allows dynamic tracking of the optimum point for maximum power extraction from an MFC combined array to help solve this problem (Carreon-Bautista , et al., Oct 2015).

Switched capacitive (SC) circuits is a more efficient method used for the voltage balancing of microbial fuel cells. A SC circuit consists of switches, capacitors and an oscillator. When the MFC's are unbalanced, the capacitor charges when it is connected to the stronger MFC_2 and discharges when it is connected to the weaker MFC_1. Thus practically a capacitor (C_{12}) is alternatively represented in parallel with the MFC at switching frequency (Khaled, et al., May 2015). See the circuit below in figure 2.20.

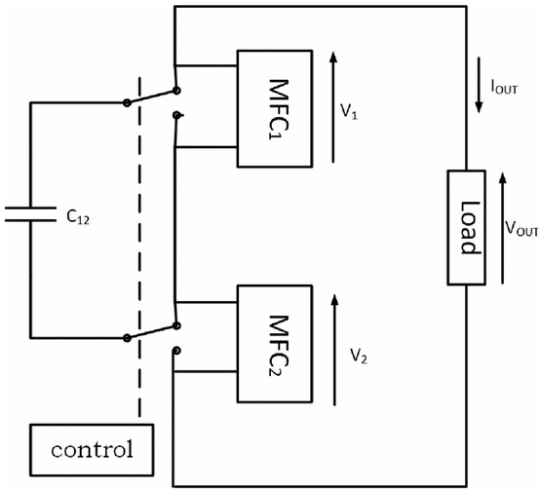

Figure 2.20: Switched capacitive circuit

(Khaled, et al., May 2015)

Eco-volt is an invention that recycles waste water into clean water as well as producing electricity. The waste water is possessed by two systems, the first system uses bacteria that facilitates the normal oxidation reaction that converts dirty water in the clean water with an EMF resultant, thus electricity.

With the second process at the cathode, the electrodes are coated with a different kind of bacteria that combines the electrons, hydrogen and carbon dioxide into pure methane gas. The Eco-volt systems thus host this process and is called electro-methano-genisis. The methane gas provides additional clean heat and energy.

2.5.3.3 Simplified Fuel Cell Stack

The two most basic input parameters for a fuel cells consists of pressure and temperature. See the basic electrical circuit representing a fuel cell in figure 2.21.

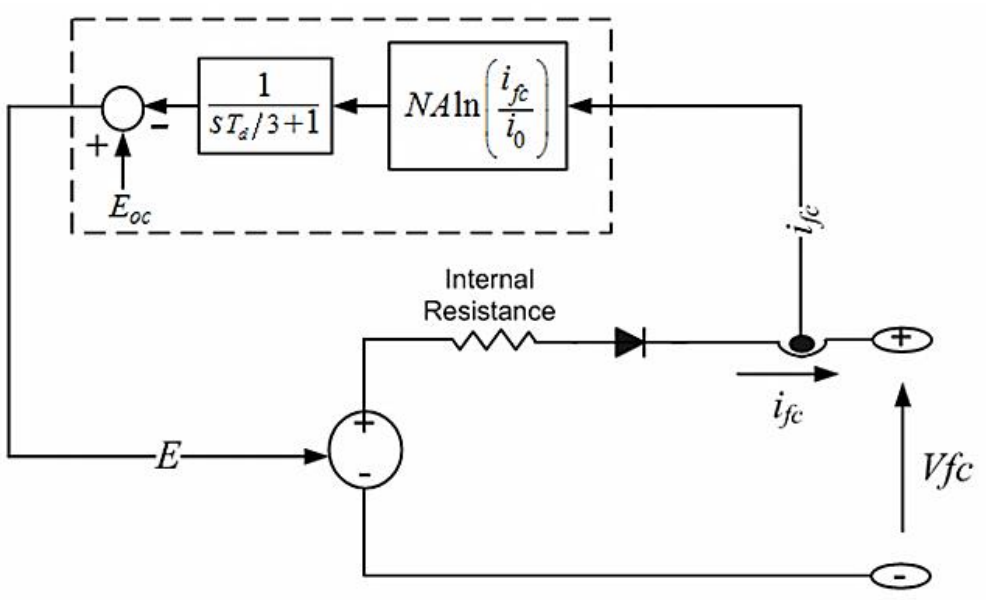

Figure 2.21: Fuel Cell Control Diagram

(Matlab, 2016)

The first region is the activation region caused by the slower initial chemical reactions taking place at the electrode surfaces. The second region is due to the resistive losses caused by the internal resistance of the fuel cell stack. The third and last region shows the transport losses caused by the change in concentration of the reactants as the fuel cell produces power. (Matlab, 2016).

2.5.4 Photo Voltaic Cells

2.5.4.1 Development of PV Technology

The PV effect was discovered by Becquerel while he studied the effect of light on electrolytic cells. Leading types of solar cells are c-Si, pc-Si, amorphous-Si (a-Si), III–V, II–VI, and I–III–VI_2 semiconductors and their alloys as well as nano-PV. There are four basic types of Pv cells: Mono crystalline, poly crystalline, thin film and transparent solar cells.

Dye sensitized solar cells (DSSCs) can reach efficiencies of 13% with simple chemical manufacturing requirements which inevitable links to lower fabrication costs. DSSC's can be integrated as PV windows complimenting and even replacing structural buildings (Sygkridou, et al., July 2015).

A photo voltaic cell is a specialized semiconductor diode that converts visible light into direct current. Some PV cells can also convert infrared or ultraviolet radiation into DC electricity. Photo simply means ‘light’ and voltaic means ‘voltage’. The sun strikes the earth’s surface at a solar constant of about 1000 watts per square meter, this can vary due to changing weather conditions as well as location.

In the past five years, photo voltaic energy has grown at an annual rate of 60%. Factors that contributed to this rapid growth are the cost reduction, increase in efficiency of the PV panels, increased environmental awareness and favourable governmental incentives (Kouro, et al., March 2015). Crystalline silicon is the dominant PV material due to its high efficiency, long service cycle and lower cost (Benda, Dec 2015).

The direct normal irradiation (DNI) per hour daily can be calculated as follow:

$$\text{DNI} = \frac{Average\ Annual\ sum\ (0ver\ 20\ years)}{\frac{365.25\ days}{24\ hour}} * 5\ \text{days (average sunlight)} \qquad 2\text{-}8$$

$$\text{DNI} = \frac{\frac{3200}{365.25}}{\frac{}{24\ hour}} * 5$$

$$= 1.83\ \text{kWh}/m^2$$

Note that a distinction must be made between solar photo voltaic power and concentrated solar power (CSP). With CSP, reflectors direct the sunlight towards a central point, where heat is concentrated. The concentrated heat drives a heat engine (sterling engine). Note that solar can also imply thermal energy where heat collection systems are used for heating geysers. Concentrating photo-voltaic (CPV) utilizes mirrors to concentrate sunlight onto PV cells to generate electricity (Hebrink, June 2009).

The trade-off of PV Cells would lie between the durably vs. efficiency on a power level as well as their financial viability. Cracks can develop in the crystalline silicon material and will lead to power losses due to increased resistances. Transportation, installation and severe climate extremes causes the PV modules to crack and weaken (Morlier, et al., Oct 2015). National Renewable Energy Laboratory (NREL) has revealed that over the past 30 years the efficiency of solar PV panel reached record levels of up to 46%. (Kazmerski, April 2011). See the following table 2.3.

Table 2.3: PV efficiency development

(Information Adapted from NREL, 2011) (Kazmerski, April 2011)

Multi junction Cells (2-terminal, monolithic)	**Efficiency**
Four-junction or more (concentrator)	46.0%
Three-junction (concentrator)	44.4%
Four-junction or more (non-concentrator)	38.8%
Three-junction (non-concentrator)	37.9%
Two-junction (concentrator)	31.1%
Single-Junction GaAs	
Concentrator	29.1%
Thin-film crystal	28.9%
Single crystal	27.5%
Crystalline Cells	
Single crystal (concentrator)	27.6%
Silicon heterostructures (HIT)	25.6%
Single crystal (non-concentrator)	25.0%
Thin-film crystal	21.2%
Multicrystalline	20.8%
Thin-Film Technologies	
CIGS (concentrator)	23.3%
CIGS	21.7%
CdTe	21.5%
Amorphous Si:H (stabilized)	13.6%
Emerging PV	
Perovskite cells (not stabilized)	20.1%
Inorganic cells (CZTSSe)	12.6%
Dye-sensitized Cells	11.9%
Organic cells (various types)	11.5%
Organic tandem cells	10.6%
Quantum dot cells	9.9%

2.5.4.2 PV Technology Locally

The heat map shown in figure 2.22 below indicates that South Africa is of one of the most suitable countries in the world regarding the irradiating intensity. Note that the Karoo especially is suitable for PV systems with constant high irradiation per square meter.

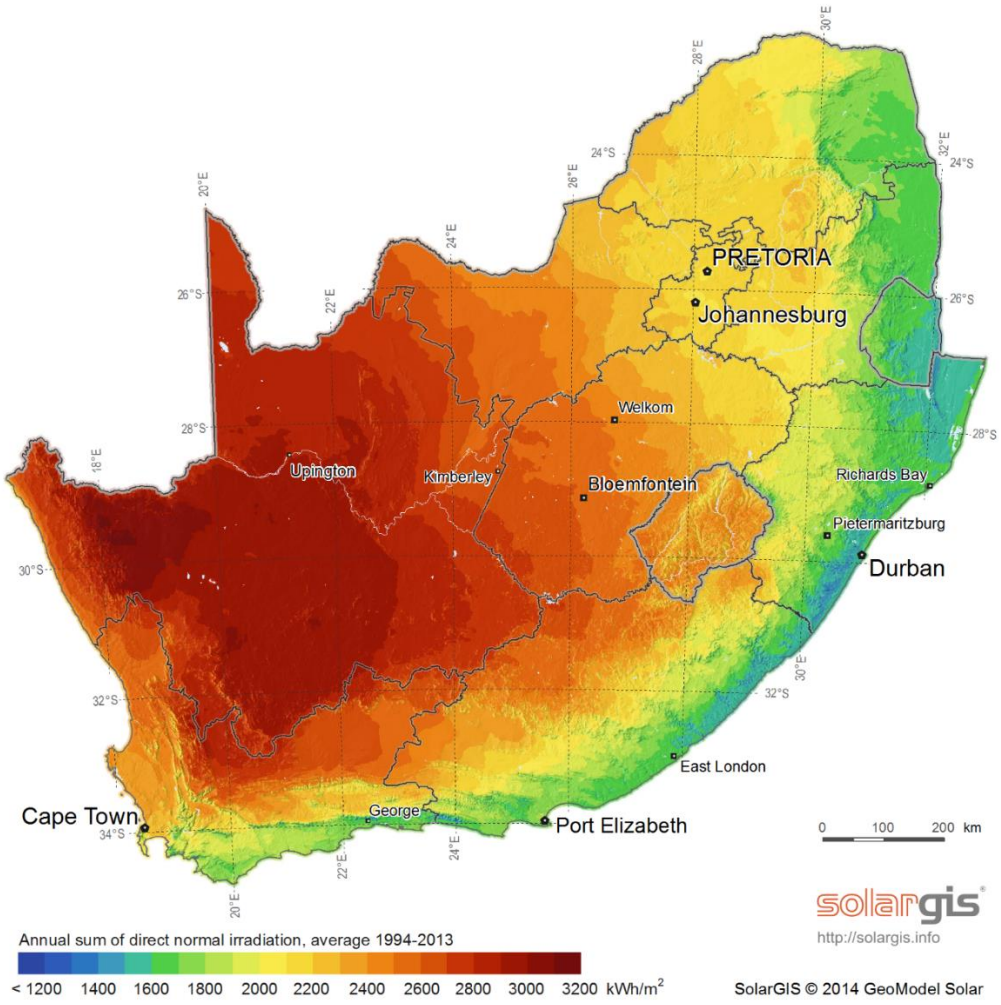

Figure 2.22: Heat Map of South Africa

(Solargis, n.d.)

PV technology is popular for residential and commercial renewable energy systems (RESs). South Africa is a developing country where PV panels are very accessible and easy to install and maintain. The unique challenge we have is that our peak demand is very marginal to our reserved energy capacity.

The other challenge is the sun can only be utilized and optimised for PV production before the countries' recognised peak demand starts, which is 17:00-19:00 in the winter and 18:00-20:00 in the summer (According to Eskom). The sun produces infinite power but only effectively on an average of five hours per day. The solution to reserve the sun's energy would be to simply store it.

The figure 2.23 below illustrates the comparison between the output power profiles of the residential load compared to the PV power generated in Singapore (Zhou , et al., May 2011).

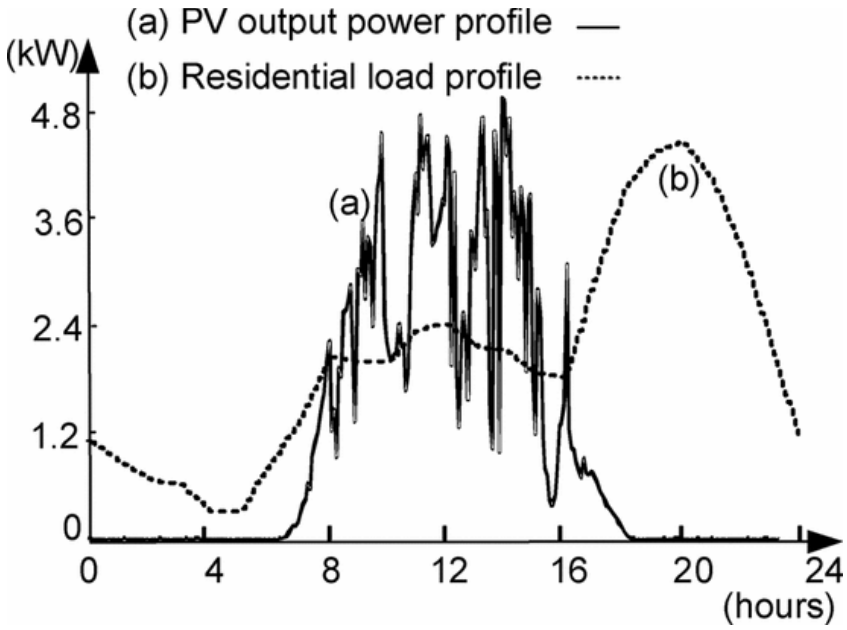

Figure 2.23: Electrical output power profile

(Zhou , et al., May 2011)

The residential peak load profile lies between 16:00H - 24:00H. The graph clearly indicates that the PV output profile provides maximum power before the peak demand of the consumer even starts. This study states the utter important role that energy storage plays in renewable energy efficiency.

3.4.2 MPPT Control

The concept of maximum power point tracking (MPPT) is to get the maximum possible power as a sum of various sources. PV cells produces a non-linear efficiency due to the main following factors: solar irradiance, temperature and cell resistance.

MPPT uses a technique to sample the output voltage of the PV cells and introduces a variable load to maintain the maximum output. A MPPT controller adjusts the output of the solar panel in order to transfer maximum energy to the batteries (Pantelimon, et al., May 2013) . It is an electronic DC to DC converter that optimizes the power efficiency.

Most PV panels produces a higher output greater than 12 volts to compensate for fluctuations (Up to 18 volts). A rated PV panel of 135 watts should produce 7.6A if the output voltage is 18 volts. But the battery only charges at 12 volts so 7.5A x 12 = 90watts. That is a 33% drop in efficiency. The MPPT converts the 7.5A to 11.25A to maximise the charging current and to keep the power output at 135 watts.

$$\begin{aligned} P &= I*V \\ &= 11.25A \text{ x } 12V \\ &= 135 \text{ watt} \end{aligned} \qquad 2\text{-}9$$

The MPPT analyses the output of the PV panels and matches it with the requirement of the battery. Most MMPT's generates conversion efficiencies between 93-97%. The conversion gain is less in the summer than in the winter. The DC input current is converted to AC, and then it is stepped down by transformer and converted back to a DC signal followed by voltage regulation for DC electrical loads.

3.4.3 PWM Control

A PWM controller forces and regulates the power output of the panels to operate at 12v, which imply some power losses. See the figure 2.24.

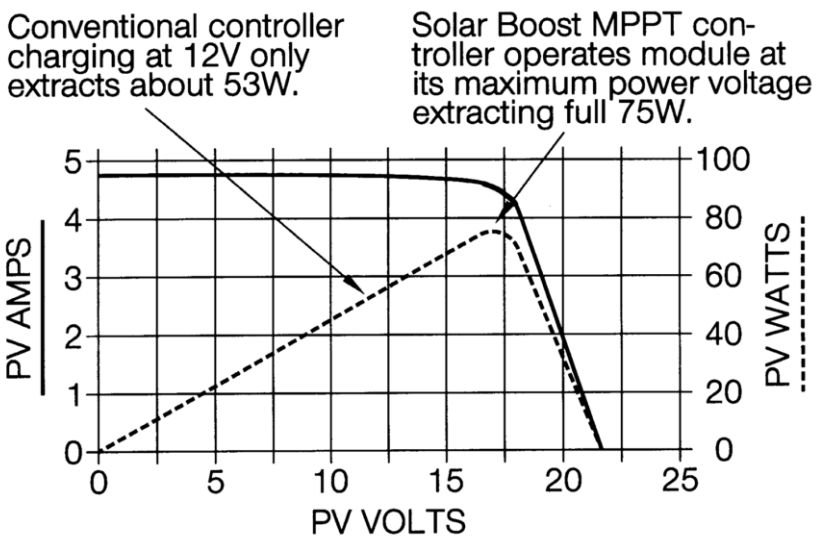

Figure 2.24: PWM versus MPPT control

(Tech Mart, 2007)

The maximum voltage of the panel in this example above is 17 V (Vmp). The MPPT extracts the full power of 75 watts, regardless of the 12v battery. The MPPT uses a DC-DC converter (buck-boost) that coverts the maximum panel voltage to match the battery voltage without losing power, thus increasing the panel output current.

Assuming 100% efficiency

$$\begin{aligned} \text{Charge current} &= \text{V-panel} / (\text{V-battery}*\text{I-panel}) \\ &= 17 / (12*4.45) \\ &= 6.30\text{A} \end{aligned} \qquad 2\text{-}10$$

With the MPPT system the current increases from 4.45 to 6.30 A, thus an increase of 42%, if one ignores the small power losses in the wiring, fuses, circuit breakers. The MPPT current increase or gain in the winter is up to 40% and in the summer 10-20%. The panel output rises with lower temperatures decreases with higher temperatures.

2.6 Energy storage technologies

2.6.1 Energy storage background

South Africa faces unique challenges with grid-tied systems. The facility to sell electricity back to the local utility is very limited and not accessible to everyone. Almost all the residential microgrid systems have to rely on its own storage component to utilize the maximum energy produced by the connected sources.

AC electrical energy cannot be stored directly as this energy is stored in different forms such as electrochemically, magnetically, kinetically as well as potential energy or as compressed air (Boicea , Oct 2014). Energy storage technologies can be classified in terms of round-trip energy efficiency, maximum power and capacity rating, energy losses over time and capital costs involved (Yang & Nehorai, June 2014).

2.6.2 Rechargeable Chemical Batteries

Battery storage of electrical energy can act as a good emergency power supply and operates without noise. A smooth and secure start-up can be ensured when sufficient energy is stored and harmful voltage perturbation can be avoided as required (Arai, et al., 2008). Battery storage provides reliable power supply when the DG's fail temporarily (Pei, et al., March 2016).

Battery manufactures may link the battery's life cycle to the applicable depth of discharge (DOD) (Gunter, et al., May 2013). Efficient charging involves three stages: constant current, constant voltage and floating charge (Eghtedarpour & Farjah, Jan 2014). A conventional battery cannot be rapidly charged and discharged due to its chemical reaction restrictions. Wind and solar generation is clean regarding its carbon footprint, but the storage of this green energy mostly uses chemical batteries which is not environmentally friendly and limited in its storage capacity (Qian, Oct 2010).

Vanadium redox battery (VRB) technologies are competitive for energy storage systems on a larger scale due to the manufacturing and maintenance costs involved. VRB's also offers high design flexibility. Higher flow rated improve energy efficiency but at high pump power losses. Low flow rates need to be optimized for battery efficiency (Binyu, et al., July 2013).

A vanadium redox battery system consists of two electrolytes separated with a proton exchange membrane. The two vanadium based electrolytes are stored in separate tanks. The advantage of VRB is that both the electrolytes contains the same metal ions which illuminates cross contamination degradation (D'Agostino, et al., May 2015).

NEC has released a high-performance battery that claims extraordinary performances. This is an intelligent battery including monitoring and control of the battery voltage and current, relative state of charge (SOC), cell voltage and temperatures, full charge and remaining capacity including the cycle count (NEC Energy Solutions, 2015).

Battery life can be enhanced when all the cells are monitored, evaluated and properly maintained because non-uniform cells limits the battery capacity and even imposes safety hazards (Ju, et al., April 2016).

The Tesla Power-wall is a rechargeable lithium-ion battery. The Power pack is a larger unit with a 100kWh capacity, used more for industrial applications. There are currently two types of batteries: The off-grid everyday battery and the backup battery. The 10kWh battery consists of a nickel-cobalt-aluminium cathode and produces about 1000-1500 cycles in its life span. Multiple Tesla batteries can also be installed together to increase the storage capacity, up to 9 batteries in total (Shahan, 2015).

2.6.3 Micro pumped Storage

Gravitational force is a force that exists in nature, attracting mass towards the earth's centre (Baral, Aug 2010). The principles of gravitational energy and methods can be used to supplement a more sufficient method of power generation rather than replacing it. Incompressible fluid could also be pumped up a large cylinder which is connected to a raising mass, thus creating and storing potential energy (Shively, et al., Nov 2008).

Hydroelectricity is generated by water driven turbines connected to generators. The turbines convert the kinetic energy in the flow of water, either in a river or from a dam, into rotation of the turbine/ generator. Hydroelectricity is widely used where climatic and geographic conditions (high rainfall etc.) are suitable.

Pumped hydro storage is considered as a more reliable standing reserve. The amount of available storage depends on the previous operating management's stored energy and not upon the 100% availability of fuel as used in gas turbines (Black & Strbac, Feb 2007).

A pumped storage scheme uses power from the grid to pump water vertically in reservoirs to be released when needed in order to generate electricity. Some benefits of this scheme include the storing of energy on a daily basis as well as storing energy during off-peak hours to be used during peak hours (Brown, et al., April 2008).

The starter is used to accelerate the pump turbine up to speed after which the main motor/generator takes over. This same device is also used for braking the unit on shutdown. The third mode of the generator is used as a synchronous condensing operation for power factor correction on the national grid. The Palmiet power station of Eskom consists of two units which produces 200 Mega Watts each (Eskom Holdings SOC Ltd, n.d.).

Underground pumped storage schemes have been investigated utilizing deserted mineshafts and quarries to mitigate potential flooding when the controls and mechanical components fail. Such flooding can cause fatalities as well as damage to protected eco systems (Hayes, et al., March 2016). Large hydropower potential is often located in nature reserves and comes with environmental preservation challenges (Varas , et al., April 2013).

2.6.4 Compressed Air Storage

With compressed air energy storage (CAES), unused electricity is drawn from the grid to power large compressors. The compressors push pressurized air into storage, mainly underground geological storage structures. Heated air expands and have more energy.

On demand the stored energy (pressurized heated air) is released back to the surface to drive turbines that generate electricity (Cleary, et al., June 2015). CAES plants that utilises underground salt caverns is relatively inefficient (< 50%) and requires a specific location including the use of hydrocarbon fuel (Saadat & Li, June 2012).

Liquid air energy storage (LAES) operates on three basic principles: charge, store and discharge. High-view power Storage Company has built such power plants where the energy is stored in the form of liquid air in large tanks. Off peak energy is used to liquefy air. The liquid air is stored in vessels at a low pressure, then it is pumped to high pressure, then evaporated and heated to drive turbines.

When air is refrigerated at -196 degrees Celsius, it turns into liquid which can be stored in standard air vessels. If the air liquid then reaches ambient temperatures it can expand up to 700 times in volume, this increase in air pressure then drives a mechanical turbine.

The advantages of a LAES system according to the chief executive officer of High-view Power Storage, is that it scales well on cost and efficiency as well as that it is backed by major original equipment manufacturer's supply chains (Brett, June 2015). The key features of a LEAS system are that it entails a low technology risk, large scale operation, efficient waste heat harnessing, it is geographically flexible and consist of favourable energy density properties (Brett & Barnett, Oct 2013).

2.6.5 Mechanical Flywheel

Flywheels store rotational energy gained by rotational input speed (Yuan, et al., May 2016). A flywheel energy storage system contains a rotating mass powered by external energy source that is coupled to an electrical drive, converting electrical to kinetic energy and vice versa. The stored kinetic energy amount is proportional to the inertia moment of the flywheel and also the square of its angular velocity (De Andrade, et al., July 2007).

Flywheel energy storage systems (FESS) comprises of bearings that is magnetically levitated, thus mitigating friction on the shaft of the flywheel. The FESS is additionally mounted in a vacuumed enclosure to reduce the resistance of air. Flywheels are better used for surge power devices. Unfortunately, a lot of FESS's can generally only supply maximum rated power for 5-30 seconds.

The flywheel is driven by an electrical machine, either a motor or a generator. The motor exerts positive torque or inertia on the flywheel till it reaches its maximum velocity, thus converting the electrical energy into kinetic energy. The energy is maintained constant by powering the mechanical or idle losses with a constant supply (Pastor, et al., Feb 2014).

When applying negative torque (braking) to the flywheel, the kinetic energy is converted back to electrical energy via the flywheel acting as a generator. Thus, releasing electricity back into the power lines. Metallic flywheels are slower, below 10000rpm. Compound flywheels can reach up to 50000rpm.

The basic principle of energy produced is equal to the energy consumed, implies that the storage of energy delays the process of energy consumed. Flywheel is called kinetic energy storage system (KESS). Advantages of KESS are the high-density levels of power and energy as well as that the power storage capacity is not linear to price increase as it arises in the case of batteries.

To conclude this chapter, the first section gave an overview of the four different renewable energy source available on the market. The second section elaborated on four different energy storage techniques which include some advantages as well as disadvantages in terms of efficiency.

CHAPTER 3: MICROGRID CONTROL ASPECTS

3.1 Overview

This chapter focusses on various control aspects and principles that work together in a universal system in order to improve the overall control efficiency. Three hierarchy control levels are unpacked as well as in some cases explained and validated along with flow diagrams, electrical circuit diagrams, software simulations and explanatory graphical illustrations.

3.2 Control background

Electrical power systems regularly experience small constant power oscillations. Power oscillations that increase in amplitude can become unstable oscillations, also called out-of-step conditions. Power system oscillations are caused by sudden load changes, switching of transmission lines, tripping or removal of generators or occurrence of systems faults (Martinez & De La O Serna, Jan 2015). A Utility system cannot accept any fluctuating power without strict voltage regulation (Mohod & Aware, Feb 2012).

A centralized control system also referred to as a supervisory control and data acquisition (SCADA) system can put a utility at risk of a national blackout. A smart grid is also known for its decentralization in the production, consumption and trading of energy including advanced intelligent control algorithms for improved power efficiency and reliability (Dasgupta, et al., July 2012). A smart grid distributes its power with active distribution networks. (Lo & Ansari, March 2013).

Conventionally microgrids trade energy directly towards a macro station. The multi-agent concept enables microgrids to share energy cooperative by exercising local control before connecting to the macro grid. This concept is called the coalitional game strategy consisting of a request exchange stage, a merge-and-split stage and a cooperative transaction stage (Ni & Ai, Jan 2016).

A researcher proposed a phenomenon stating that in order to improve the reliability index of an energy producer the storage capacity has to be doubled. A large storing capacity implicating high financial repercussions only ensure a small probability of energy deficiency (Dong, et al., March 2016).

There is a trade-off between affordability and reliability, and alternative control concepts has to be implemented in conjunction with electricity storage to stabilize the power output of a microgrid.

In conventional grids, the power is balanced by changing the frequency of the system through the spinning energy storage reserves that possesses inertia. In a microgrid where no inertia is present, the energy storage in the DC bus imitates the inertial DG through the power that is released proportionally to the derivative of the system frequency (Vandoorn , et al., Dec 2013).

3.3 Primary control

In conventional grids, unbalances between the generated electrical power and the simultaneous power consumption is rectified and balanced by the rotating inertia of the system. Thus the frequency adjustments implement the power changes. This control action is rapid which takes action in approximately 5-30s.

3.3.1 Droop control

Droop control compensates for frequency and voltage fluctuations. Also called tune slip control (Gu, et al., May 2012). After the frequency falls, the loading increases and more active power is required to maintain the set point. Frequency droop control is advantageous for multiple generators that are connected in parallel for automatic compensation with a fast control action (Bevrani & Shokoohi, Aug 2013).

Power-frequency droop control and reactive power-voltage magnitude droop control is commonly used in decentralized power systems which emulates the operation of a common synchronous generator (Xiu , et al., Sep 2011). Output line impedances causes the Q-V droop control to weaken (Lu & Chu, July 2015). It is so far almost impossible to control inverters with inductive/capacitive impedances in parallel (Zhong & Zeng, March 2016).

Droop control benefits to an autonomous grid by sharing the total real and reactive according to the microgrid capacities (Ashabani & Mohamed, July 2013). The disadvantage would be that when the main system frequency drops the droop control will follow that change accordingly. Secondary and tertiary control would be needed to rectify the system frequency to its nominal value.

Droop control does not rely on external communication which makes it more reliable but with a small error that can be ignored. In the figure 3.1 below, f_0 and U_0 are the rated frequency and grid voltage where P_0 and Q_0 are the momentary set points for the active and reactive power of the inverter (De Brabandere , et al., July 2007).
Refer to figure 3.1 below.

$$f - f_0 = -k_p(P - P_0) \quad 3\text{-}1$$

$$U - U_0 = -k_q(Q - Q_0) \quad 3\text{-}2$$

Where

f - System frequency
f_0 - Base frequency
k_p - Frequency droop control setting
P - Active power of the unit
P_0 - Base active power of the unit
V - Voltage at the measurement location
V_0 - Base voltage
Q - Reactive power of the unit
Q_0 - Base reactive power of the unit
k_q - Voltage droop control setting

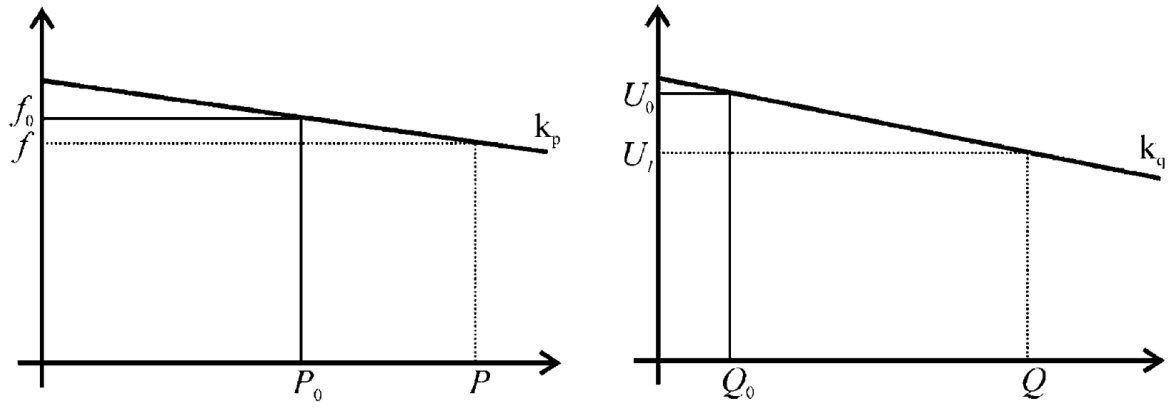

Figure 3.1: Characteristics of frequency and droop control

Frequency-active power droop control is ideal in the transition from grid connected mode to stand-alone mode; self-isolation control is used for a smooth transfer. With the transition from stand-alone mode to grid connected mode, self-synchronization control is adopted. (Chen & Mei, May 2015). The voltage magnitude, phase and frequency needs to match to the main grid accordingly before connection.

In the following simulation, a combination of governor & excitation compensation triggered by a load disturbance was modelled in stand-alone mode**.** A load was introduced to the inertial simulated generator as indicated in figure 3.2 below.

This conventional droop control acts immediately and the steady state response of the power and frequency output settles at a slightly higher value after the disconnection takes place. Note that the values are represented as per unit. See the figures 3.3 and 3.4 below. With this simulation the load was disconnected at 1s and reconnected again after 1.5s. The droop control responds immediately and the three-phase stator current was measured in per unit.

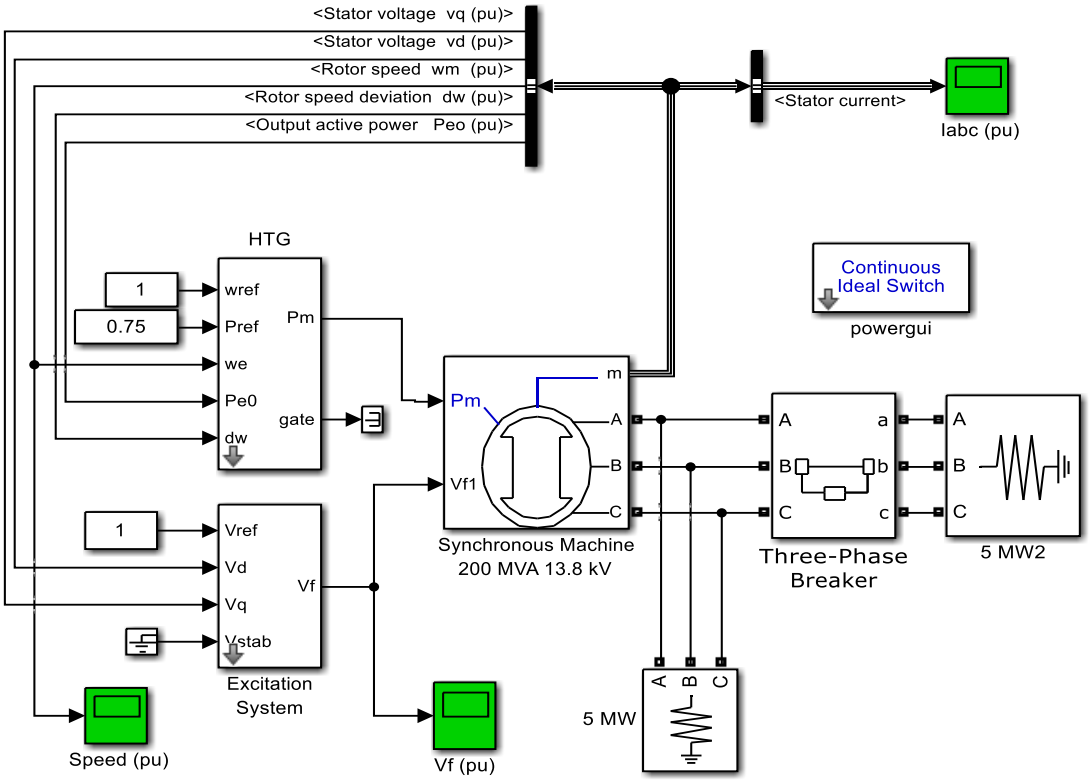

Figure 3.2: Synchronous Machine model

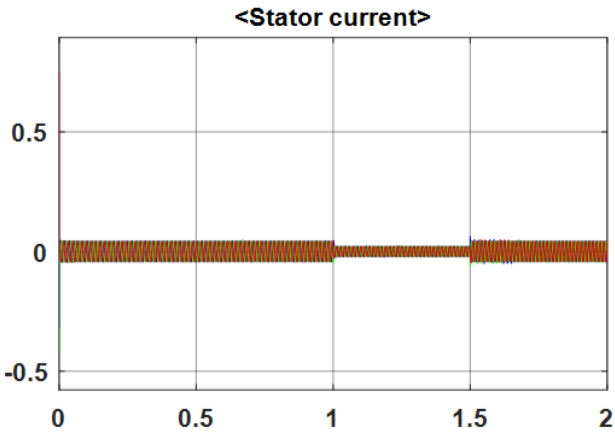

Figure 3.3: Stator Current Output

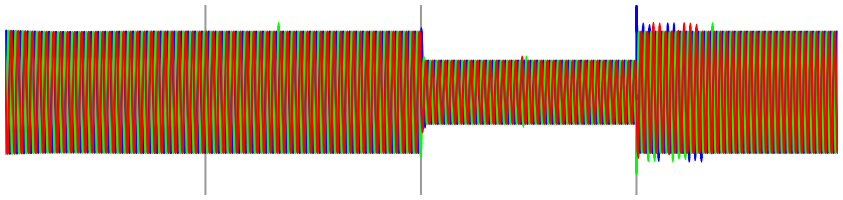

Figure 3.4: Stator current zoomed in

3.3.2 Droop & PQ Control

The PQ control method could be operated in islanded mode because its reference voltage is obtained from the droop control at the point of common coupling before transitioning to the autonomous mode. Figure 3.5 below illustrates the three DGs' that are connected in parallel in islanded mode.

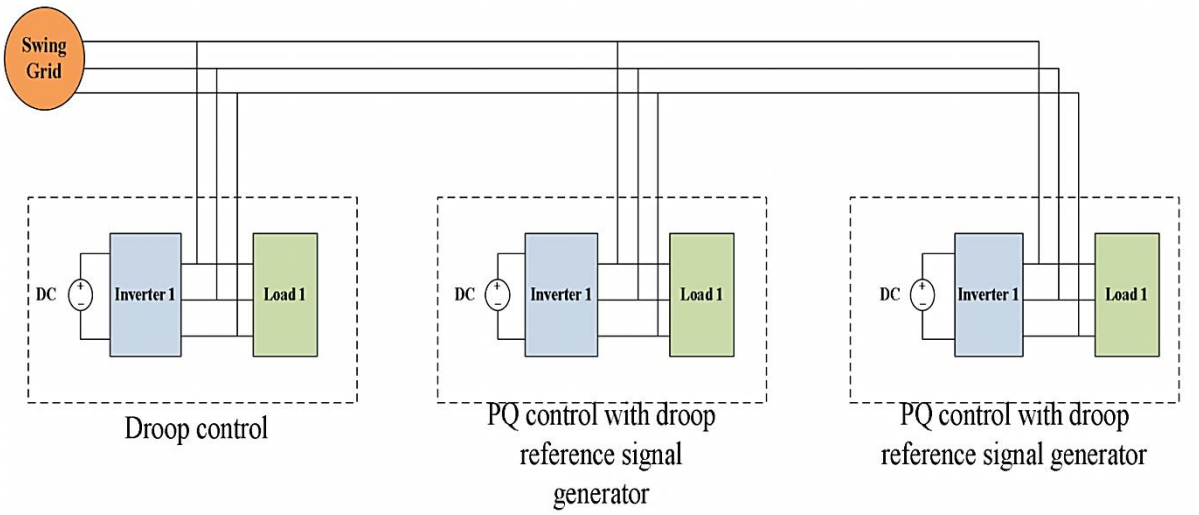

Figure 3.5: Simulated system configuration

(Niu, et al., Oct 2014)

The output current at the inverter 1 that is connected to DG1 fluctuates much more that when the other two inverters DG2 & DG3 were connected due to the lack of the added PQ control method. The distortion that occurs at DG2 & DG3 is smaller during the switch over period from the grid mode to the autonomous mode. Note that the main reason is because the PQ method generates the required real and reactive power instead of merely sharing the power with all the related DG's in the system. This trend is shown in figure 3.6 as well as 3.7 below.

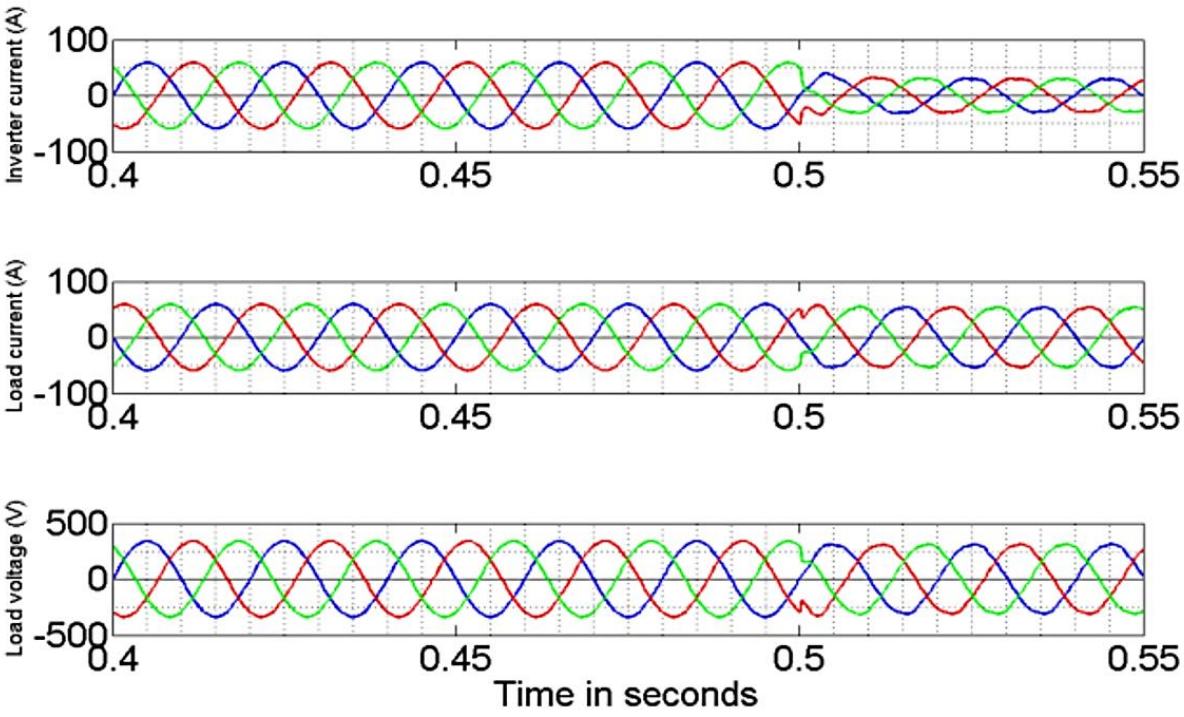

Figure 3.6: Inverter output current DG1

(Niu, et al., Oct 2014)

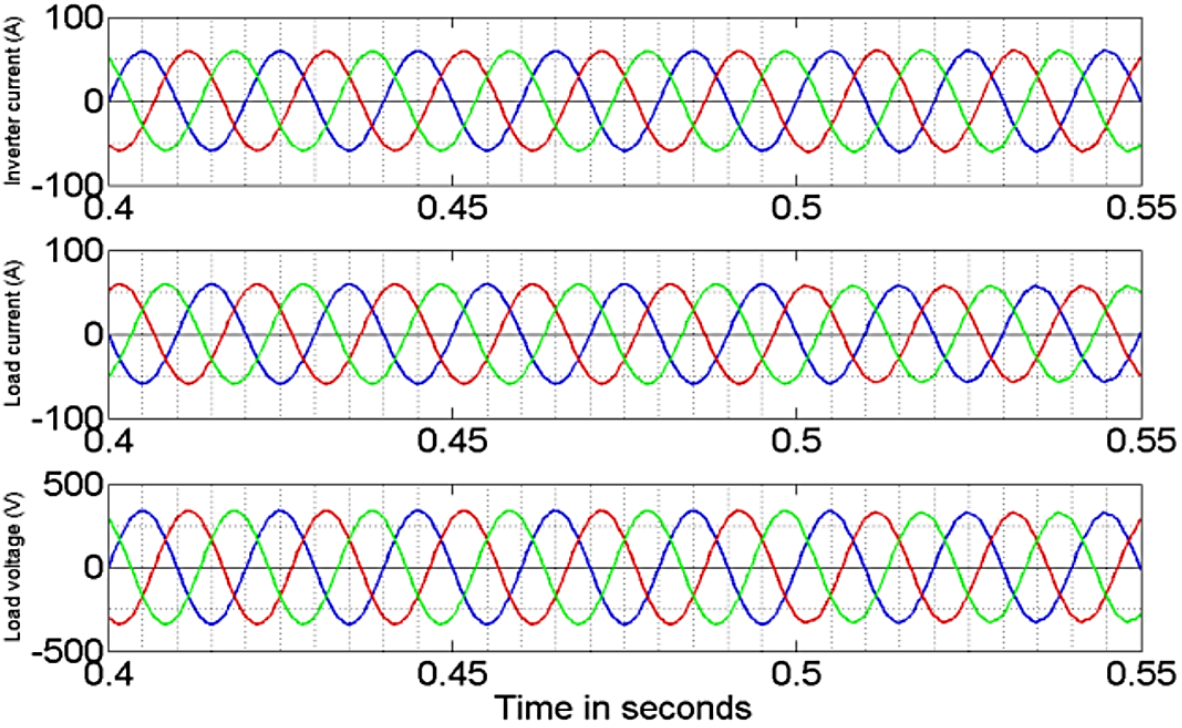

Figure 3.7: Inverter output current DG2

(Niu, et al., Oct 2014)

The simulation results in figure 3.8 shows that at the transition between grid connected and autonomous mode, DG1 shows more current fluctuations that DG2 (and DG3 not indicated in the figure). In figure 3.8 it is evident that the power distortion is more pronounced in DG 1 than DG 2 & DG 3 in the same graph.

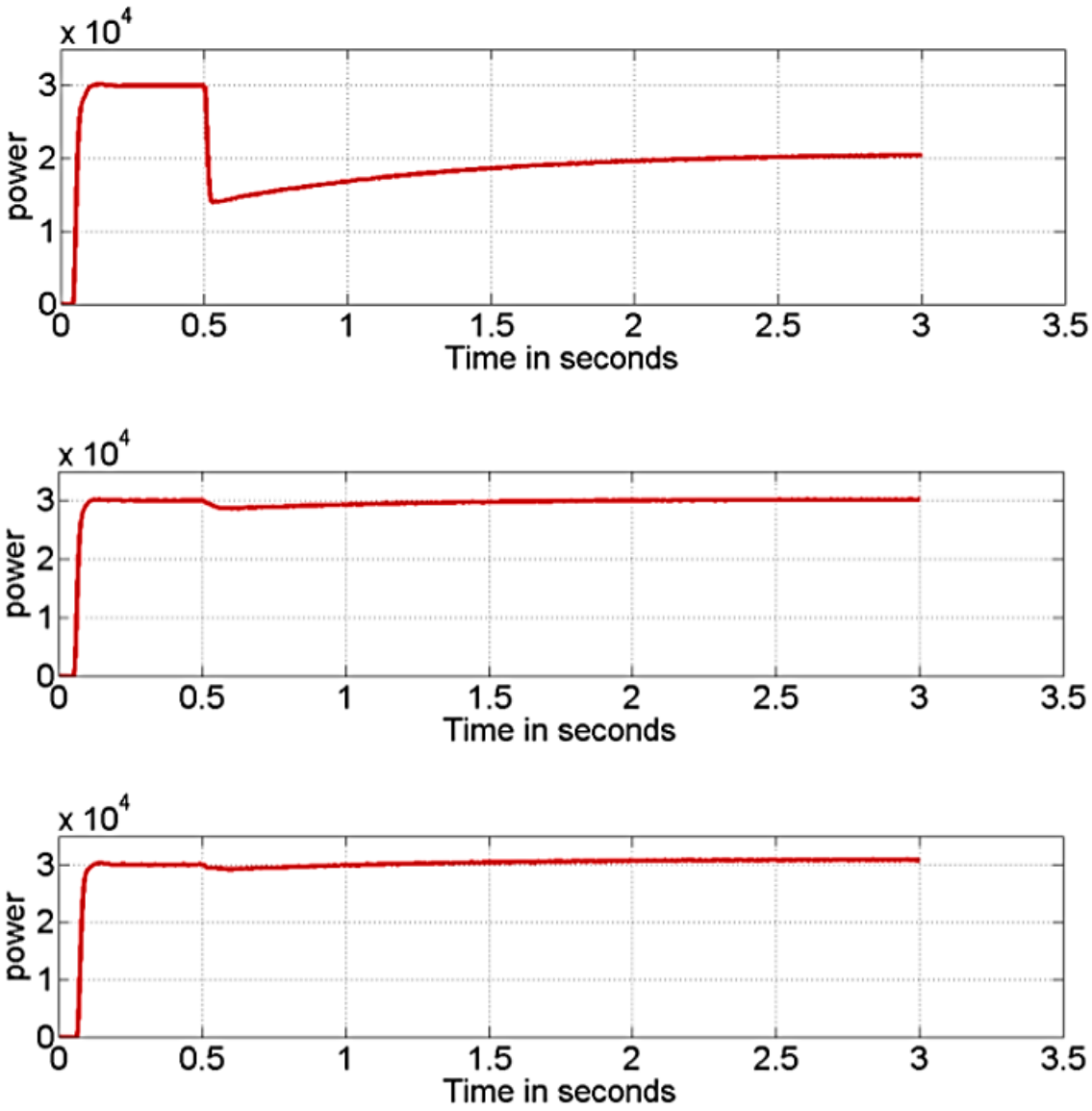

Figure 3.8: Power output of all three inverters

(Niu, et al., Oct 2014)

The aforementioned case study's simulation in Matlab/Simulink confirms that droop control combined with PQ control is more effective than conventional droop control unaided. DG1 implements only droop control after it switches to islanding mode (Niu, et al., Oct 2014). DG2 & DG2 employs the droop control as well as additional PQ control after islanding mode of operation.

3.4 Secondary Control

The secondary controls restore the deviations caused by the primary control (Guerrero , et al., Nov 2009). With islanded microgrids that consists of interfaced power electronics, the inertial component is missing. Secondary control sends reference signals to the primary local controllers to reduce voltage imbalances (Savaghebi, et al., Dec 2012) . The secondary control returns the frequency back to its nominal value and resets the primary control reserves in approximately 5-15 minutes (Vandoorn , et al., Dec 2013).

3.4.1 PID Control

For power converter applications, it is important that the output signal of a closed loop system closely tracks the desired trajectory with minimal control effort. Each aspect of a microgrid subsystem corresponds to an energy generation system, an energy consumption system and connection points to loads or a utility grid (Ornelas-Tellez, Nov 2014).

There are three aspects of the control namely proportional, derivative and integral control, also known as PID control. PID control systems are widely used in industrial control applications (Yukitomo, et al., 20-23 July 2004). Gain values can be tuned to manipulate the output response (Bisht , Oct 2014). See figure 3.9 for a basic control design and figure 3.10 for a corrected output signal.

The mathematical equivalent transfer function of PID control would be:

$$\mathrm{u(t)} = K_p e(t) + K_i \int e(t)\,dt + K_d \frac{de(t)}{dt} \qquad 3\text{-}3$$

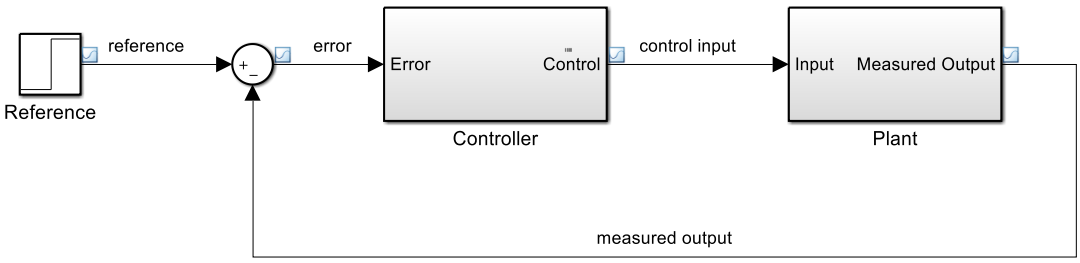

Figure 3.9: PID Control Diagram

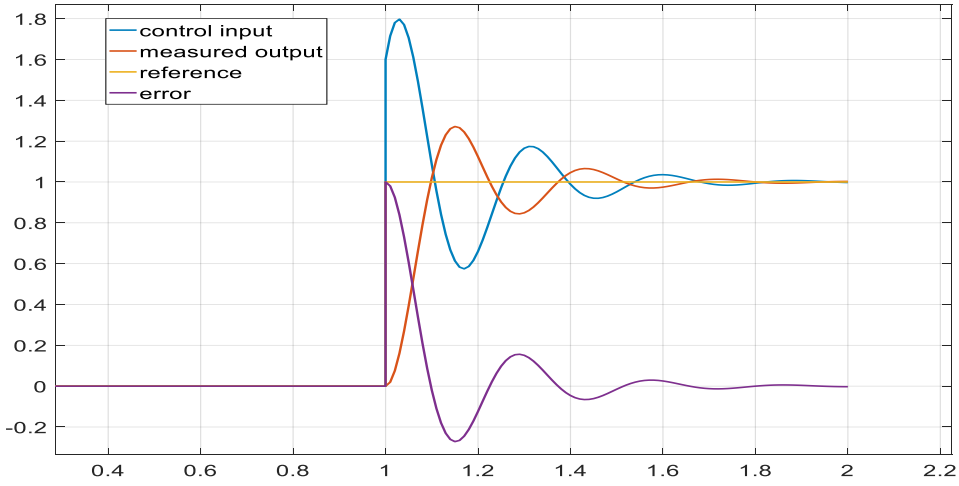

Figure 3.10: Signal corrected with PID Control

The second graph (brown) reflected the best output, in order to demonstrate a steady state response in Simulink as indicated in figure 3.11 and figure 3.12 Note that the gain was adapted and decreased to a value of 0.3 (proportional control) in order to prolong the steady state output as shown in the figures 3.13 to 3.14.

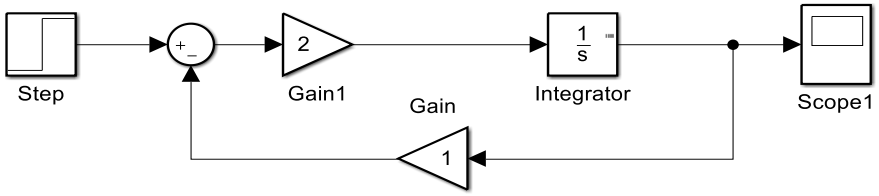

Figure 3.11: PI Control tuned with higher gain input

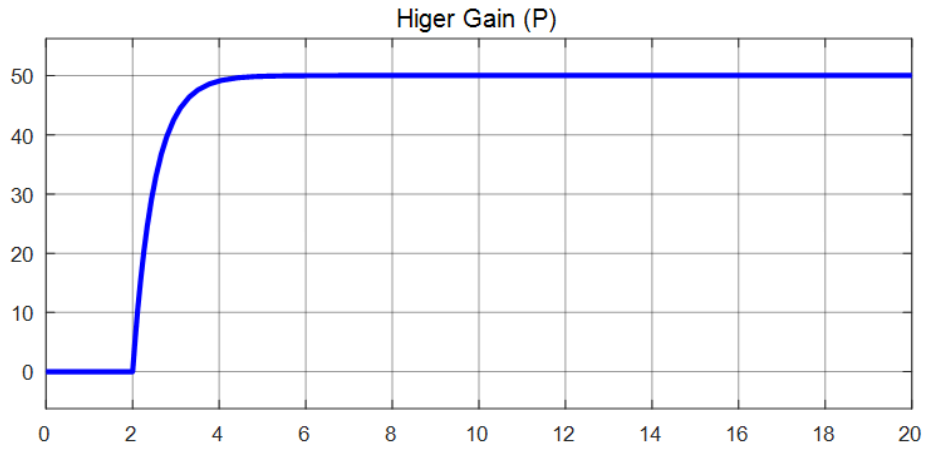

Figure 3.12: Steady state output responses of PI control

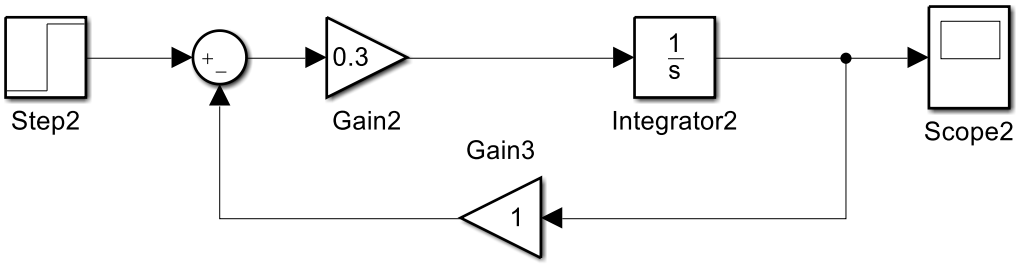

Figure 3.13: PI Control tuned with lower gain input

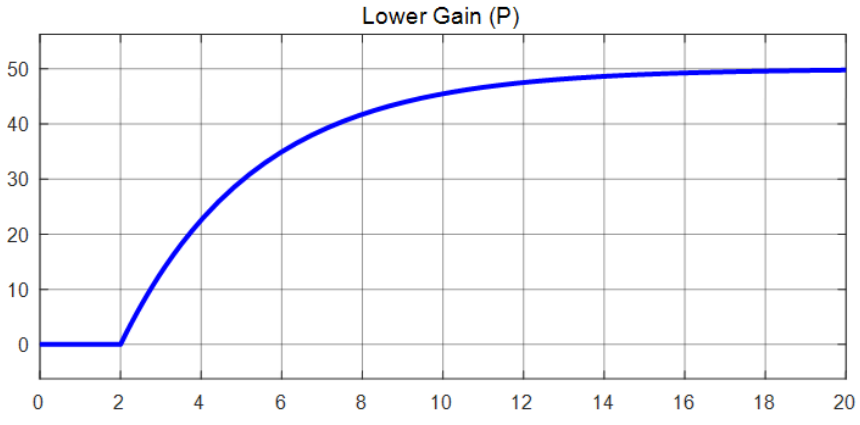

Figure 3.14: Steady state out responses of PI control

3.4.2 Switch mode inverters

A switch mode inverter is can also be configured as a transformer-less inverter with higher efficiency conversions, lower costs, smaller size and lightweight compared to a conventional transformer (Islam & Mekhilef, March 2016). Currently transformer-less inverters are the most efficient grid-connected converters on the market (Barater , et al., Feb 2016).

3.4.2.1 DC-AC Inverter

The input to the switch inverters will be assumed to be a dc voltage source, also referred to as voltage source inverters (VSI's). Inverters used for very high power AC drives is called the current source inverters (CSI's). The VSI's can be divided into three categories: Pulse width modulated inverters, square wave inverters and single phase inverters with voltage cancellation.

With Pulse width modulated inverters, the input dc voltage is constant, the inverter controls the magnitude and frequency of the ac voltage output and includes a sinusoidal PWM. With square wave inverters, the input dc voltage is controlled to control the magnitude of the output ac voltage, the inverter only controls the frequency of the output ac voltage and the output ac voltage similar to a square wave. Single phase inverters with voltage cancellation combines the characteristics of the aforementioned two inverters.

With the PWM, A sinusoidal control signal at the preferred frequency is compared with a triangular wave form. The triangular frequency inverter is kept constant along with its respective amplitude and its frequency establishes the inverter switching frequency.

Control can be exercised on inverters by manipulating the modulation index. With Non-Inertial sources**,** the modulation index can be described as the ratio between the modulated variable of the signal and the unmodulated signal. In this case, it would be the amplitude root mean square (RMS) magnitude of the AC sine wave versus the input of the DC carrier signal. It can also be called the modulation index factor and consists of a value between 0 and 1 in most cases.

The output frequency of the inverter is determined by the rate at which the IGBT device is switched on and off. The modulation index determines the amplitude. The figure 3.15 below shows the inverted AC output signal diagram when the improved PI controller is not implemented. The modulation Index (Ma) is almost the full value from the start. The value is 0.75 in order to control the inverted output voltage. The figure 3.16 below displays the inverted AC signal on the scope.

The next figure 3.17 shows the inverted AC signal diagram when the improved PI controller is implemented. The modulation Index (Ma) will increase gradually within 0.8 seconds to a value of 0.75 in order to control the inverted output voltage, thus it reaches steady state at a longer period as shown in figure 3.18.

The modulation index for both cases is calculated with the following formula. Note that a value of 827.38 V had to be used to get a peak to peak value of 537.4 V, thus 380 volts RMS.

$$\begin{aligned} \text{Ma} &= [\text{VDC} * 0.612] \,/\, \text{VLL (RMS)} \\ &= [827.38*0.612]/380 \\ &= 0.75 \end{aligned} \qquad 3\text{-}4$$

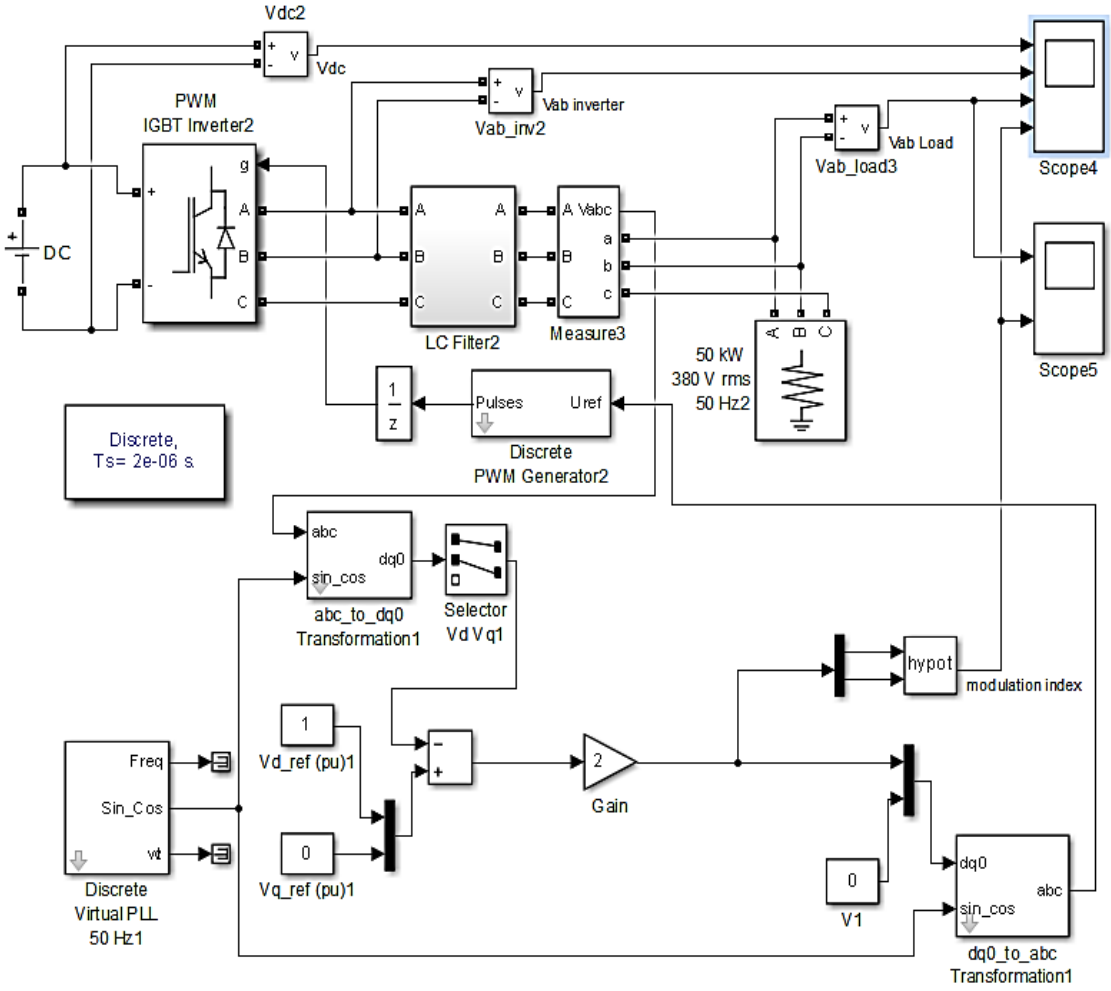

Figure 3.15: Inverter without PI control model

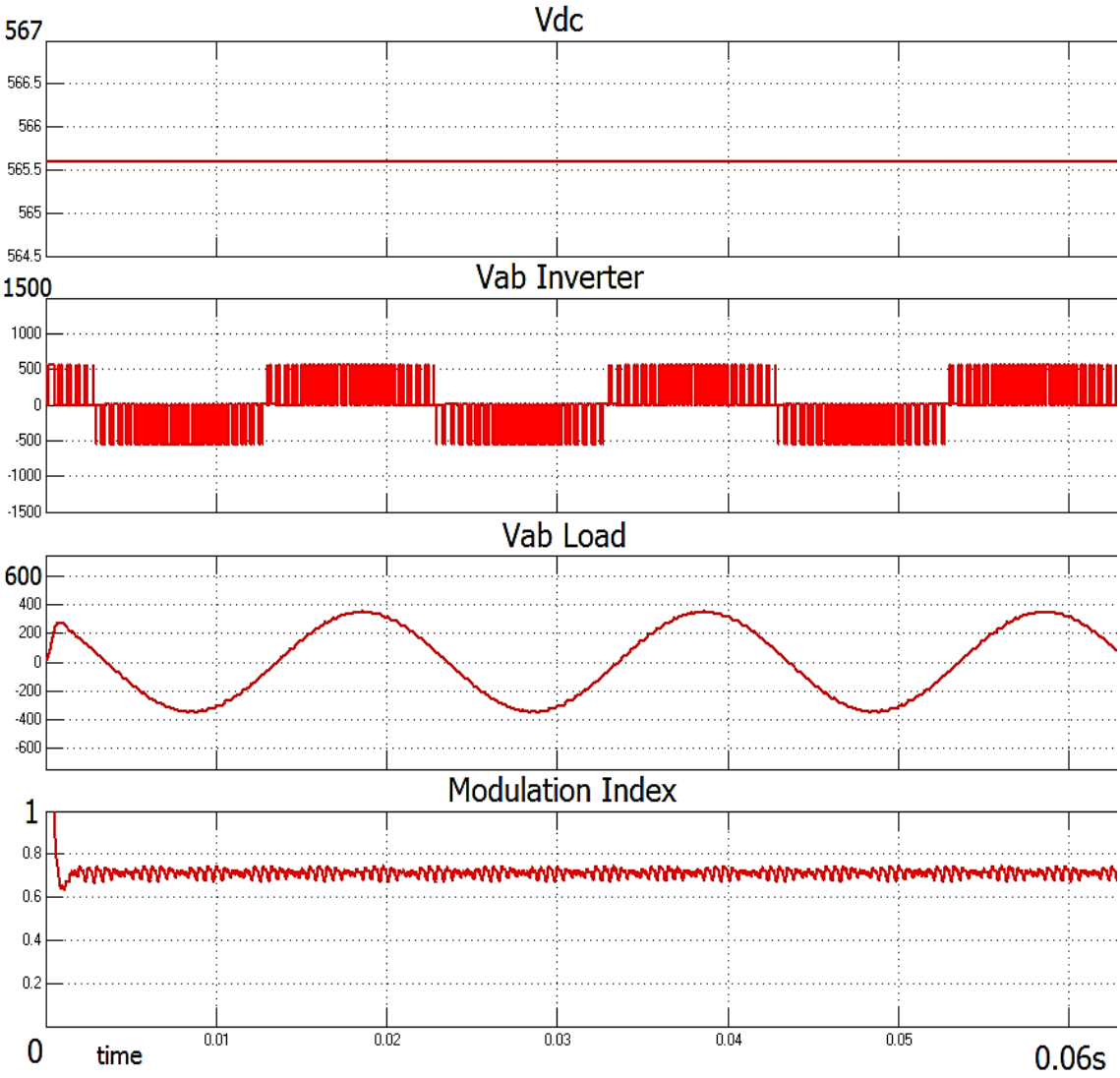

Figure 3.16: Inverter without PI control output response

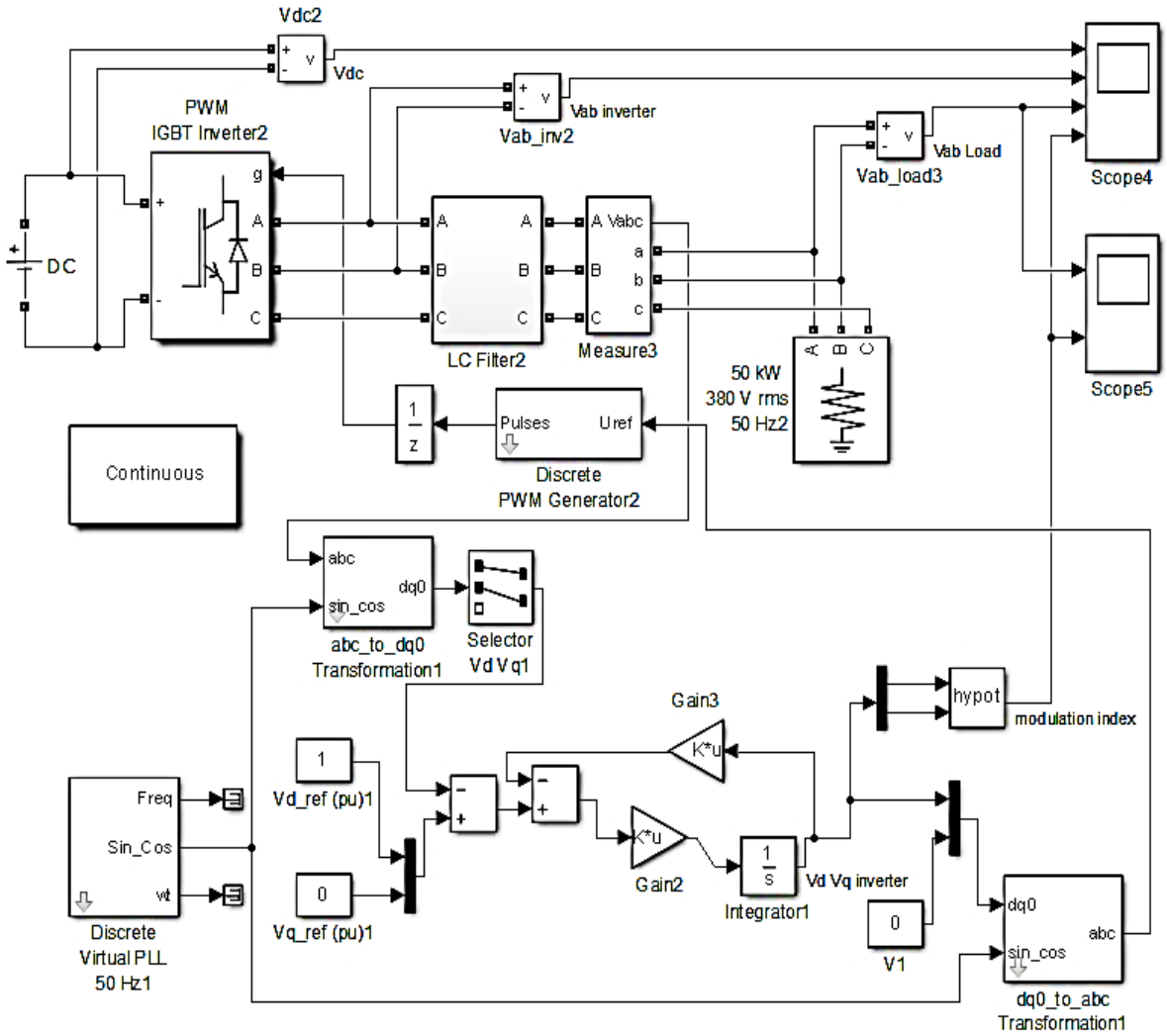

Figure 3.17: Inverter including PI control model

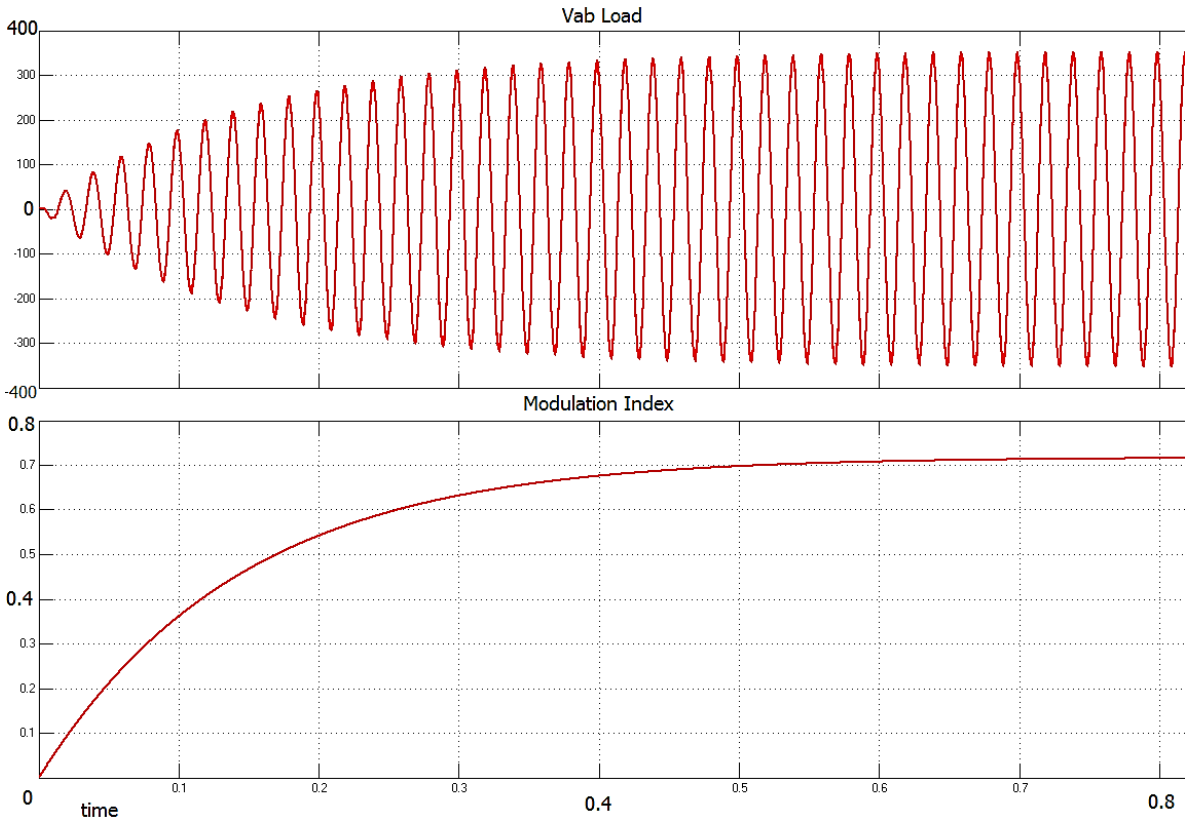

Figure 3.18: Inverter including PI control output response

In order to control the inverter, output the three-phase power represented by the ABC single line diagram, the ABC signal had to be converted to the DQ0 signal. The direct-quadrature-zero method simplifies the three AC components to two DC magnitudes for the use of less complicated calculation (Chen, et al., Sept 2015). See Appendix A for further derivation of the park transformation equations.

The DQ0 signal is then manipulated by the PI controller that causes the voltage and power output to reach the transient steady state at a slower rate. After the PI control the DQ signal gets converted back to an ABC signal which is fed into the PWM to convert it into a switching signal. See the figure 3.19 below regarding the signal conversion.

The smooth critically damped response of the output will cause less power and frequency oscillations when the inverter is connected to the diesel generator in the microgrid. The PI control action is clearly seen by looking at the scope output of the modulation index shown in figure 3.18 above.

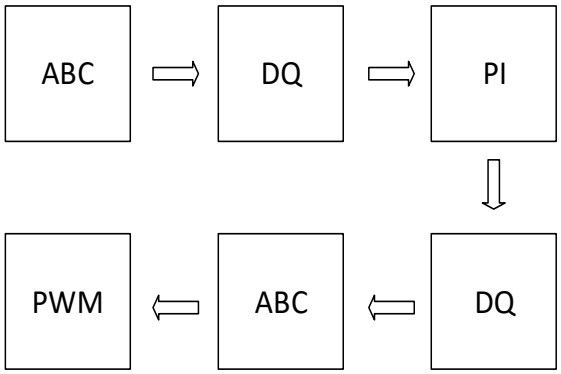

Figure 3.19: Signal conversion flow diagram

3.4.2.2 DC-DC Converter

Switch mode dc-dc converters converts unregulated DC input to a controlled DC output at an anticipated voltage level. This output voltage level is controlled via constant switching technology, by adjusting the switching frequency and duration of the switch to control the average output voltage.

In PWM switching, the switch control (on/off) is generated by comparing the control voltage with a repetitive saw tooth wave from, see figure 3.20. This saw tooth wave forms the switching frequency depicted in figure 3.21.

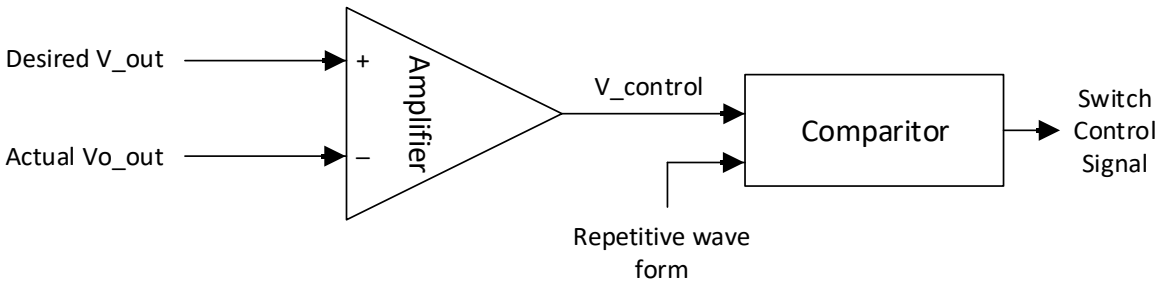

Figure 3.20: On/Off control

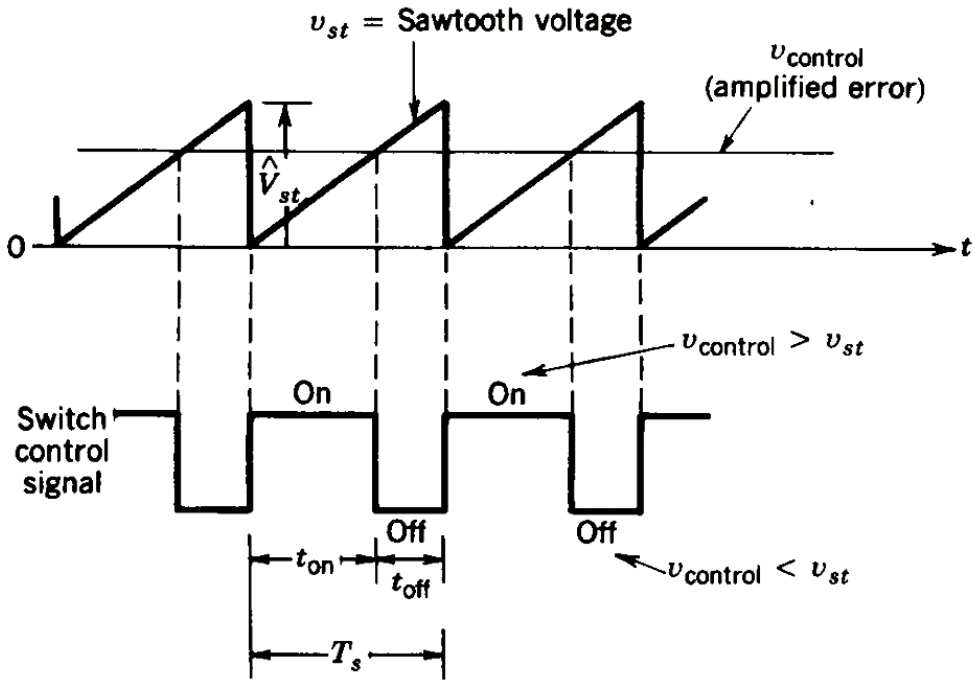

Figure 3:21 Saw-tooth voltage compared to Switch Control Signal

(Mohan, et al., 2003)

Note: Switching frequency above mentioned $f_s = \frac{1}{T_s}$ 3-5

$$D = \frac{t_{on}}{Ts} = \frac{V_{control}}{V_{st}} \quad (3\text{-}6)$$

$$V_0 = \frac{1}{T_s}\int_0^{T_s} V_0(t) \quad (3\text{-}7)$$

$$= \frac{1}{T_s}\left(\int_0^{Ton} V_d dt + \int_{t_{on}}^{T_s} 0 dt\right)$$

$$= \frac{t_{on}}{T_s} V_d$$

$$= DV_d$$

Substituting for D in Equation 3-7 from Equation 3-6;

$$V_o = \frac{V_d}{V_{st}} v_{control} = k v_{control} \quad 3\text{-}8$$

Where:

$$k = \frac{V_d}{V_{st}} = \text{constant} \quad 3\text{-}9$$

The following buck converter was built and modelled in a software called Power-sim. The Voltage settles at 50V after 10ms, see figures 3.22 and 3.23.

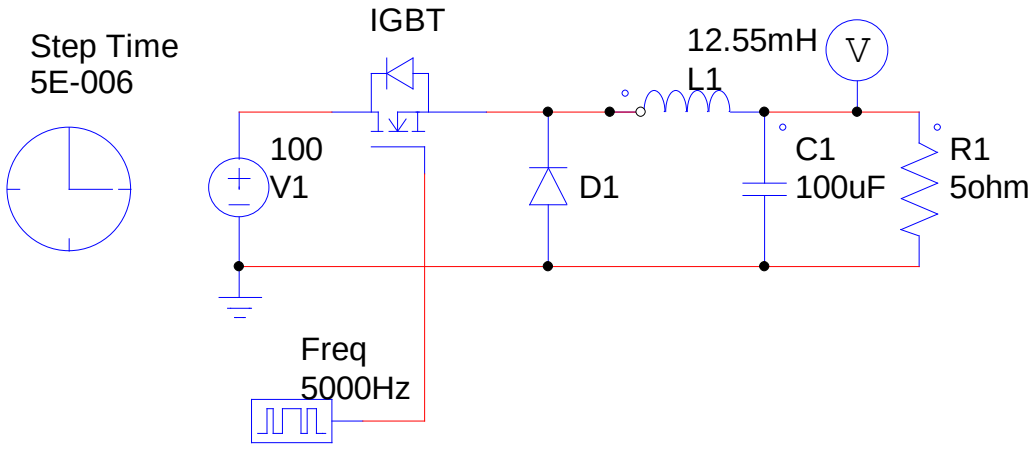

Figure 3.22 PI LC Circuit diagram

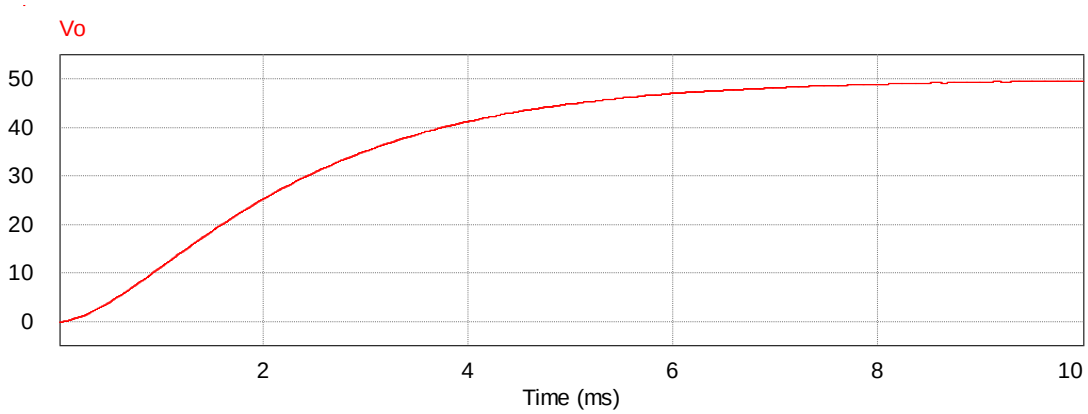

Figure 3.23 PI LC Circuit voltage output

The previous LC circuit was modified; the L1 inductor value was decreased, the step time was changed and the switching frequency was increased. Noted that the decreased inductor value causes the system voltage to settle before 5ms, thus the settling time is shorter than the previous model. See figures 3.24 and 3.25.

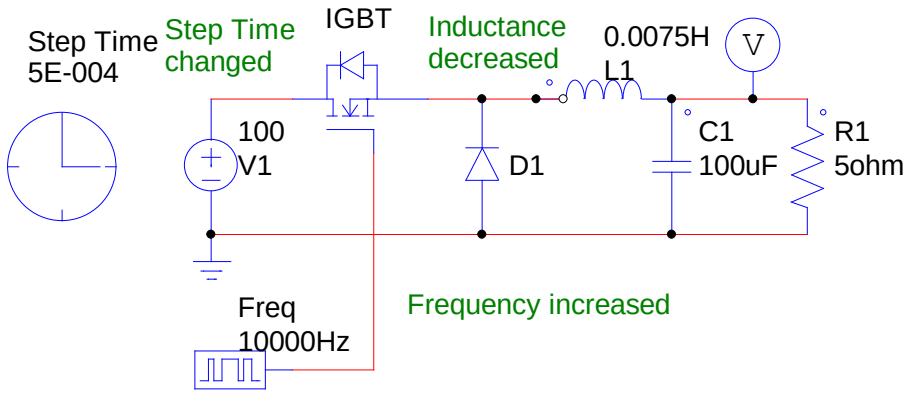

Figure 3.24 PI LC Circuit diagram with decreased inductance

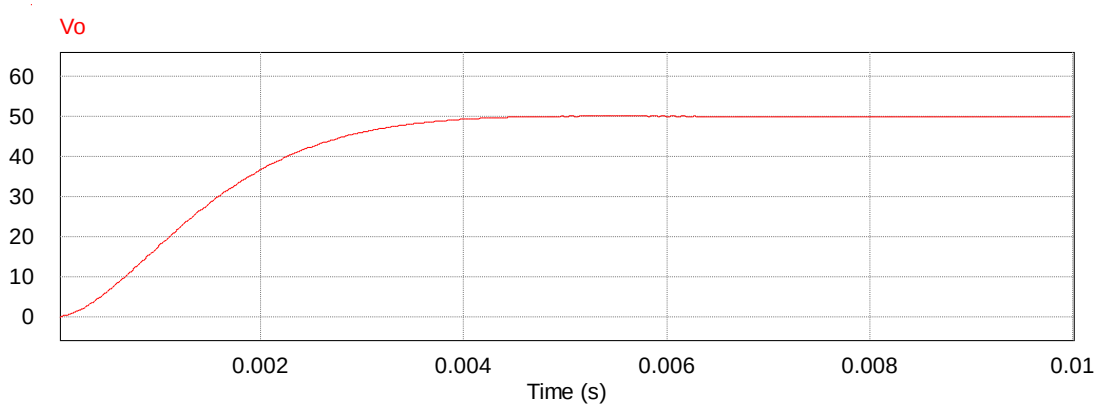

Figure 3.25 PI LC Circuit voltage output due to decreased inductance

3.5 Tertiary control

The tertiary control is a centralized control strategy including communication aspects usually an integrator on a software level to provide subsidiary services. The tertiary (and secondary) controllers manipulates the primary control set points.

The electricity usage has to be monitored in order to understand the generation and consumption of the electricity in a microgrid. The user also needs to act upon such

information in order to control the grid and to maximise the efficiency. Software platforms can automate these systems.

3.5.1 Carbon track software

For small home grids, ‘Carbon-Track’ is a technology that monitors the system energy consumption in real time. The information also gets displayed on HMI’s for the user to view the events thus providing a better understanding of own system (carbonTRACK, n.d.). Carbon track allows user to implement changes on their systems to utilise their power devices better and more efficiently.

3.5.2 Wonderware software solution

The ‘Wonderware’ corporate energy management system also includes the SCADA HMI software enables real time management (Schneider Electric Software, LLC, n.d.) Data is not only acquired and displayed but also processed to inform the various levels of work force involved in the energy management and production. This software also monitors deviations and provide the context needed for precise root-cause analysis.

3.5.3 Victron Control Solution

Vicrtron Energy Group offers a complete microgrid solution which includes the hardware and software. With various hub configurations, one can implement a custom-made system including monitoring and managing the system with their colour control (CCGX) latest firmware available (Victron Eneregy, n.d.).

Appendix C consists of a diagram representing a 5 kW microgrid for residential usage. PV panels provides power during the day and gets regulated/maximized by the MPPT which charges the battery bank. The Inverter provides AC power to the varying load. When the batteries SOC reaches below a set value the AC load gets connected to a generator or the utility grid.

The communication protocol, VE.Can connects the components to each other over unshielded twisted pair (UTP) cabling. The voltage and temperature sensing mainly consists for battery monitoring. Note that the anti-islanding device (when connected to the grid as well) is imperative to prevent excess power generated by the PV panels to export electricity to the main grid, especially in South Africa. The generator should have its own non-return connection or diodes.

Victron also released its own software package called VEConfig. Victron inverters needs to be programmed in order to maximise its full abilities. The Victron Quattro Inverter is globally used thus the system frequency has to be set to 50 Hz in South Africa.

The Victron Quattro range consists of 2 AC inputs; the first input would be connected the utility and the second one to a back-up generator. The battery capacity must be set to the value of the actual battery bank capacity. The bulk charge mode value should be set to the recommended value of its applicable battery bank capacity.

3.6 Energy storage microgrid control

3.6.1 Battery Storage in microgrid control

Energy storage systems increases the consistency and viability of renewable DG's like wind and PV generation. These aforementioned DG's produces irregular power due to its strong weather dependence and uncontrollable peak production that does not necessarily match the instant demand of the consumers (Hussein, et al., June 2012).

An autonomous microgrid requires a more complex control due to the lack of the main grid as a base support. Reliable main power sources are required to support stable frequency and voltage conditions. Energy storage systems (ESS) can facilitate steadiness in terms of voltage and frequency instabilities and act as a base support (Tang , et al., December 2015).

Uninterruptable power supplies (UPS') plays a key role in stabilizing the power output in microgrids when the main supply is off. An UPS is able to supply regulated and conditioned power to critical loads as well as assisting in a seamless transition from main power to back-up power and vice versa (Zhao , et al., May 2013).

Research also have shown that 20-30% of energy consumed in buildings can be recovered by implementing optimized energy management without significant structural, hardware configuration and energy supply changes (Guan, et al., July 2010).

The following energy systems are commonly used in in a typical commercial build microgrid; solar power, wind power, combined cooling, heating, and power generation, the high temperature chiller, the liquid desiccant fresh air unit, the battery, and the

power grid . Three types of loads are illustrated as electricity, sensible heat, and latent heat load (Jia, et al., 15-18 May 2011) (Jia, et al., Dec 2012).

Distributed energy storage systems (DESS) benefits the consumer in power quality and reliable improvement as well as reducing the time related to the use demand charges. The smart grid operator can save in electricity prices by storing energy for the duration of off peak times and supply energy during peak load stages. DESS reduces the need for of VAR generation from renewable energy systems (Carpinelli, et al., May 2013).

Battery- or super-capacitor based ESSs produces a faster response to power fluctuations with limited energy capacity power support. The battery based ESS disintegrates faster the more frequently it is used. Mechanical ESSs such as pumped hydro and compressed air possesses a larger energy storage capacity with a slower response time (Niu & Santoso, June 2016). Optimal battery sizing can increase efficient operation of the grid while reducing related costs (Bayram, et al., August 2015).

In PV applications, a battery back-up is connected in parallel to inject or absorb active power through a bi-directional converter interface. When the battery is absorbing power, the converter operates in buck mode. When the battery injects power to the grid, the converter operates in boost mode (Adhikari & Li, April 2014).

Energy conversions that generates heat should be avoided because it diminishes the conversion efficiency. Pumped hydro generates minimal heat and the concept of a heavily load car on a railway can use the over supply of electricity to thrusts itself uphill and return energy by coasting downhill. (Pickard, August 2015) .

To evaluate the performance of ESS's in terms of energy, and energy performance index calculation is used. E_{fail} refers to energy that an ESS fails to supply. E_{demand} refers to the total energy for the ESS from other components in the microgrid (Tran & Khambadkone, August 2013).

$$\text{EPI}\ (\%) = (1 - \frac{E_{fail}}{E_{demand}}) * 100\% \qquad 3\text{-}10$$

3.6.2 Ultra-Capacitor Hybrid Arrangement

Ultra-capacitors are advantages to microgrid control and is ideal for short-term energy storage or burst-mode power delivery. There are mainly three types: electrostatic double-layer capacitors, electrochemical pseudo capacitors and Hybrid capacitors.

Ultra-capacitors have low specific energy, high specific power, short charge times, high cycle life as well as a low self-discharge and high cost per watt attributes.

Ultra-capacitors can storage large amounts of energy and release it rapidly when required (Bakhoum , Feb 2009). Ultra-capacitors can be combined with batteries responding to short and large current demands in order the preserve the lifetime of the battery (Hredzak, et al., Sept 2013).

Below is a basic example of a 500 micro farad capacitor that discharges with the resistor once the source is disconnected from the rest of the circuit at a 2 second time stamp as shown in figures 3.26 and 3.27 below. The switch is assumed to be ideal.

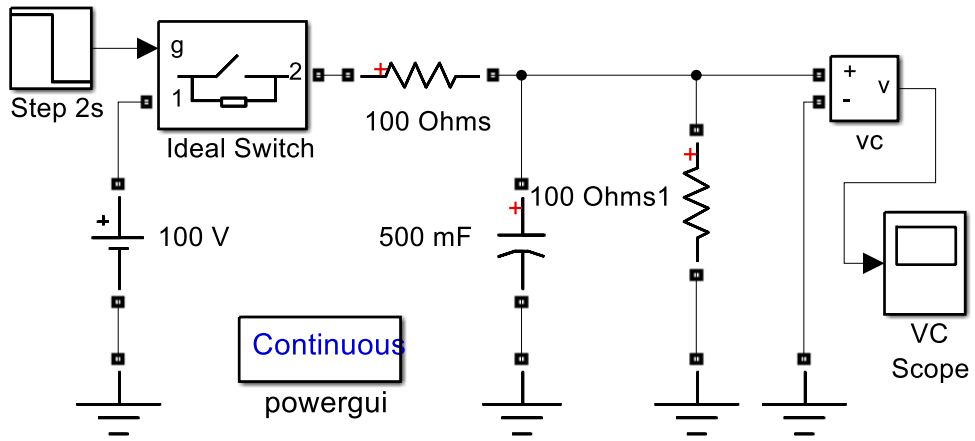

Figure 3.26: Ultra capacitor in a circuit diagram

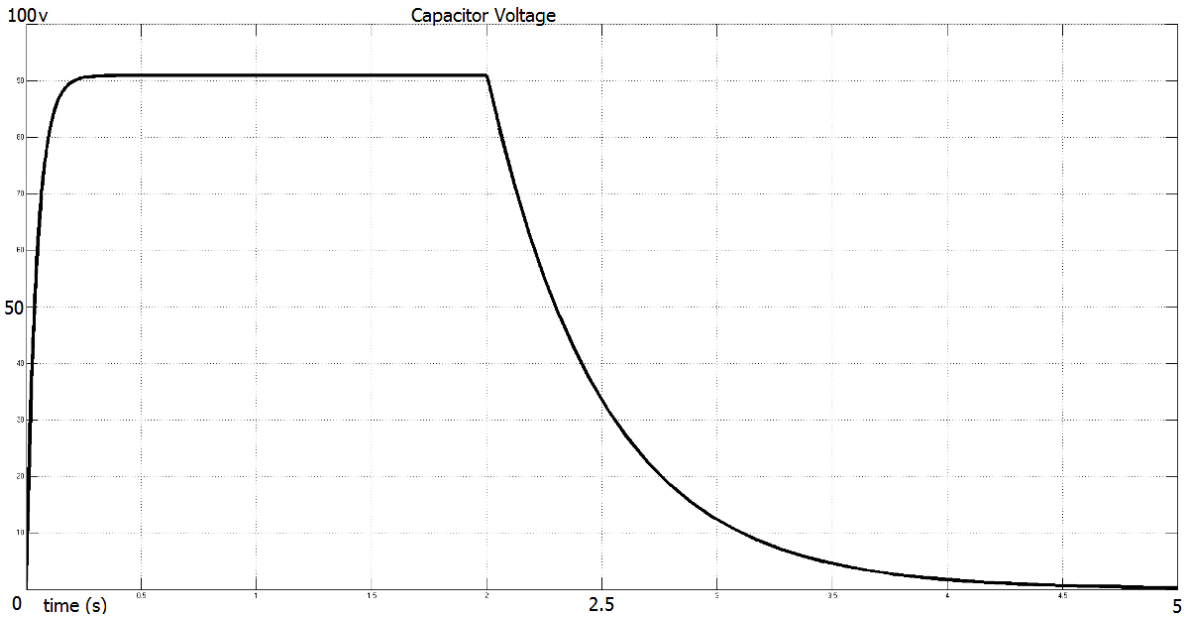

Figure 3.27: Output Voltage of Ultra capacitor

When the capacitor size decreases from 500mF to 10 mF, the discharge rate also lengthens. Note in the graph that the larger capacitor maintains 90% of its initial value for 18s, where the smaller capacitors maintains 90% of its initial value for only milliseconds. See figures 3.28 and 3.29 below.

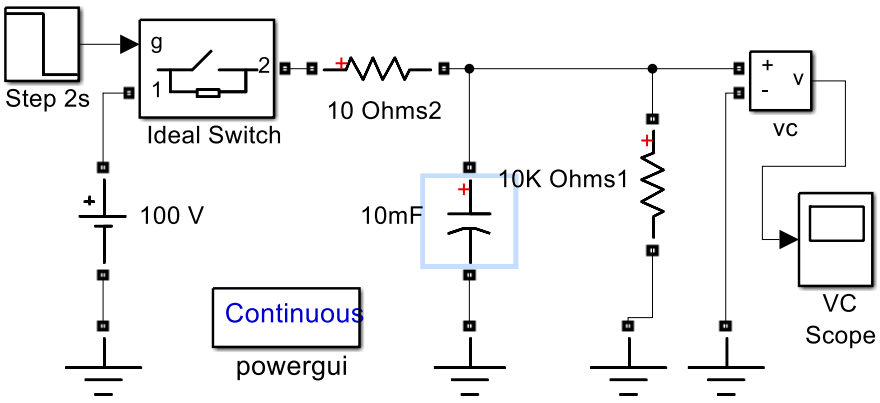

Figure 3.28: Modified Ultra Capacitor Circuit Diagram

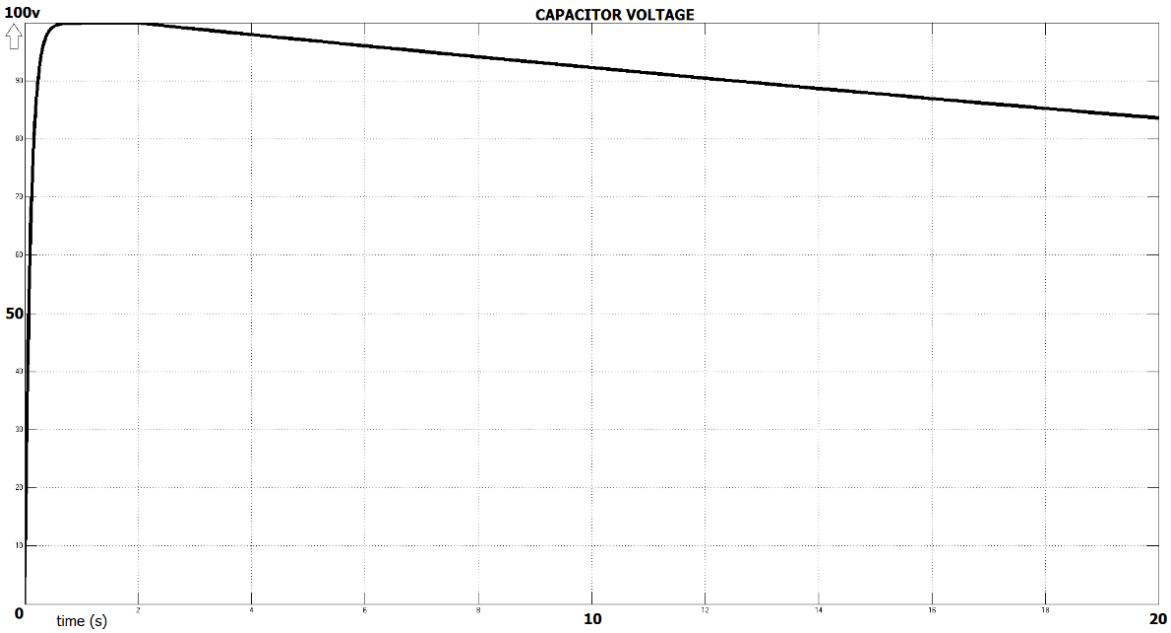

Figure 3.29: Slower discharge rate of capacitor voltage

3.6.3 Superconductor

Superconducting magnetic energy storage (SMES) improves the operation of power systems due to its quick response and high power density (Gong, et al., April 2016). This energy storage process loses the least amount of energy in a system than most other storage methods because the electric current encounters almost zero resistance. The small energy loss is only due to the inverter/rectifier stages.

SMES systems is a technology where energy in the magnetic field created by the flow of DC current in a super conducting coil is stored (Ali, et al., April 2010). The coil has to be cooled down cryogenically below its superconducting critical temperature. The coil can then be discharged to release the energy back to the power network.

SMES is also advantageous due to its very short time delay compared to pumped storage and compressed air that involves mechanical inertia. A very high power output can be achieved in an instant which provides grid stability due to large sudden disturbances like load changes and uncontrolled voltage fluctuations.

Superconducting fault current limiters (SFCL's) are current limiting devices with a higher fault-current level success rate. When a short circuit appears in the main network the superconductor sends a trip signal to disconnect the DG's from the grid to an islanded mode (Zheng, et al., Feb 2015).

The figure below shows a schematic of a basic microgrid. The SFCL will detect the fault current and disconnects the DG'S at the point of common coupling from the main grid to operate in an islanded mode as shown in figure 3.30. The SFCL will also activate the energy storage as a master DG to stabilize the power fluctuations in the new autonomous grid mode.

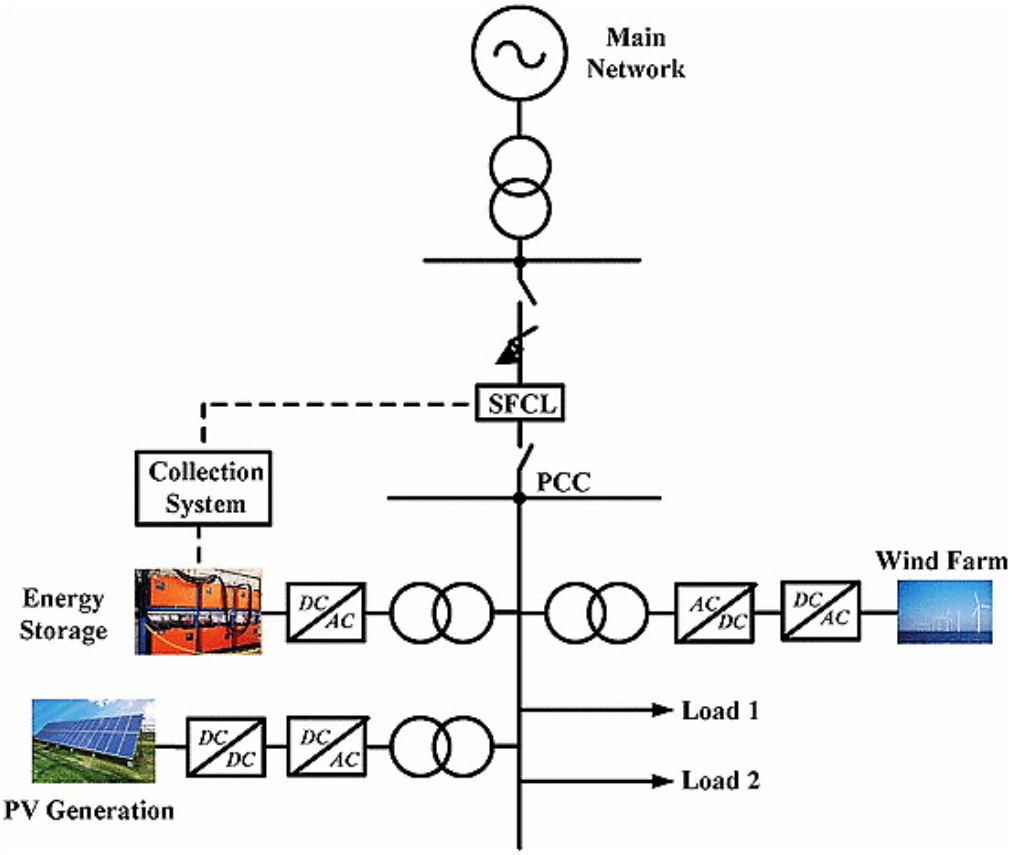

Figure 3.30: Microgrid integrated with a SFCL

(Zheng, et al., Feb 2015)

3.6.4 Superconducting Magnetic Energy Storage Control

The output power of a solar cell and a wind turbine will vary due to irregular sunlight irradiation and fluctuating of wind flow. The superconducting magnetic energy storage system can balance those varying power fluctuations and is linked to the PV system with the DC bus between diode 8 (D8) and diode 9 (D9) as indicated in the figure 3.31 below.

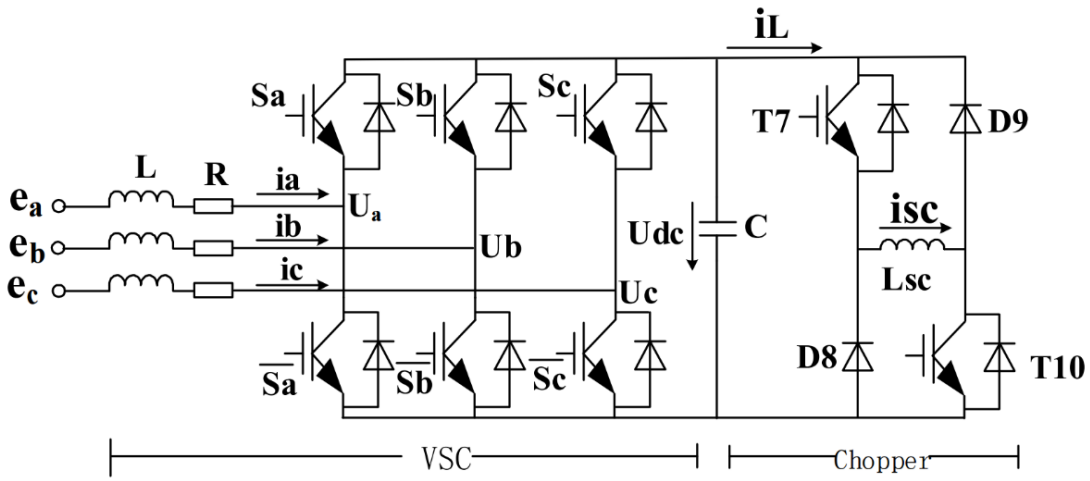

Figure 3.31: Circuit diagram of SMES

(Xie, et al., Nov 2014)

The following microgrid comprises of a PV cell array, PV side DC/DC converter, DC chopper, superconducting magnet, wind turbine, wind converter and the grid side converter. The SMES is structured and simulated as an inductor, pulsed DC chopper, capacitor, pulsed voltage source converter, grid inductor and an enabling soft starter that is connected to bus 4 (B4).

The DC chopper manages the energy passing through the superconducting magnet by the charging and discharging of the current of the superconducting magnet. The voltage source converter (VSC) controls the active and reactive power (Xie, et al., Nov 2014). See the figure 3.32 where the SMES is connected in parallel to the PV system, wind turbine and utility grid.

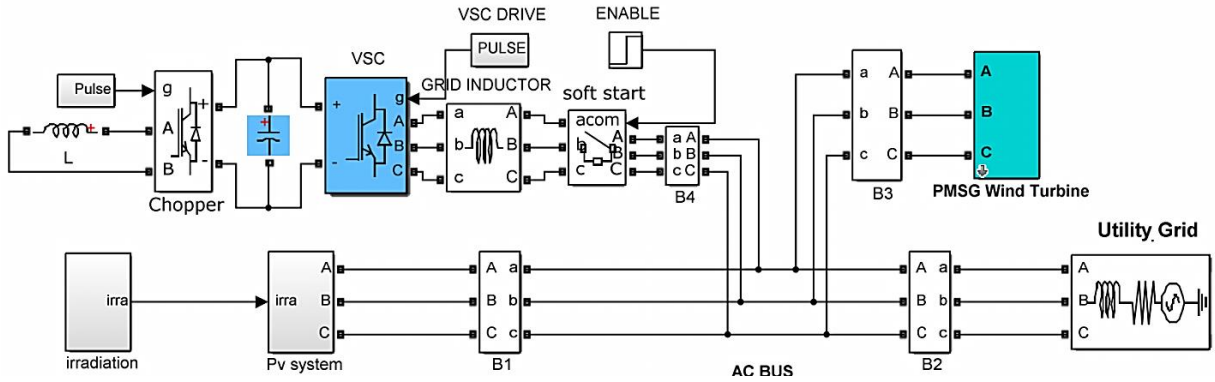

Figure 3.32: Simulink model with SMES

(Xie, et al., Nov 2014)

This first simulation shows that the grid side current cannot meet the demand as the grid absorbs power from the PV instead as indicated in figure 3.33 below.

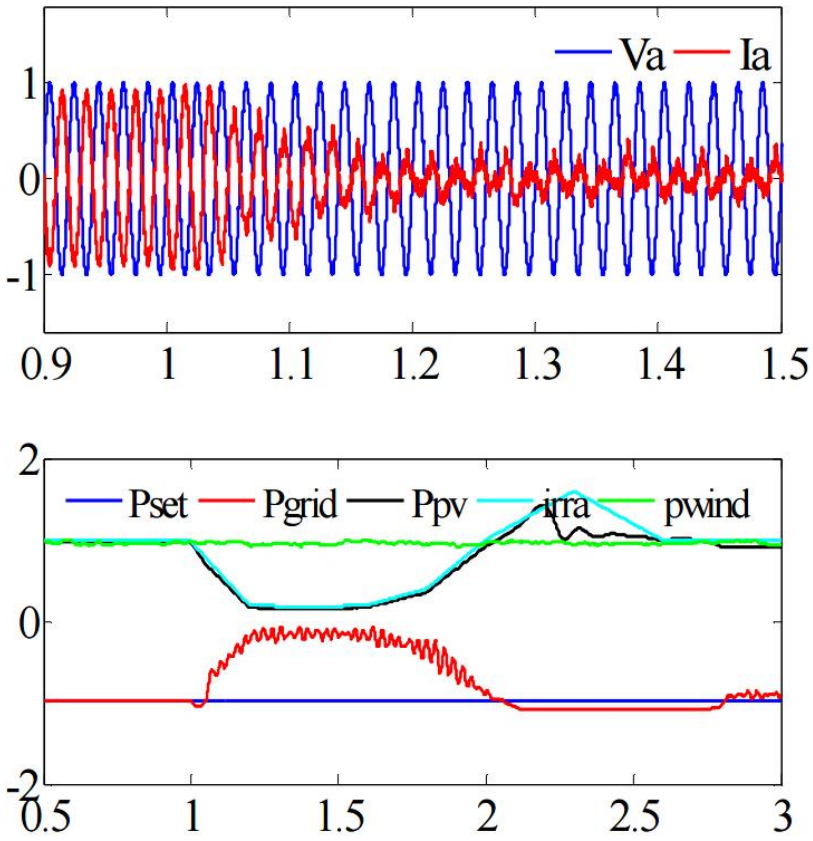

Figure 3.33: PV output result without the SMES

(Xie, et al., Nov 2014)

The second simulation includes the SMES, the grid side voltage and the current is in high power factor. The grid absorbs the matched power demand. The SMES straighten out the power fluctuations as indicated in figure 3.34 below.

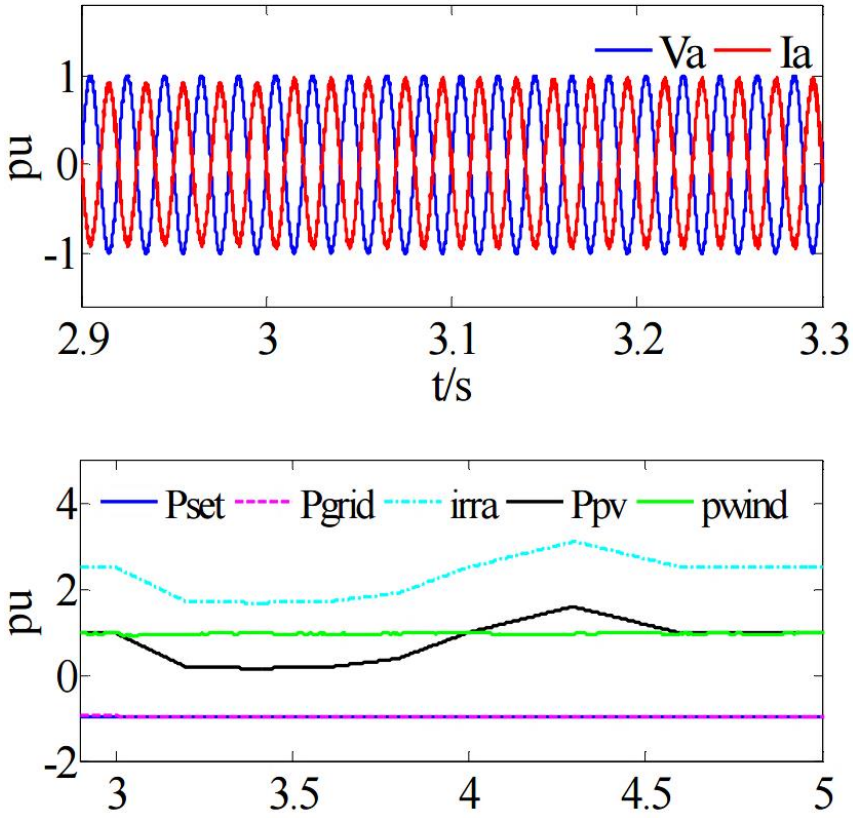

Figure 3.34: PV Output result including the SMES

(Xie, et al., Nov 2014)

CHAPTER 4: MICROGRID COMPONENTS CONTROL SYSTEMS

4.1 Overview

This chapter defines parameters for fuel cells, solar panels, wind turbines as well as batteries and capacitors including simulations. Some parameters are developed and aided with explanatory software simulations. The Matlab/Simulink software program (Created by Mathworks) was used to do the modelling in Simulink with its applicable toolboxes. Matlab/Simulink is a language for technical computing whereas Simulink is a graphical model based simulator designed for physical systems modelling.

4.2 Control Parameters for Distributed Generators

4.2.1 Fuel Cell Stack Detailed Parameters

A 24 V PEM Fuel cell stack comprising of a 100 fuel cells was simulated in Simulink. The flow rate regulator gets its reference signal from the output current in order to adjust the fuel input accordingly in order to maintain a constant voltage output. Figure 4.1 displays the circuit diagram and figure 4.2 shows the voltage output.

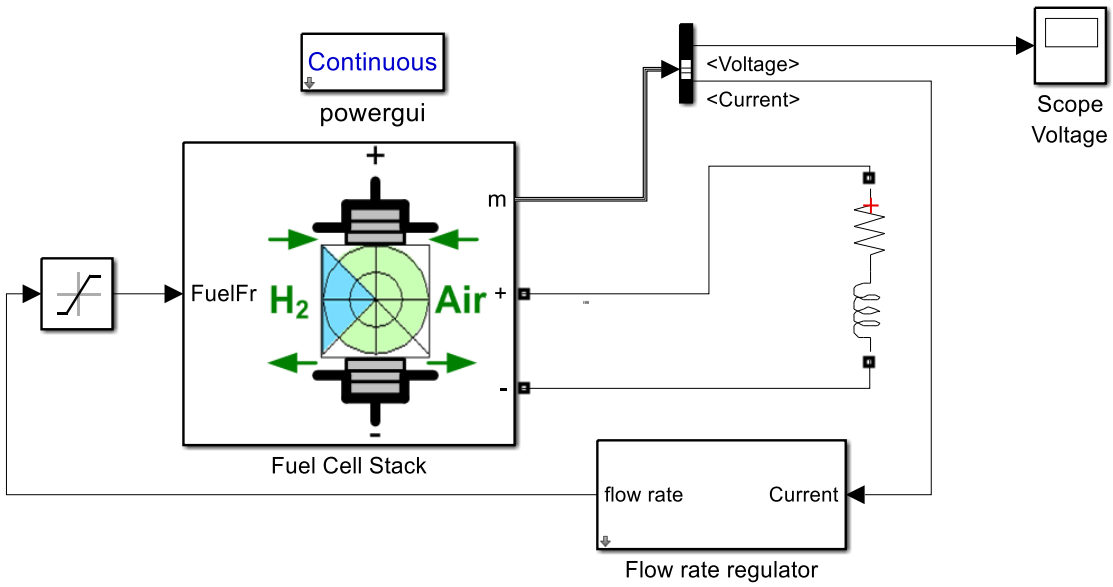

Figure 4.1: Fuel cell diagram

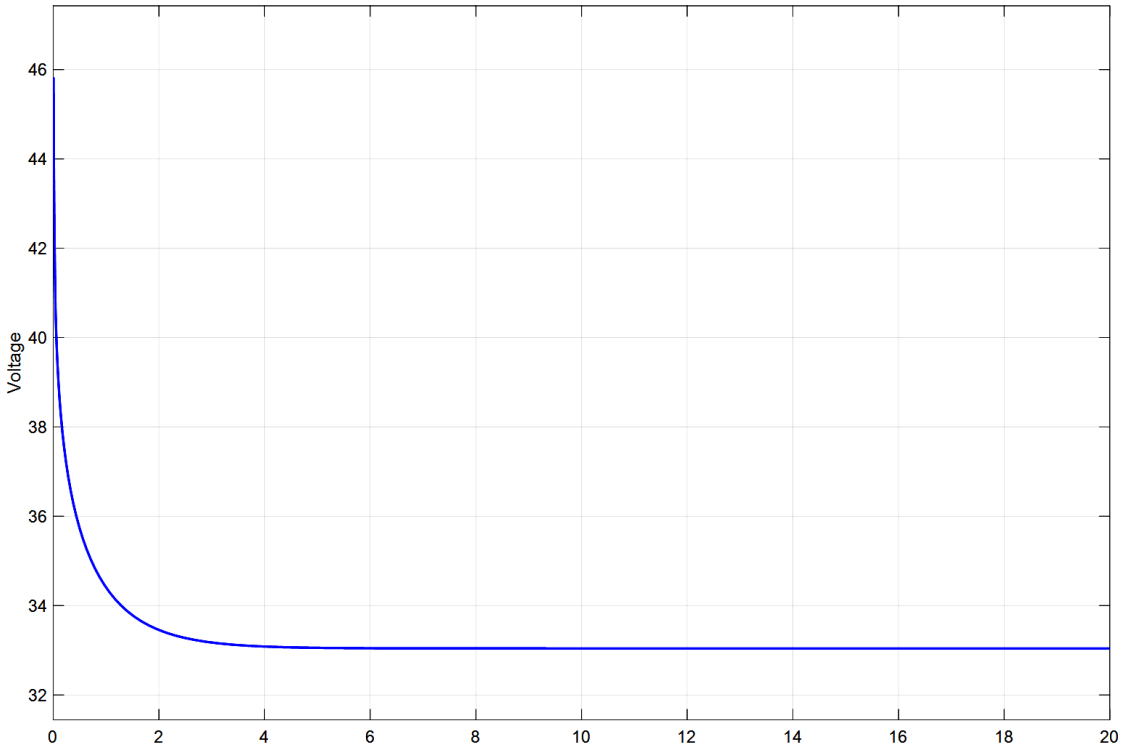

Figure 4.2: Fuel Cell Output control

The input parameters for fuel cells includes: pressure, temperature, and composition, flow rate of fuel and air variants. The above-mentioned variations affect the open circuit voltage (E_{oc}), the exchange current (i_o), and the slope (A).

$$E_{oc} = K_c E_n \tag{4-1}$$

$$i_o = \frac{zFk\,(P_{H_2} + P_{O_2})}{R_h} e^{\frac{-\Delta G}{RT}} \tag{4-2}$$

$$A = \frac{RT}{z\alpha F} \tag{4-3}$$

R = 8.3145 J/(mol K)

F = 96485 A s/mol

z = Number of moving electrons

E_n = Nernst voltage, which is the thermodynamics voltage of the cells and depends on the temperatures and partial pressures of reactants and products inside the stack (V)

α = Charge transfer coefficient, which depends on the type of electrodes and catalysts used

P_{H_2} = Partial pressure of hydrogen inside the stack (atm)

P_{O_2} = Partial pressure of oxygen inside the stack (atm)

k = Boltzmann's constant = 1.38 × 10−23 J/K

h = Planck's constant = 6.626 × 10−34 J s

ΔG = Size of the activation barrier which depends on the type of electrode and catalyst used

T = Temperature of operation (K)

K_c = Voltage constant at nominal condition of operation

4.2.2 Photovoltaic Inverter Parameters

PV solar cell modelling with a basic DC voltage source is represented. The figure 4.3 below illustrates a basic circuit that represents a DC source, such as provided by a solar cell. The voltage and current scope respectively indicates a voltage of 0.6V and a current of 7.3V, as shown in figures 4.4 and 4.5 respectively. The value of the resistor is less than one Ohms.

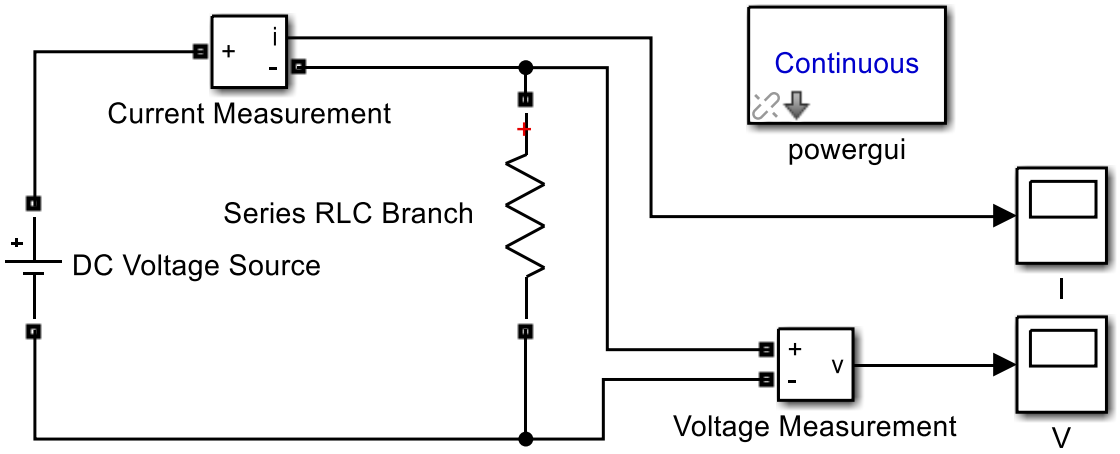

Figure 4.3: DC Voltage Source Model

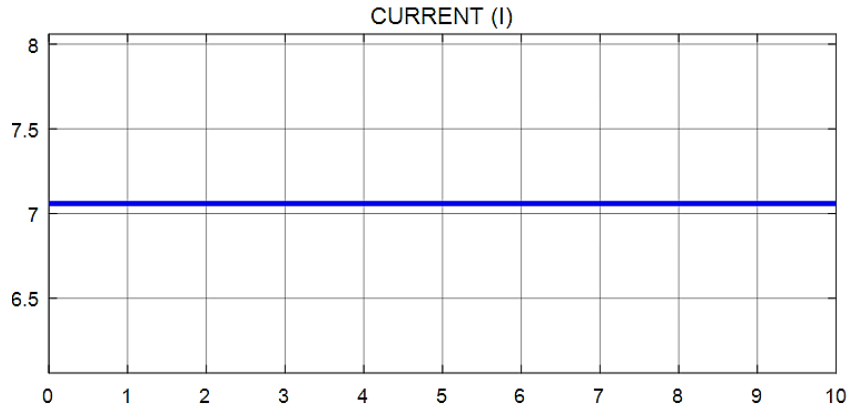

Figure 4.4: DC Current Output

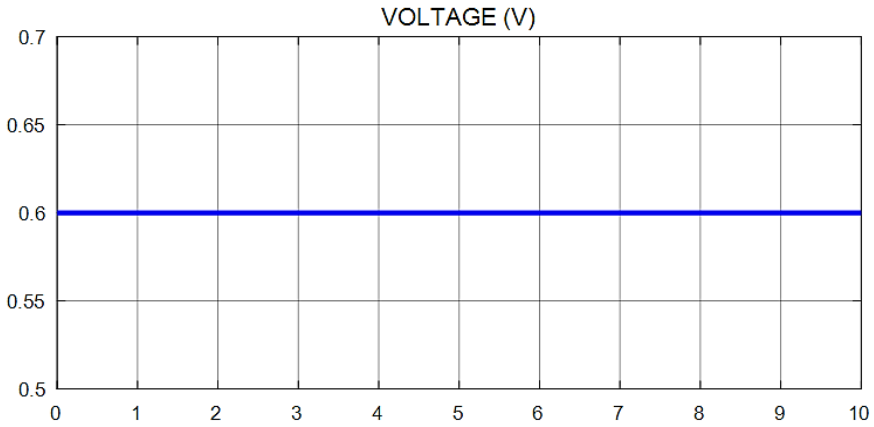

Figure 4.5: DC Voltage Output

The next circuit replaces the conventional DC source with a single solar cell. This solar cell below is found in the Sim-Electronics domain of Simulink; thus it can't interface with the higher powered circuit components found in Sim-Power-Systems toolbox. Matlab/Simulink 2013 doesn't allow for such a connection to be made.

The solution is to add a current source that is controlled by the signal output of the solar cell. A current sensor is added to sense the solar cell signal; this signal is converted by the PS-S Simulink converter into a Simulink signal that regulates the current source output.

A constant block is added that represents the irradiance value of the sun. This constant block effects the output of the solar cell just when it varies up to a saturated point. The configuration solver specifies the parameters that the model needs to accommodate during the simulation; this solver finds the steady state for a stable input.

This current source output then represents the actual current signal produced by the solar cell, see the figure 4.6 below. The measured current is 7.34A and the measured simulated actual voltage is 0.6V that confirms the original/actual rating of the solar cell that is 0.6V. The Matlab/Simulink software possesses of a power electronics compatible output. See figures 4.7 and 4.8 below.

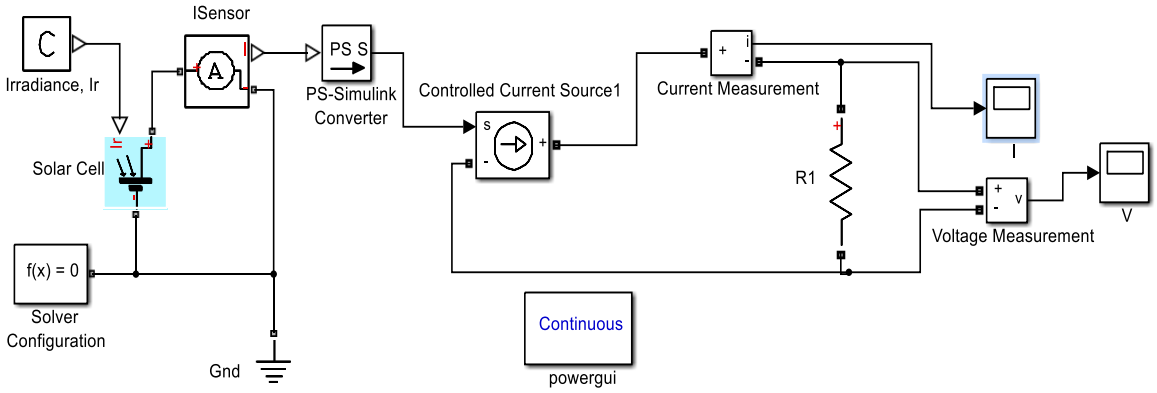

Figure 4.6: Controlled Current Source Model

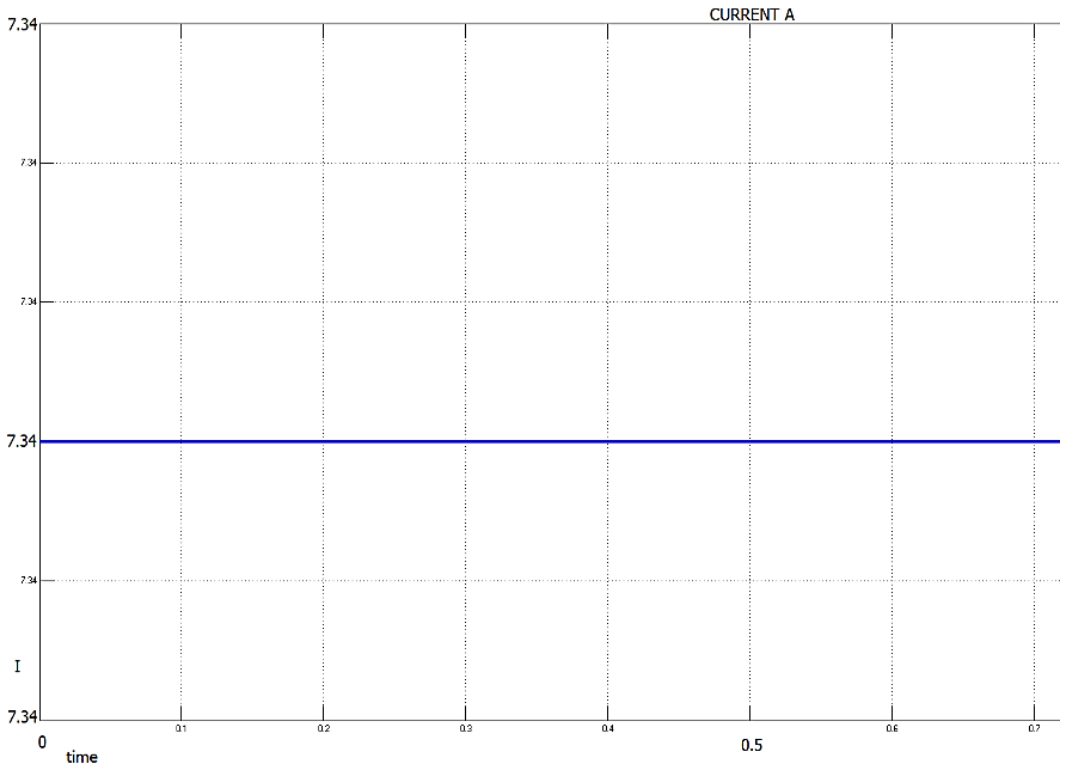

Figure 4.7: Controlled Current Source Voltage Output

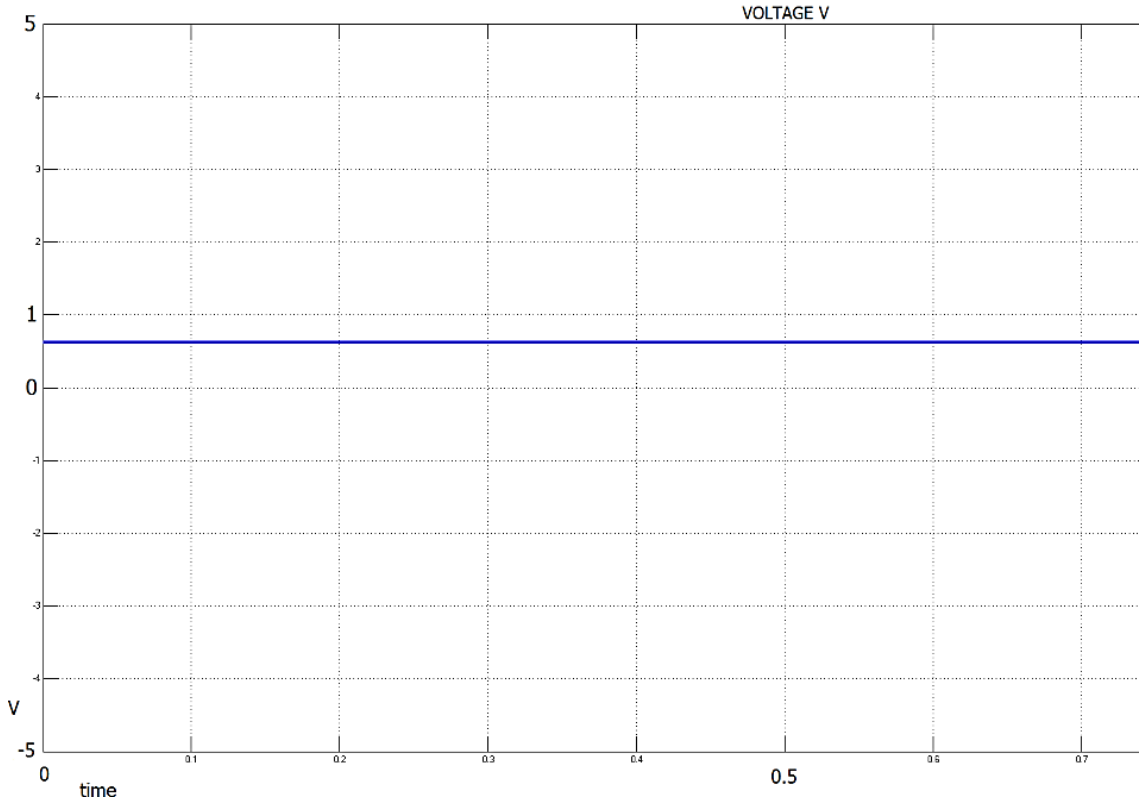

Figure 4.8: Controlled Current Source Current Output

The next step is to add a frequency switch in the circuitry to test the compatibility of the controlled switch. An IGBT was added with a pulse generator as a DC-DC converter. The final voltage and current output successfully stayed unchanged, see in the graph below that the current output is still exactly 7.34A and the voltage output is 0.6V. Refer to figures 4.9 to 4.11 below.

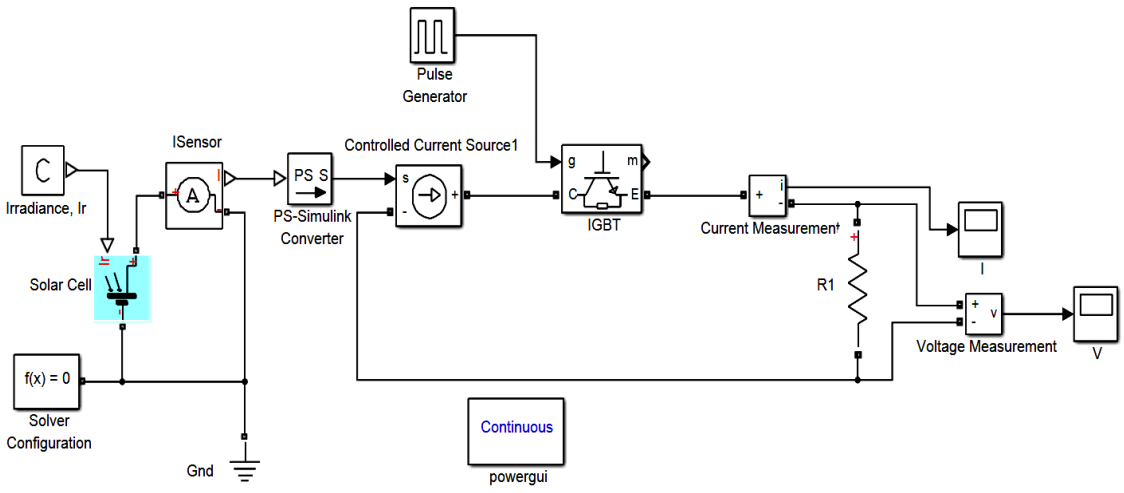

Figure 4.9: Solar Cell IGBT Model

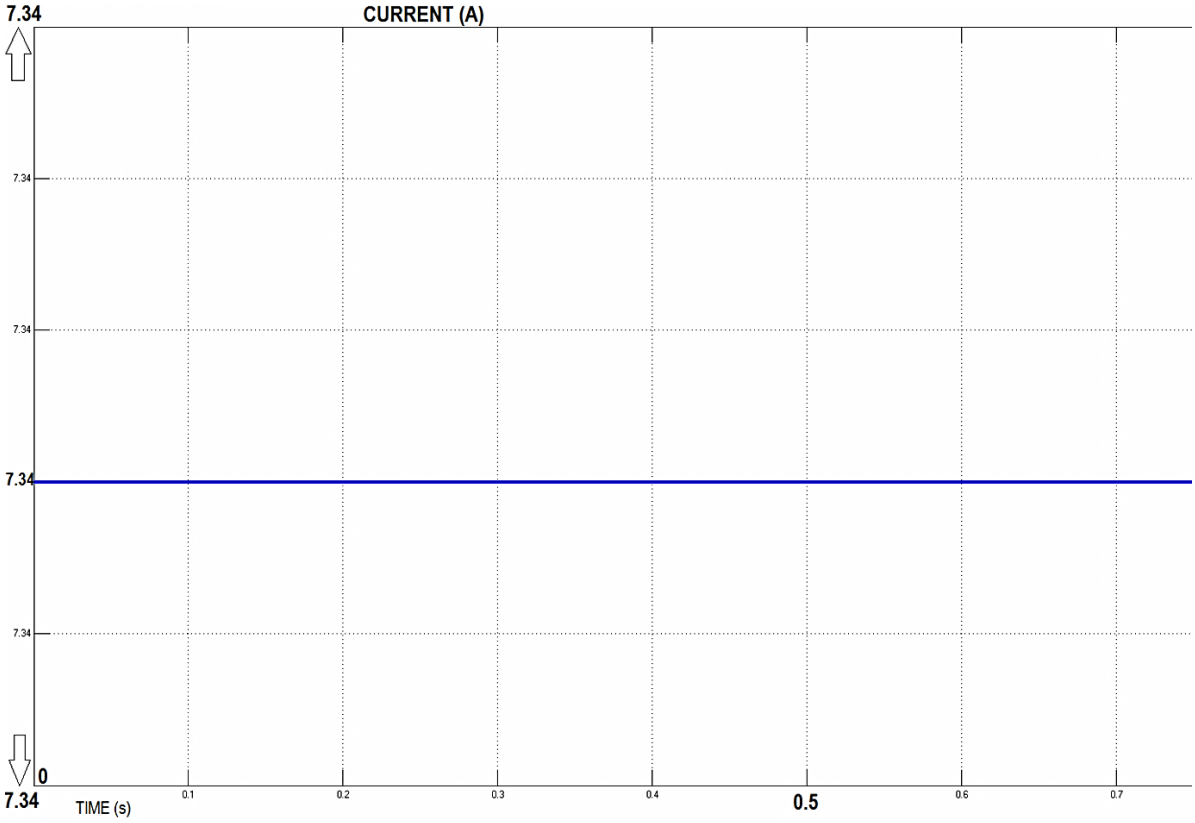

Figure 4.10: Solar Cell IGBT Voltage Output

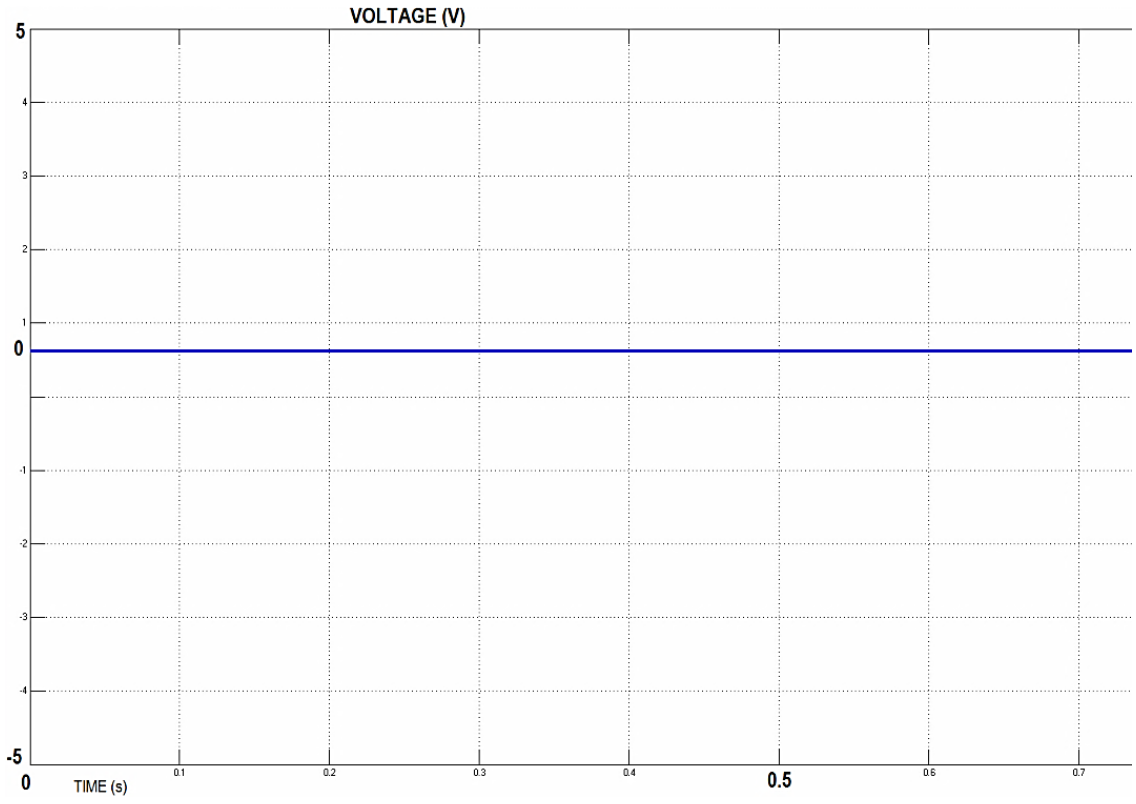

Figure 4.11: Solar Cell IGBT Current Output

In the circuit below, indicated in figure 4.12, the number of solar cells are increased into an array to represent two PV panels connected in parallel with an open circuit voltage of 25V and with a closed circuit current rating of 10A. A three-phase, two level converter is implemented to invert the DC voltage an AC voltage.

The following IGBT configuration includes two three-arm bridges, twelve-switches in an H configuration. A carrier frequency of 1080Hz was implemented as well as a modulation index of 0.85. Note that the measured voltage output on the load is a steady 30v AC signal as shown in figure 4.13.

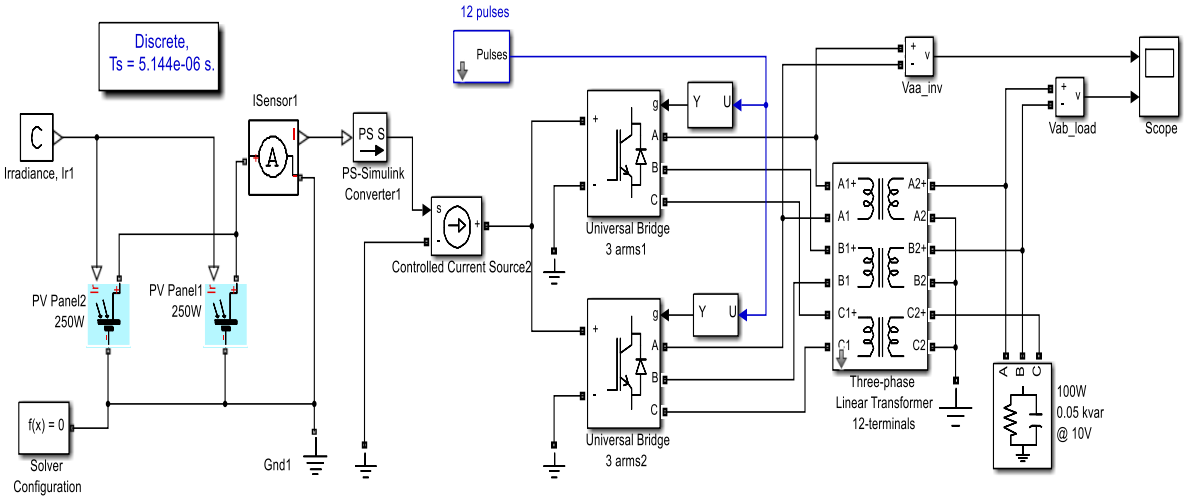

Figure 4.12: Solar Cell Array Inverter Model

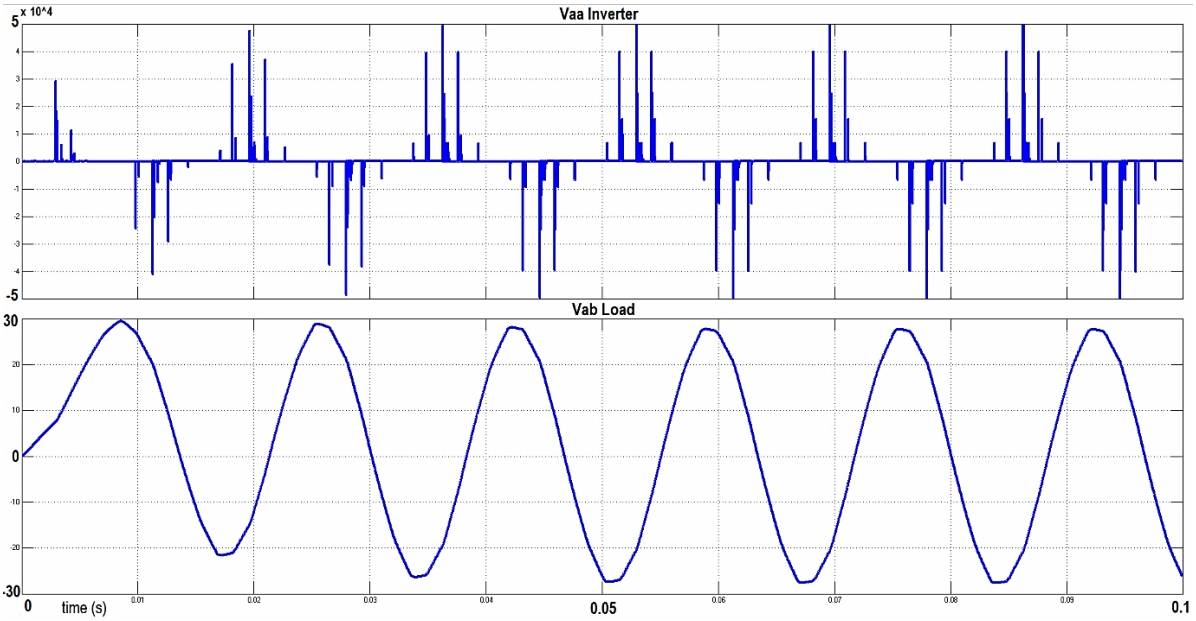

Figure 4.13: Solar Cell Output

The following are the input parameters for the PV System in Matlab/Simulink

I_{pv} - Current output of a PV module

I_{Ph} - Light generated photocurrent

I_D - Diode current

I_{Sh} - Leakage current

R_p - Cell shunt resistance

T_a- Ambient Temperature (Kelvin)

G - Solar Irradiation (kW/m^2)

G_n- Beam radiation measured in the following direction:

- the rays on the (n day) of the year in W/m2 and n is the day
- number of the year (varies between 1 and 365)

K - Boltzmann's constant (1.380658* 10-23 J/K)

q - Electron charge (1.6*10-19 C)

Eg - Band gap energy for semiconductor (1.12eY for the silicon)

I_{OR} - Reverse saturation current of diode in ampere

V_t - Thermal voltage in volt

V_{pV} - Output voltage from the PY module

Φ- Latitude of the location in degrees

δ- Declination of the sun in degrees

ω- Solar hour angle in degrees

$$I_{pv} = I_{Ph} - I_D - I_{Sh} \quad (4\text{-}4)$$

$$I_{Ph} = I_{SC}G(1 + k_i(T_C - T_R)) \quad (4\text{-}5)$$

$$T_C = T_a + 0.2G \quad (4\text{-}6)$$

$$I_D = I_S\left(\exp\left[q\frac{\frac{V_{PV}}{n}+I_{pv}R_S}{AKT_C}\right] - 1\right) \quad (4\text{-}7)$$

$$I_S = I_{OR}\left(\frac{T_C}{T_R}\right)^{\frac{3}{A}} \exp\left[\frac{qE_g}{KA}\left(\frac{1}{T_C} - \frac{1}{R_C}\right)\right] \quad (4\text{-}8)$$

$$I_{OR} = \frac{I_{SC}}{\exp\left[\frac{V_{OC}/n}{V_c}\right]-1} \quad (4\text{-}9)$$

$$V_t = \frac{AKT_R}{q} \quad (4\text{-}10)$$

Newton Raphson's method was applied to simplify the non-linear equation in order to obtain numerical values for I_{PV} & V_{PV} to calculateP_{PV}. See figure 4.14 below.

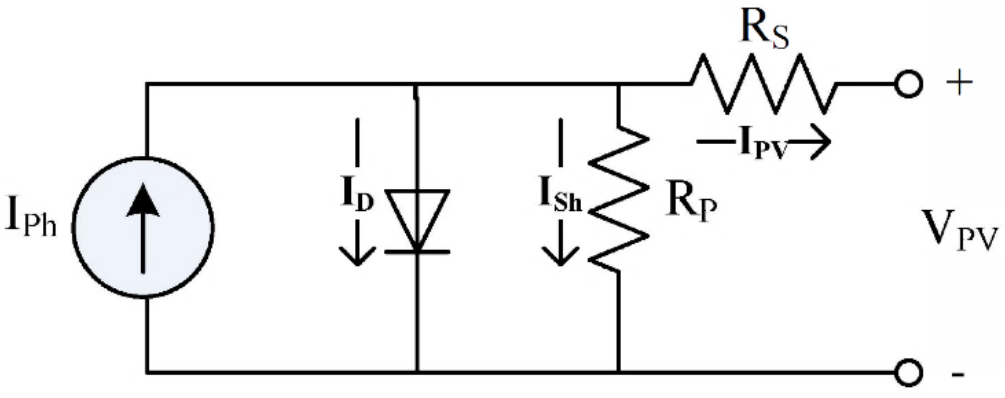

Figure 4.14: One-Diode PV Circuit

Thus

$$P_{PV} = I_{PV} * V_{PV} \quad 4\text{-}11$$

$$P_{PVA}(DC) = N_p I_{PV} . N_S V_{pV} \quad 4\text{-}12$$

$$G = \frac{G_n}{1000} \sin\Phi \sin\delta \cos\Phi \cos\delta \cos\omega \quad 4\text{-}13$$

A mathematical description of the current/voltage terminal characteristic for photo voltaic cells has been known for a long time as the double-exponential equation (Gow & Manning, Mar 1999). See the equivalent basic circuit design below in figure 4.15.

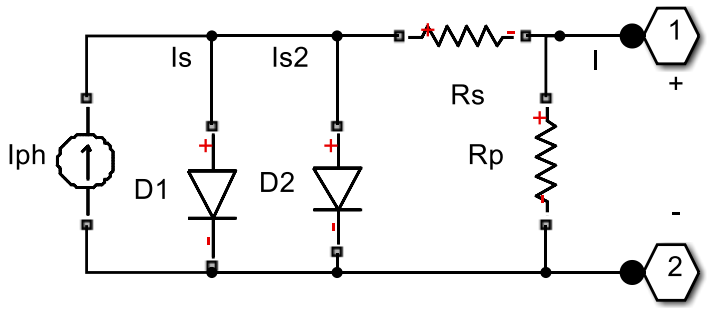

Figure 4.15: Double Diode PV circuit

The output current I is:

$$\mathrm{I} = I_{ph} - I_s * [e^{(V+I*R_s)/(N*V_t)} - 1] - I_{s2} * [e^{(V+I*R_s)/(N2*V_t)} - 1] - (\mathrm{V} + \mathrm{I} * R_s)/R_p \quad 4\text{-}14$$

Where:

I_{ph} Is the solar-induced current:

$$I_{ph} = I_{ph0} * \frac{I_r}{I_{r0}} \quad 4\text{-}15$$

Where:

I_r = the irradiance (light intensity) in W/m2 falling on the cell.

I_{ph0} = measured solar-generated current for the irradiance Ir0.

I_s = saturation current of the first diode.

I_{s2} = saturation current of the second diode.

V_t = thermal voltage, kT/q, where:

k = Boltzmann's constant, 1.38 x 10-23 I/K

T = Device simulation temperature parameter value

q = elementary charge on an electron.

V = solar cell terminal voltage

Rs = cell series resistance

Rp = cell shunt resistance

N = quality factor (diode emission coefficient) of the first diode.

$N2$ = quality factor (diode emission coefficient) of the second diode.

Temperature dependence:

$$I_{ph}\,(t) = I_{ph} * [1 + TIPH1 * (T - T_{measured})] \quad \text{4-16}$$

$$I_{s1}(T) = I_{s1} * [\frac{T}{T_{meas}}]^{(\frac{TXIS_1}{N})} * e\,\wedge\,[EG * (\frac{T}{T_{meas}} - 1) / (N_1 * V_1)] \quad \text{4-17}$$

$$I_{s2}(T) = I_{s2} * [\frac{T}{T_{meas}}]^{(\frac{TXIS_2}{N_2})} * e\,\wedge\,[EG * (\frac{T}{T_{meas}} - 1) / (N_2 * V_1)] \quad \text{4-18}$$

$$R_s\,(T) = R_s * [\frac{T}{Tmeas}]^{TRS1} \quad \text{4-19}$$

$$R_p\,(T) = R_p * [\frac{T}{Tmeas}]^{TRP1} \quad \text{4-20}$$

4.2.3 Wind Turbine Control Parameters

The next few calculations including its derivations and implemented substitutions will explain wind power in terms of its mathematical modelling. Refer to the definitions of various variables used:

E	=	Kinetic Energy (J)
ρ	=	Density (kg/m3)
m	=	Mass (kg) A = Swept Area (m2)
v	=	Wind Speed (m/s)
Cp	=	Power Coefficient
P	=	Power (W)
r	=	Radius (m)
dt/dm	=	Mass flow rate (kg/s)
x	=	distance (m)
dt/dE	=	Energy Flow Rate (J/s)
t	=	time (s)

Under constant acceleration, the kinetic energy of an object having mass *m* and velocity *v* is equal to the work done *W* in displacing that object from rest to a distance *s* under a force *F* (Bird, 2007)*:*

$$E = W = Fs \quad (4\text{-}21)$$

Newton's Law: $F = ma$ (4-22)

Substitution: $E = mas$ (4-22 into 4-21) (4-23)

Third equation of motion: $v^2 = u^2 + 2as$

Derivation: $a = \frac{(v^2 - u^2)}{2_s}$ (4-24)

Since initial velocity is zero (u=0): $a = \frac{v^2}{2s}$ (4-25)

Substitution: $E = \frac{1}{2}mv^2$ (4-25 into 4-23) (4-26)

Rate of change in energy (P_{wind}): $P = \frac{dE}{dt} = \frac{1}{2} v^2 \frac{dm}{dt}$ 4-27

Mass flow rate is: $\frac{dm}{dt} = pA\frac{dx}{dt}$ 4-28

Rate of change in distance: $\frac{dx}{dt} = v$ 4-29

Substitution: $\frac{dm}{dt} = pAv$ (4-29 into 4-28) 4-30

Substitution: $P = \frac{1}{2} pAv^3$ (4-30 into 4-27) 4-31

Including Betz limit (16/27): $P = \frac{1}{2} pAv^3 * \frac{16}{27}$ 4-32

The formula for power that can be used to calculate Wind power is the following:

$P = T\,\omega$ 4-33

Where:

P = power (W)
T = torque or moment (Nm)
ω = angular velocity (rad/s)
1 rad = $360^o / 2\,\pi =\sim 57.29578^o$

The circuit diagrams in figure 4.16 below was built and simulated in P-sim. The two input parameters were limited to wind speed and the pitch angle of the blades. The model comprises of a wind turbine, speed and torque sensors and a mechanical load.

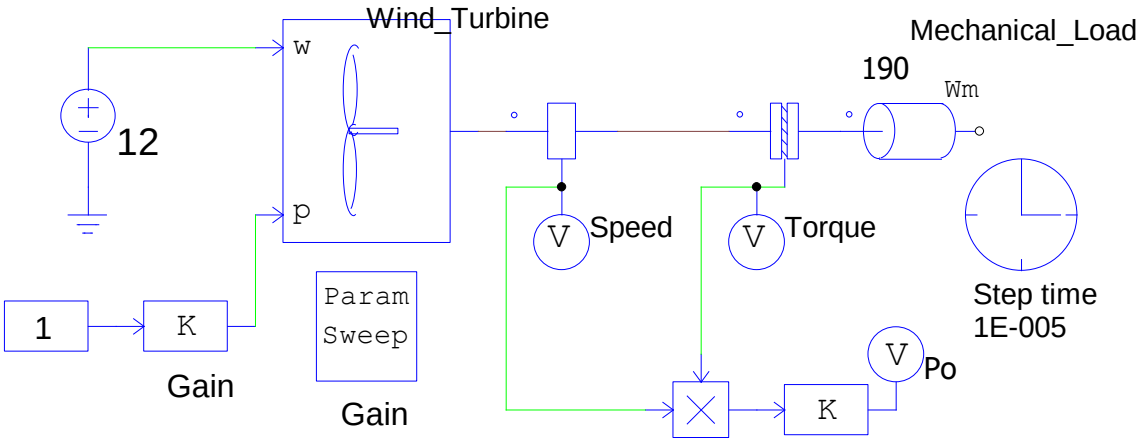

Figure 4.16: Wind turbine control circuit

Assuming the wind speed is constant, when the mechanical load increases in value, the torque and power output decrease over time and the speed thus frequency stays the same as it is directly proportional to the constant wind speed as shown in figure 4.17 and figure 4.18 below.

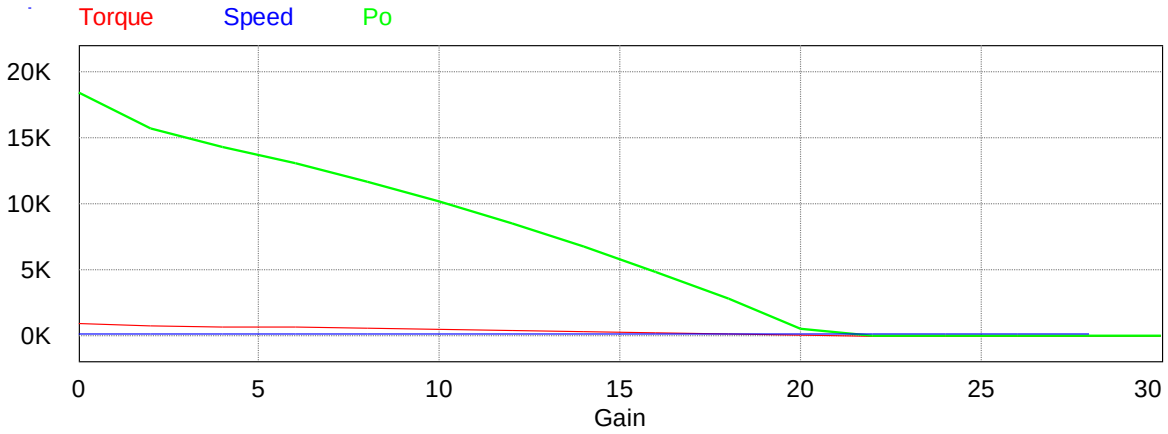

Figure 4.17: Wind Turbine power output values

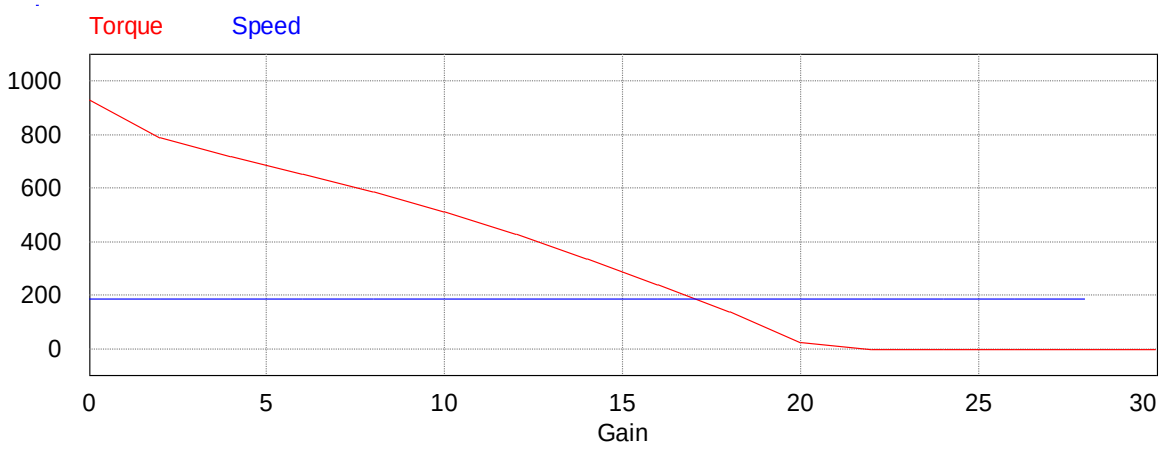

Figure 4.18: Wind Turbine torque output values

The following circuit diagram consists of a wind turbine, a speed and torque sensor respectively and includes an electrical power control system connected via an electrical mechanical interface. Refer to figure 4.19 below. The power output varies as the gain values changes via the power control interface. See figures 4.20 and 4.21.

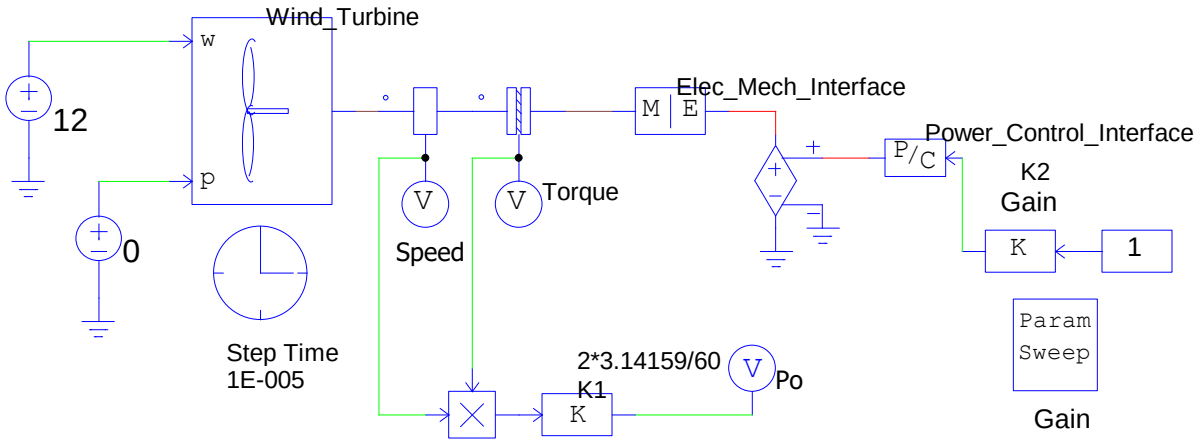

Figure 4.19: Extended Wind turbine control

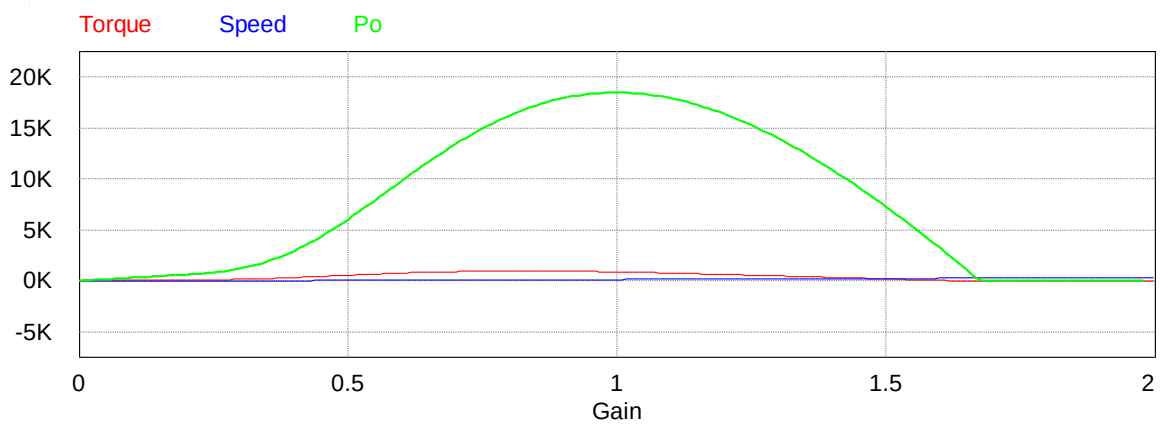

Figure 4.20: Extended Wind turbine power output value

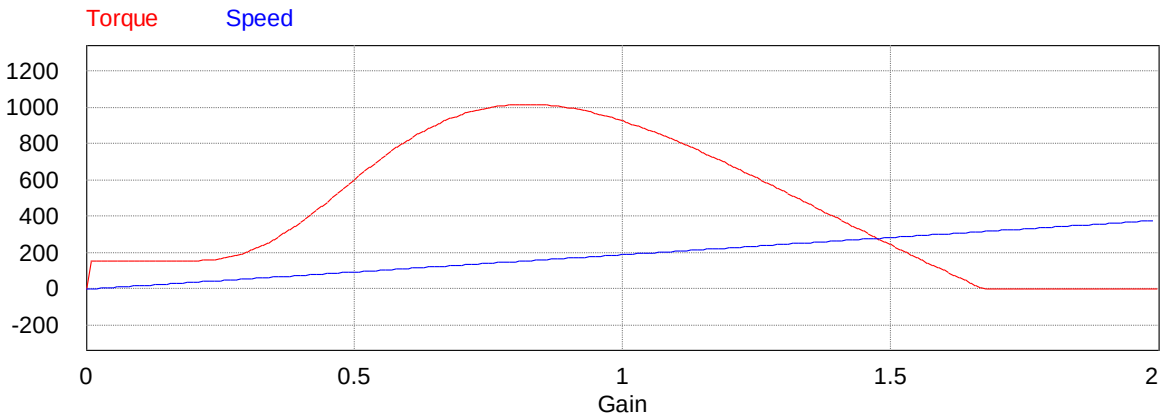

Figure 4.21: Extended Wind turbine torque output value

The following are the input parameters for a wind turbine:

$$P_m = C_p\,(\lambda, \beta)\,\frac{pA}{2}\,v_{wind}^3 \qquad 4\text{-}34$$

Where:

P_m	=	Mechanical output power of the turbine (W)
C_p	=	Performance coefficient of the turbine
p	=	Air density (kg/m3)
A	=	Turbine swept area (m2)
V_{wind}	=	Wind speed (m/s)
λ	=	Tip speed ratio of the rotor blade tip speed to wind speed
β	=	Blade pitch angle (deg.)

Three phase per unit (pu) system:

$$\text{Ibase} = \frac{S_{base}}{V_{base} \times \sqrt{3}} = 1\text{pu} \quad (4\text{-}35)$$

$$\text{Zbase} = \frac{V_{base}}{I_{base} \times \sqrt{3}} = 1\text{pu} \quad (4\text{-}36)$$

$$\text{Ybase} = \frac{1}{Z_{base}} = 1\text{pu} \quad (4\text{-}37)$$

Thus:

$$P_{m\_pu} = k_p C_{p\_pu} V_{wind\_pu}^3 \quad (4\text{-}38)$$

P_{m_pu} = Power in pu of nominal power for particular values of ρ and A

C_{p_pu} = Performance coefficient in pu of the maximum value of C_p

V_{wind_pu} = Wind speed in pu of the base wind speed. The base wind speed is the mean value of the expected wind speed in m/s.

k_p = Power gain for C_{p_pu}=1 pu, V_{wind_pu}=1 pu, k_p is less than/equal to 1

$$C_p(\lambda, \beta) = C_1(C_2/\lambda_i - C_3\,\beta - C_4)\, e^{-\frac{C_5}{\lambda_i}} + c_6\lambda \quad (4\text{-}39)$$

With:

$$\frac{1}{A_i} = \frac{1}{\lambda + 0.08\beta} - \frac{0.035}{\beta^3 + 1} \quad (4\text{-}40)$$

Calculated Coefficients:

$C_1 = 0.5176,\ C_2 = 116, C_3 = 0.4, C_4 = 5, C_5 = 21, C_6 = 0.0068$

4.2.4 Battery and Super Capacitor Parameters

The next model represents a Lead-Acid battery connected to a 13A current source in series, as indicated in figure 4.22. This 200V battery is rated at 6.5 Ah, thus the battery should drain within more or less in one hour's time (3600s). See the simulated results below indicated in figure 4.23 and 4.24.

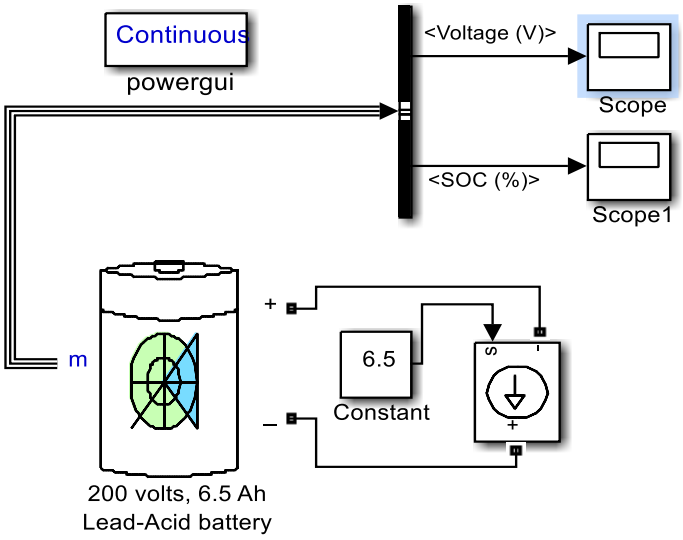

Figure 4.22: Lead-Acid Battery Model

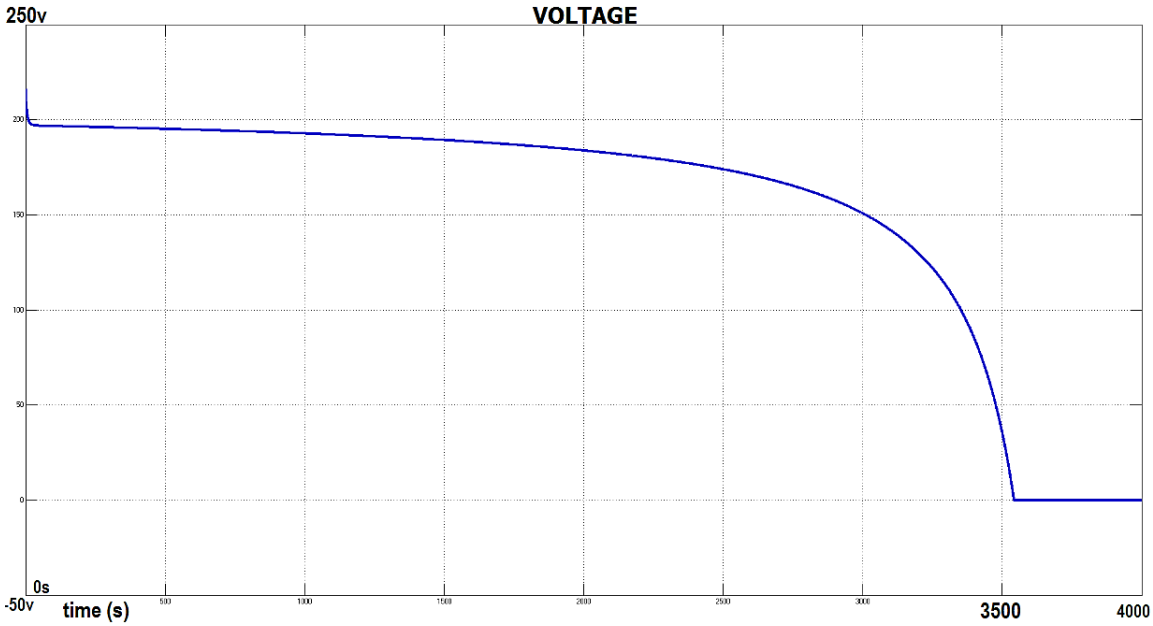

Figure 4.23: LA Battery Drain Voltage Output Simulation

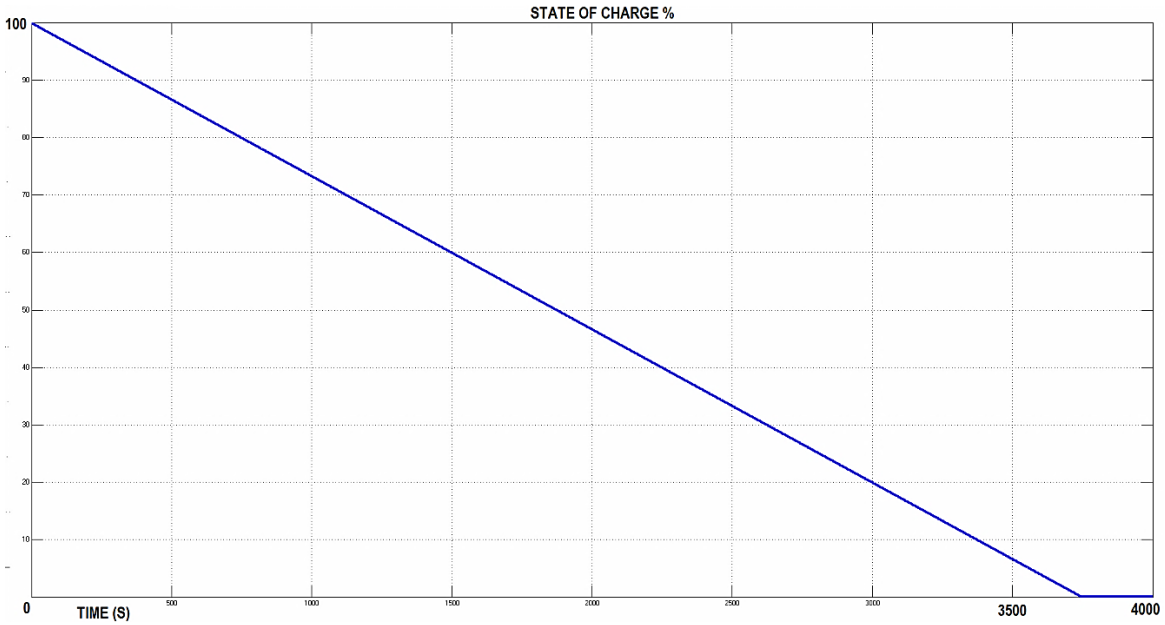

Figure 4.24: LA Battery drain SOC Output Simulation

Note that the following Nickel-Metal-Hydrate battery is connected to a 13 Ah current source as indicated in figure 4.25. Thus the battery should drain twice as fast than the previous example because the load has doubled. The battery should drain at half the time (1800 seconds). See figures 4.26 and 4.27.

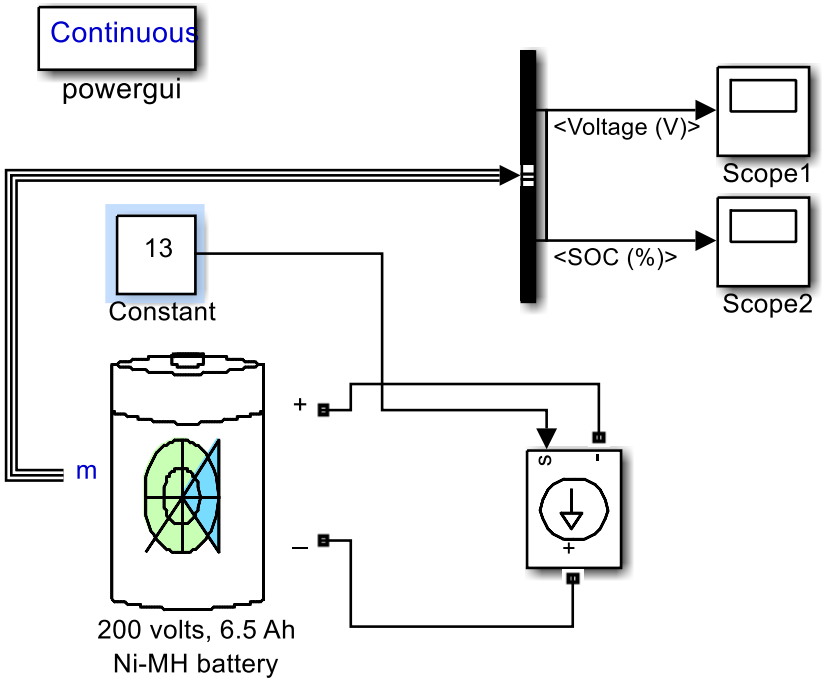

Figure 4.25: Ni-MH Battery Model

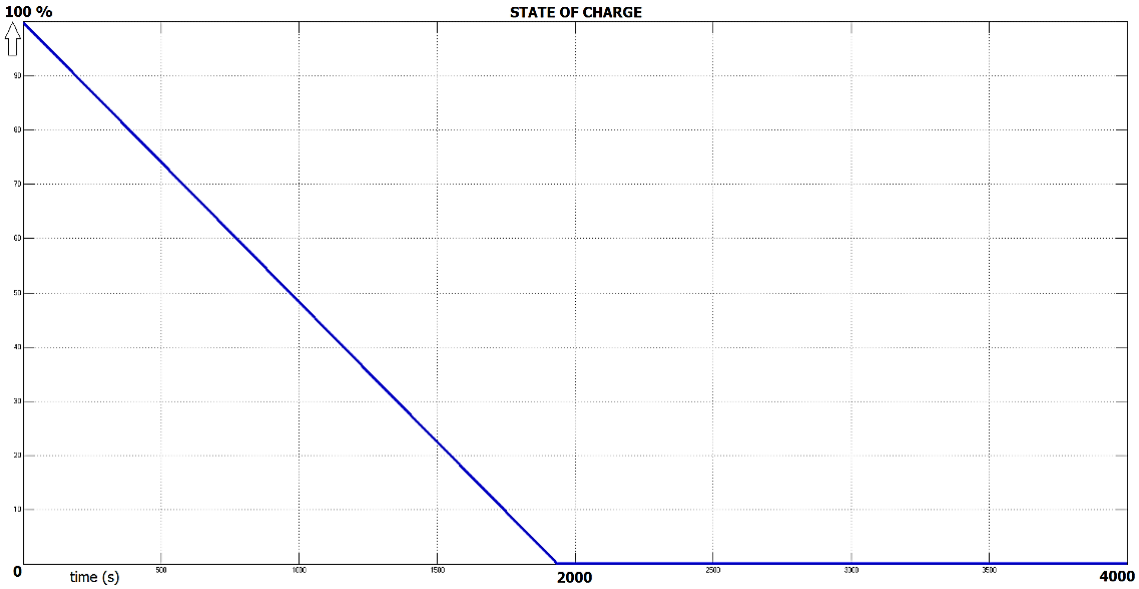

Figure 4.26: NI-MH Battery drain SOC Output Simulation

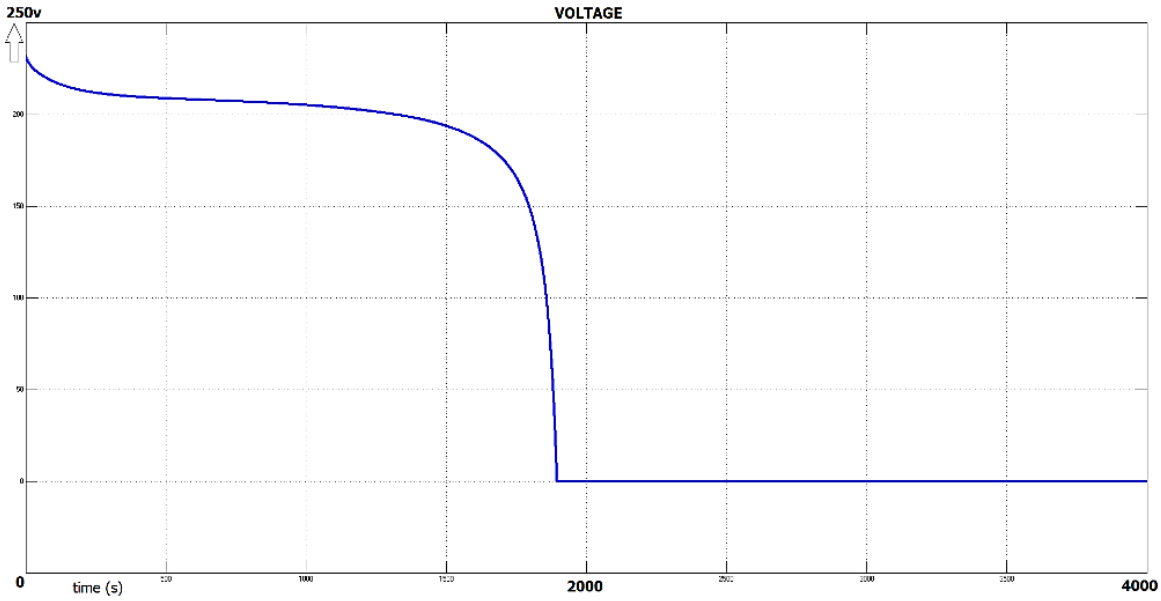

Figure 4.27: NI-MH Battery Drain Voltage Output Simulation

CHAPTER 5: MICROGRID CONTROL STRATEGIES

5.1 Overview

Case studies of different control strategies of previous researchers are analysed and summarized including simulations from the current researcher's battery and capacitive compensator control designs. Storage methods are integrated into a microgrid in order to improve output power fluctuations.

5.2.1 Battery Compensation

In the following model, a NI-MH battery is connected to an AC load of 6.5 A. A DC machine is also connected in parallel with the load with no initial torque. See figure 5.1 below. The current source drains the battery till the sate-of-charge is under 50% (SOC).

The relay which is pre-set to 0.5 (50% SOC) connects the negative torque to the DC machine, acting as a generator that starts to charge the battery. The relay is additionally pre-set to 0.9 in order to disconnect the DC generator from the circuit for an over charge protection mode. When the generator is disconnected, the currents source starts to drain the battery power again till 50% SOC.

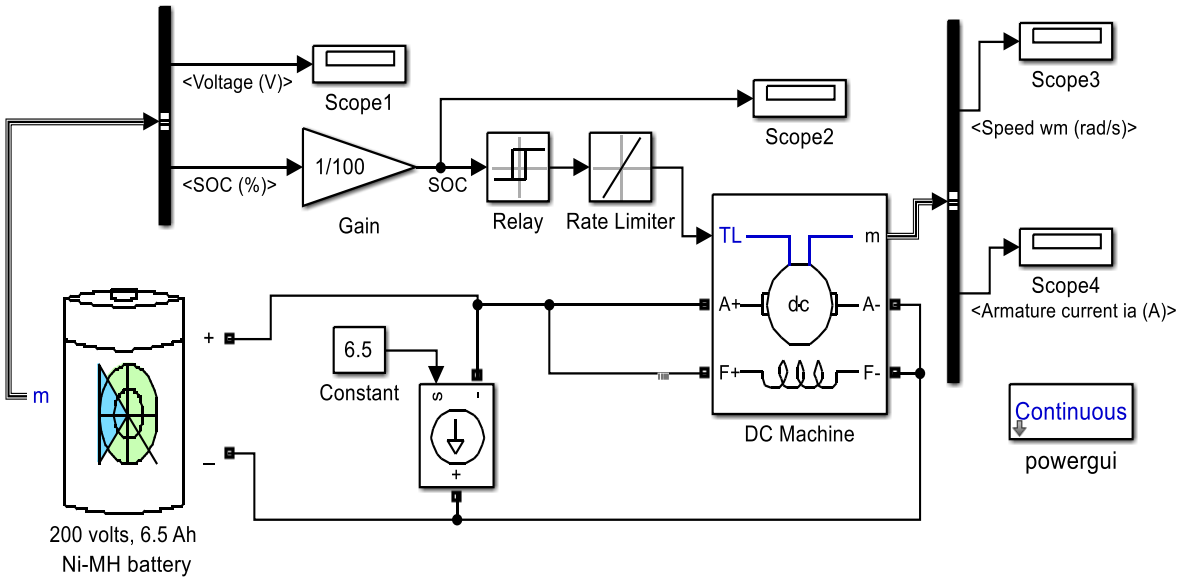

Figure 5.1: Battery and DC Generator Model

The voltage is maintained above 200V which is the rating of the battery bank via the DC generator. The value of the negative torque is 200N (-200N). The figure 5.2 below shows how the system voltage rises till 350V and then disconnects from the DC generator to discharge the power rapidly at 1500 seconds.

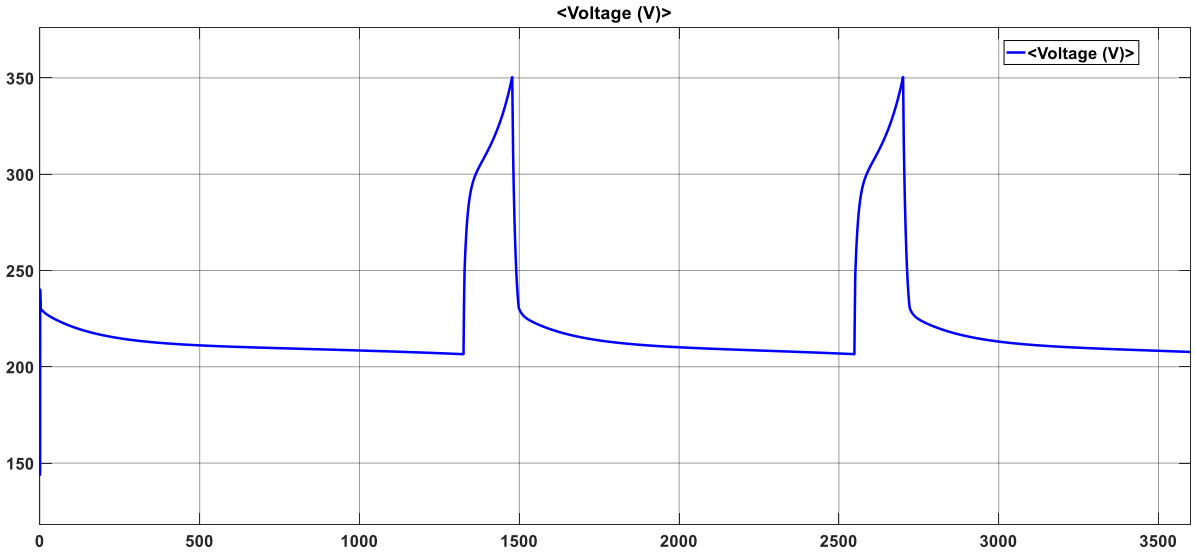

Figure 5.2: Combined Voltage Output

As soon as the battery is drained till 50% SOC, the DC generator compensates and charges the battery till 90% SOC where it is disconnected again by the relay. See figure 5.3 below.

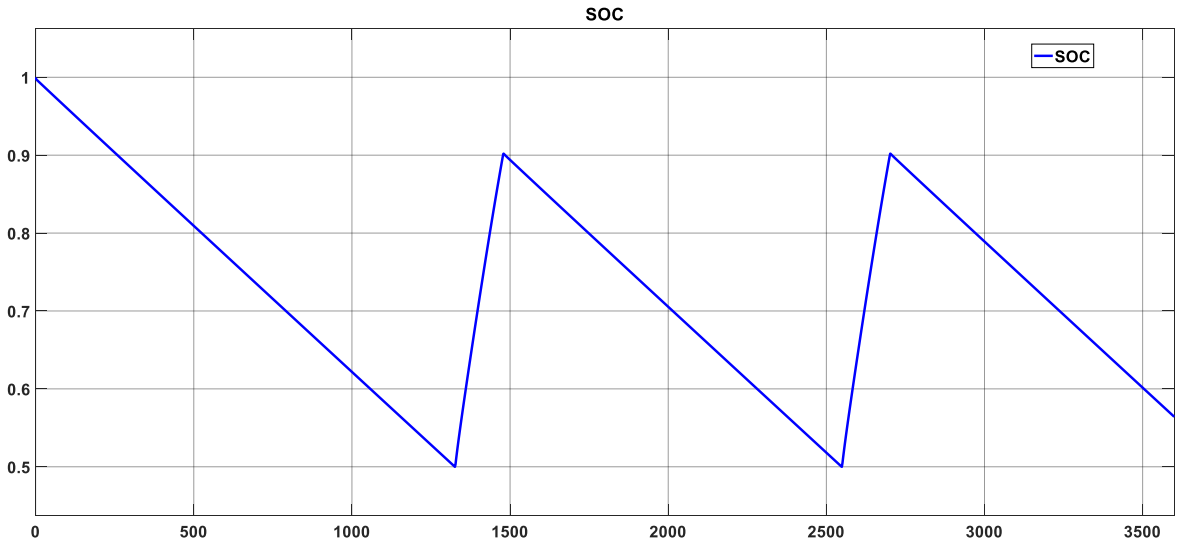

Figure 5.3: Recovery of SOC Output

Note that in figure 5.4 and figure 5.5 there is a difference between the two torque settings. The first torque setting is -200N where in the second simulation it is -1000N. The higher the torque, the quicker the recovery time of the speed of the machine is.

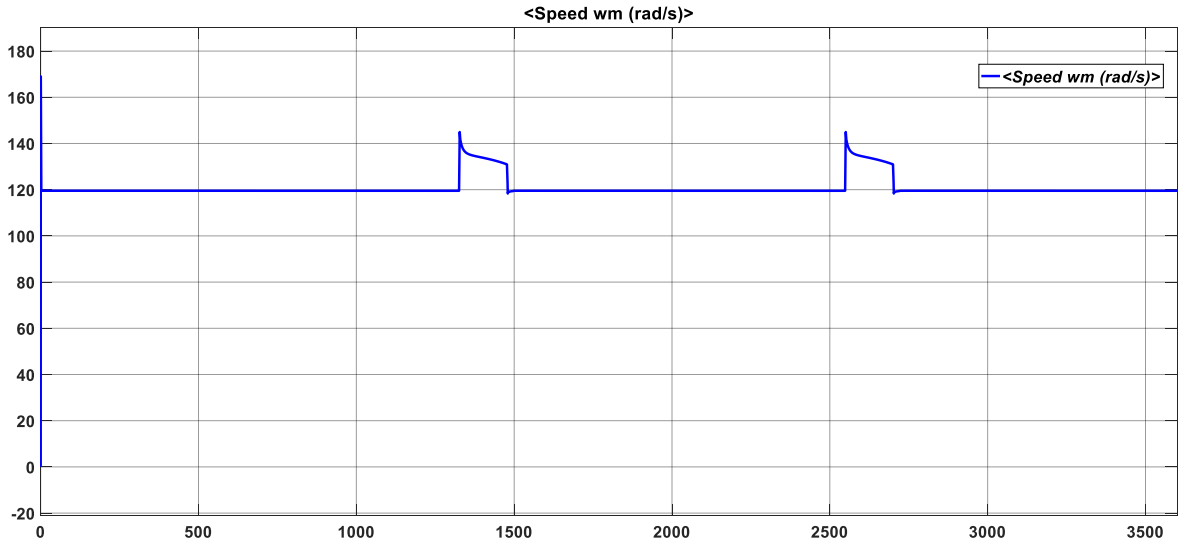

Figure 5.4: Slower DC Generator Speed Recovery

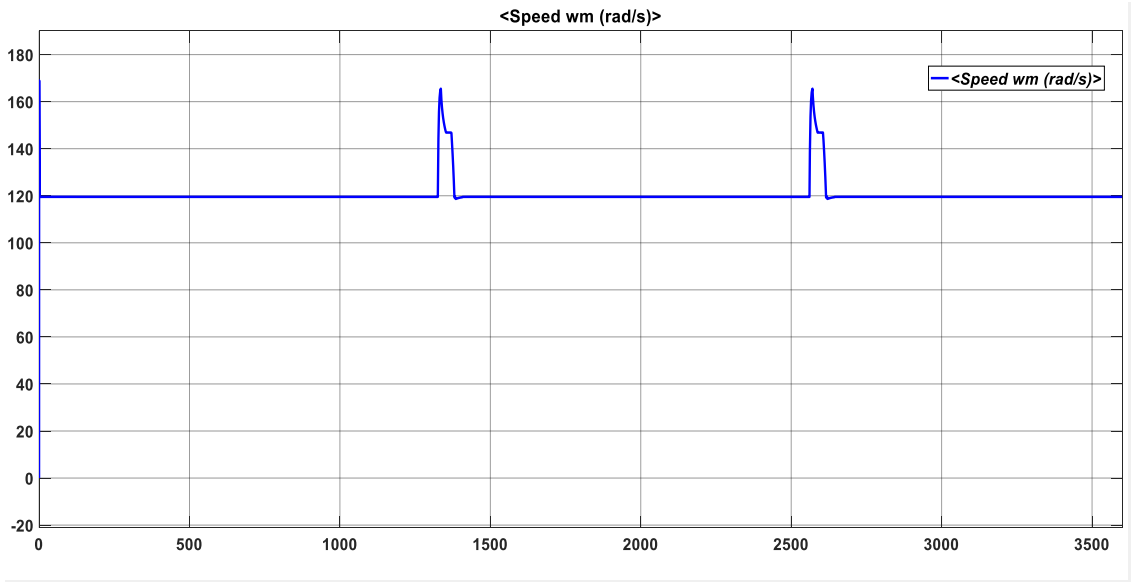

Figure 5.5: Faster DC Generator Speed Recovery

The following control system illustrates the combination of two Solar Cell systems in a microgrid; one base battery, two current sources (one negative, one positive), one DC machine (generator) as well as measurement instruments and scopes. The system battery and the two PV systems provides a base voltage of 14.75V. See figure 5.6.

At 2000s the top PV System disconnects using a breaker and the system voltage drop to under 14.5V. At 4000s the first current source (negative) is added to the microgrid (representing an active load) and the system voltage drops to a further 13.25V. If the SOC reaches below 50%, the relay switches the DC generator on, which generates a negative torque of 800N (generation mode) which then increases the system voltage every time the voltage drops below 12.4V (50% SOC).

When the system voltage reaches above 90% of the SOC, the relay then switches the DC generator off and the battery gets drained again by the negative current source (load). The second current source (connected positive-positive) adds constant power to the grid at 8000s. Note that the system voltage rises slightly and the rate by which the battery gets drained slows slightly down as shown in figures 5.7 and 5.8.

The SOC takes a longer period to reach its maximum and minimum levels. This is due to the second PV system that injects more power into the microgrid. The more power injected, the longer it takes for the batteries to discharge to its minimum set point. This is phenomenon is shown in figure 5.9.

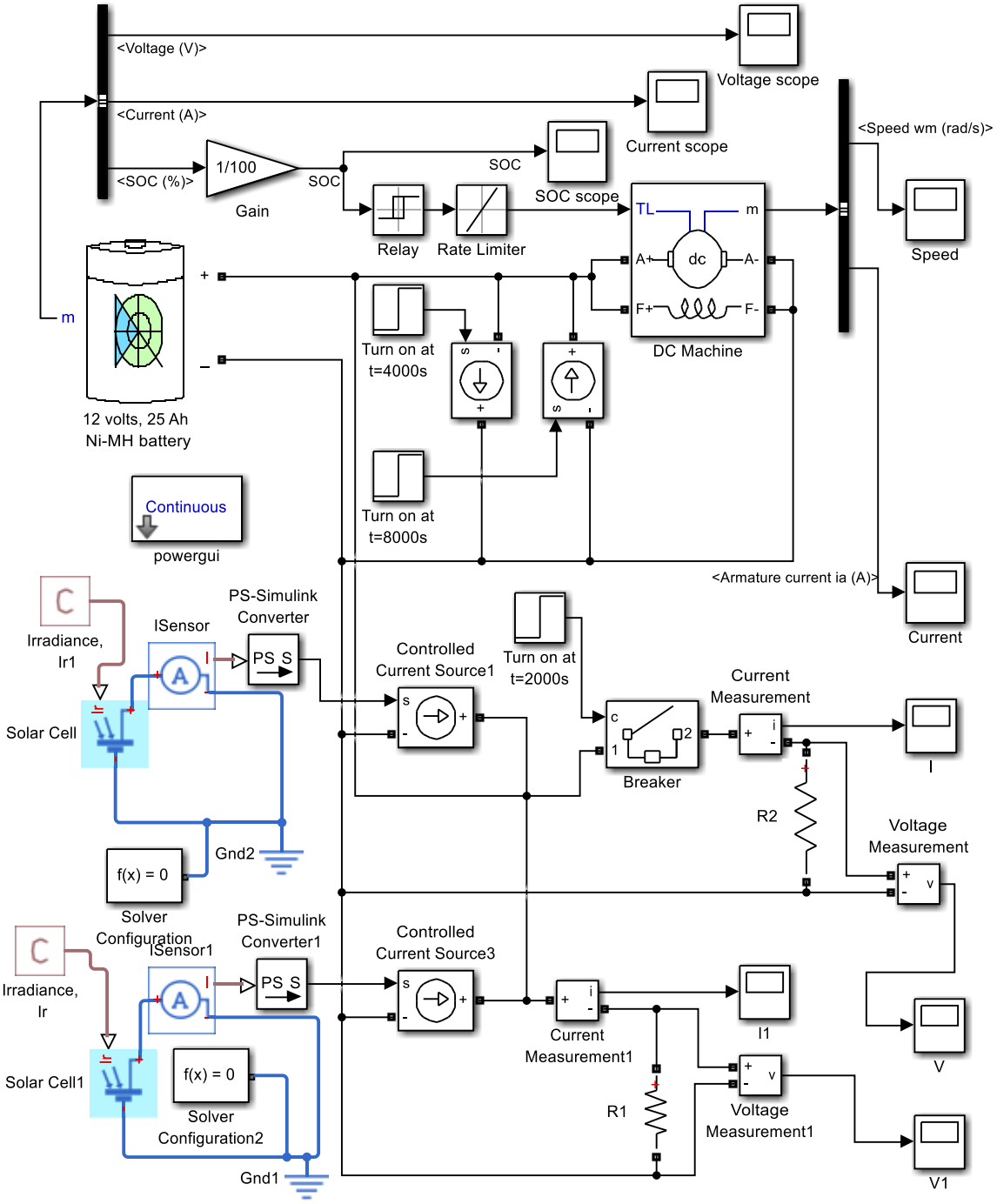

Figure 5.6: Combined Microgrid

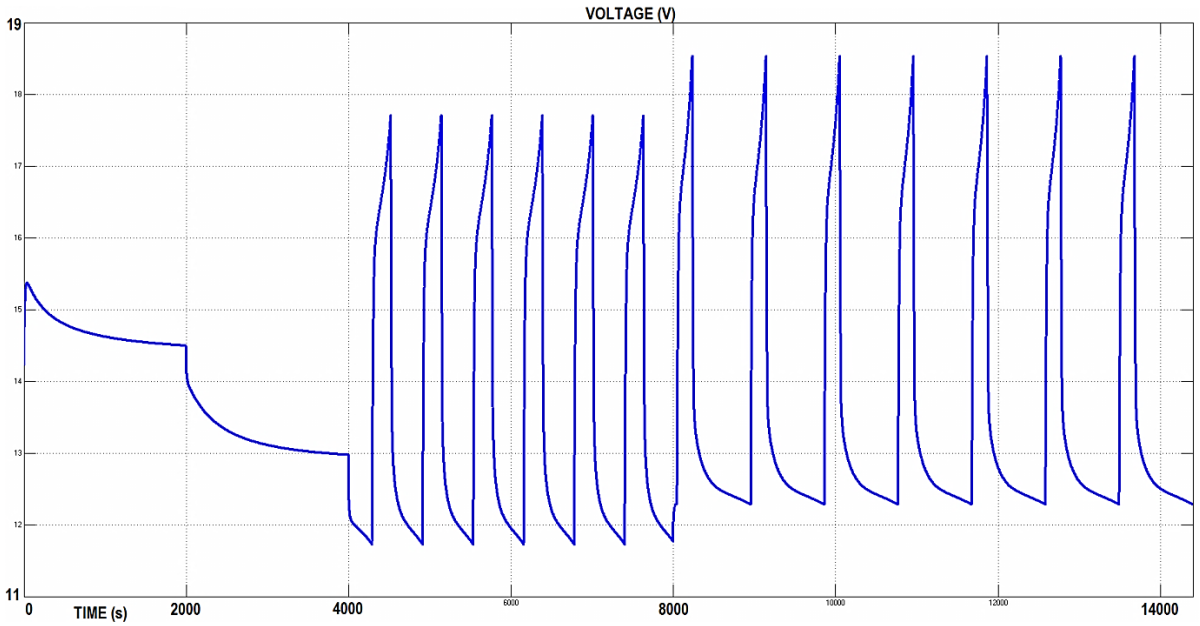

Figure 5.7: Combined Microgrid Voltage Output Results

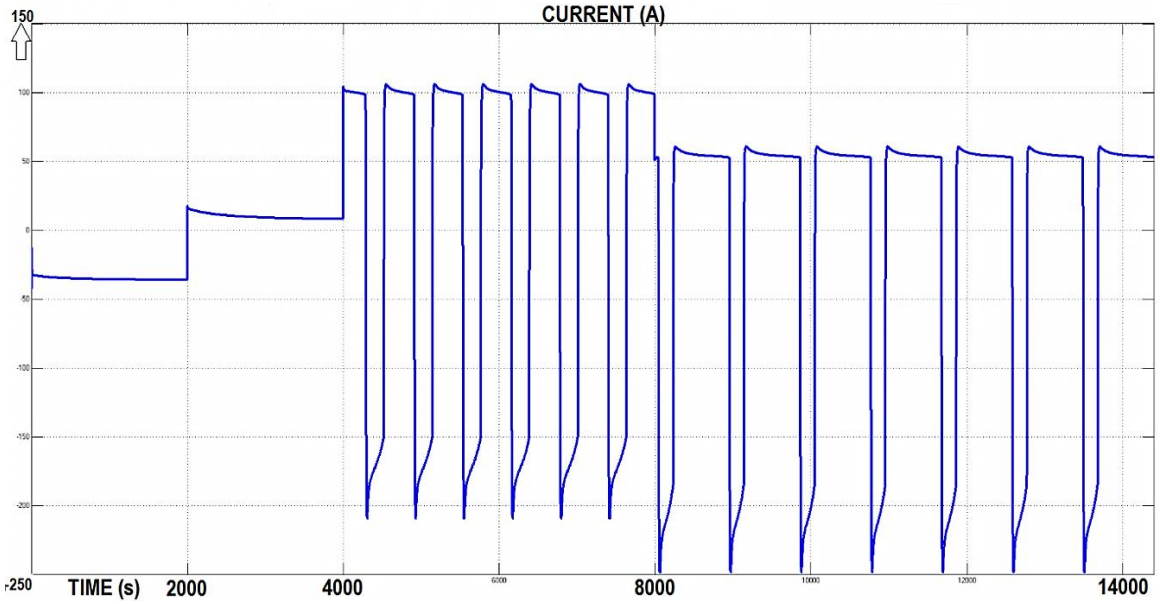

Figure 5.8: Combined Microgrid Current Output Results

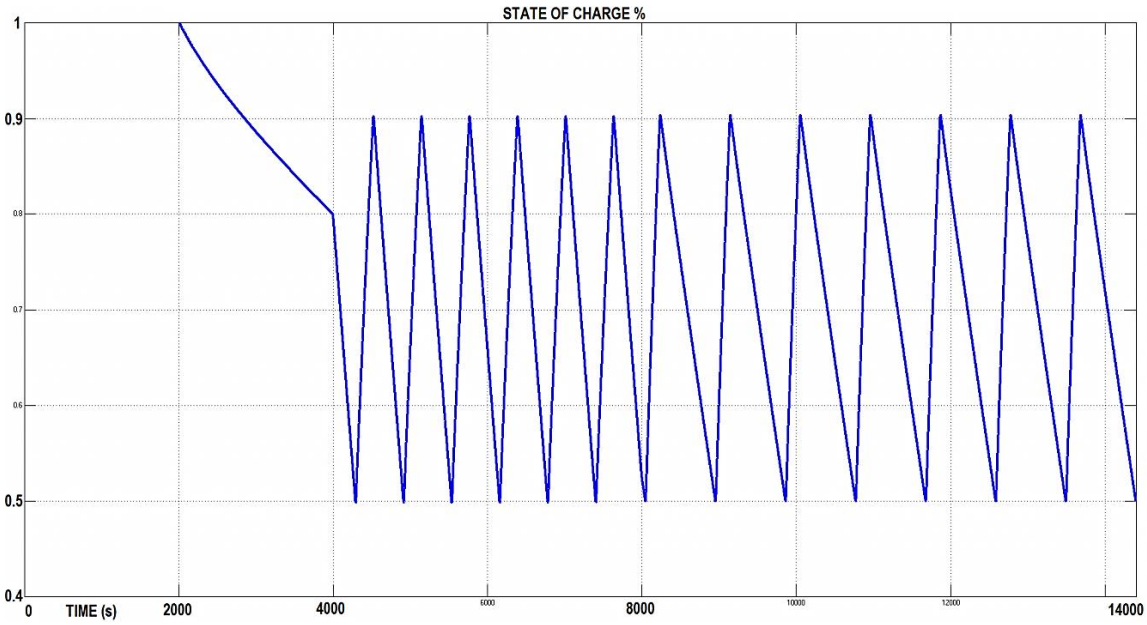

Figure 5.9: State of Charge (SOC)

In the following model displayed in figure 5.10, the irradiance of the sun fluctuates due to its intermittency as depicted in figure 5.11. The output is directly proportional to the fluctuation input. An additional battery is connected in parallel with the ten solar panels of 250 watts each to absorb the PV panel's DC input in order to mitigate the volatile fluctuations.

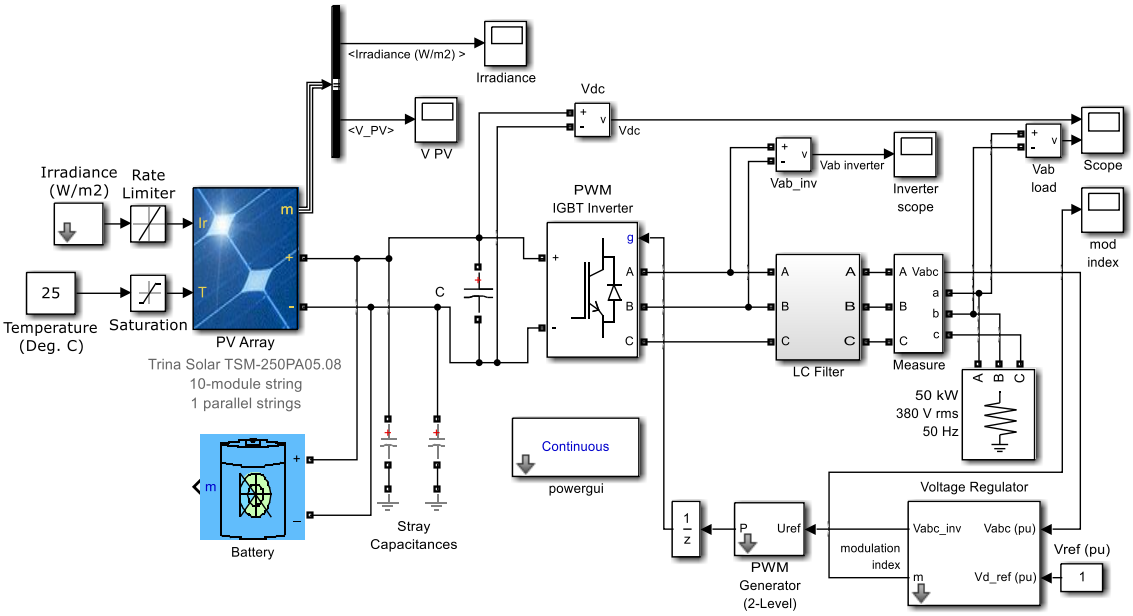

Figure 5.10 Intermitted input power

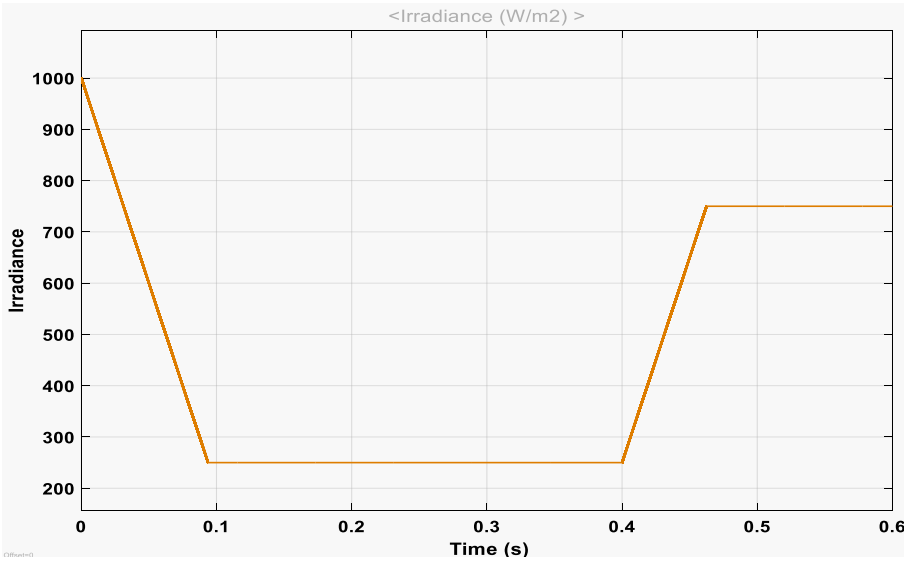

Figure 5.11 Renewable intermitted property

The battery stays disconnected and the voltage measured before the power electronic conversion stays directly proportional to the intermitted simulated input power produced by the irregular irradiance as shown in figure 5.12.

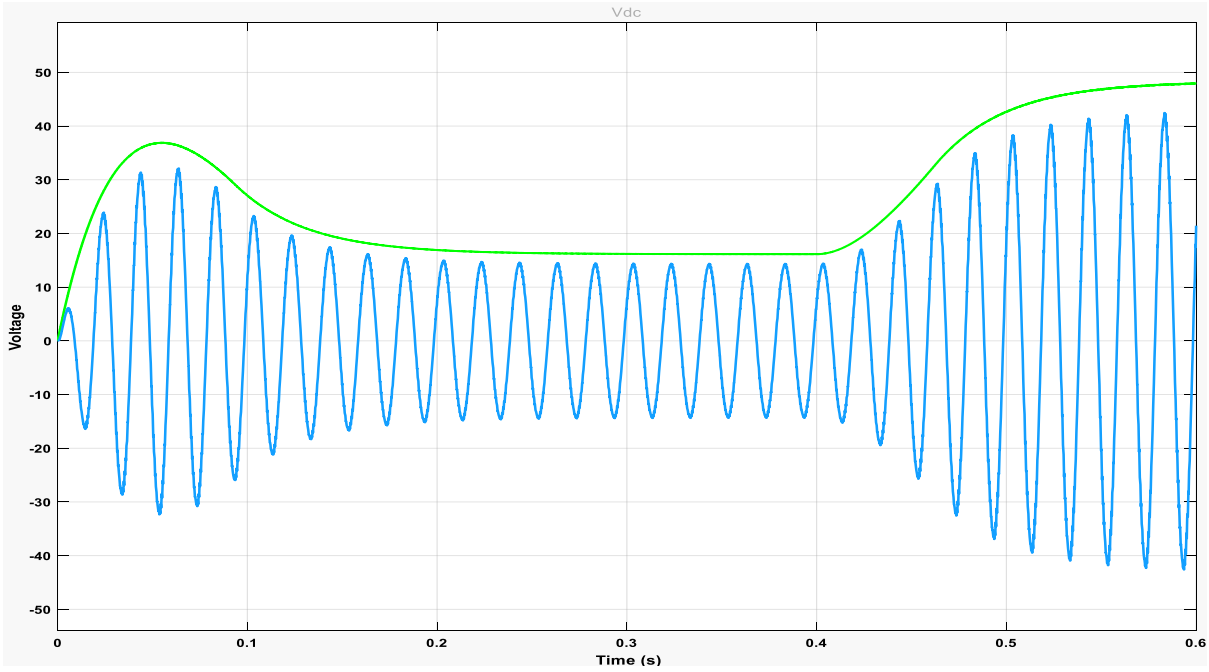

Figure 5.12 Unregulated voltage output

Once the battery is connected to the circuit, it stabilizes the voltage output as it provides reverse capacity irrespective of the radial irregularity. This storage method acts as an input control method to help stabilize the power output in a microgrid. See figure 5.13.

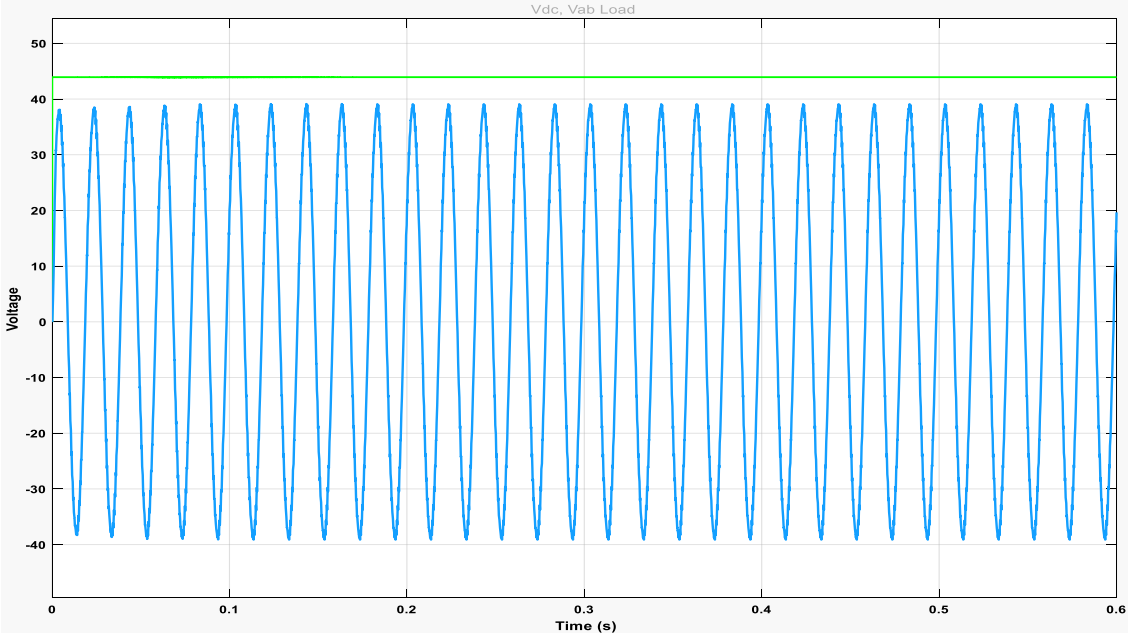

Figure 5.13 Battery regulated input voltage

In the following model, the 500-kW load is connected and disconnected at [0.1 0.2 0.3 0.4] seconds respectively as shown in figure 5.14. An AC source represents the stable power output of an inertial generator which gets inverted to a DC voltage.

Note that the DC output voltage fluctuates accordingly to the load changes implemented. As soon as the battery is connected via the breaker in parallel at 0.25 seconds, the excess battery power compensates for the disconnected load resulting in minimal voltage output variation. This behaviour is shown figures 5.15 and 5.16 below.

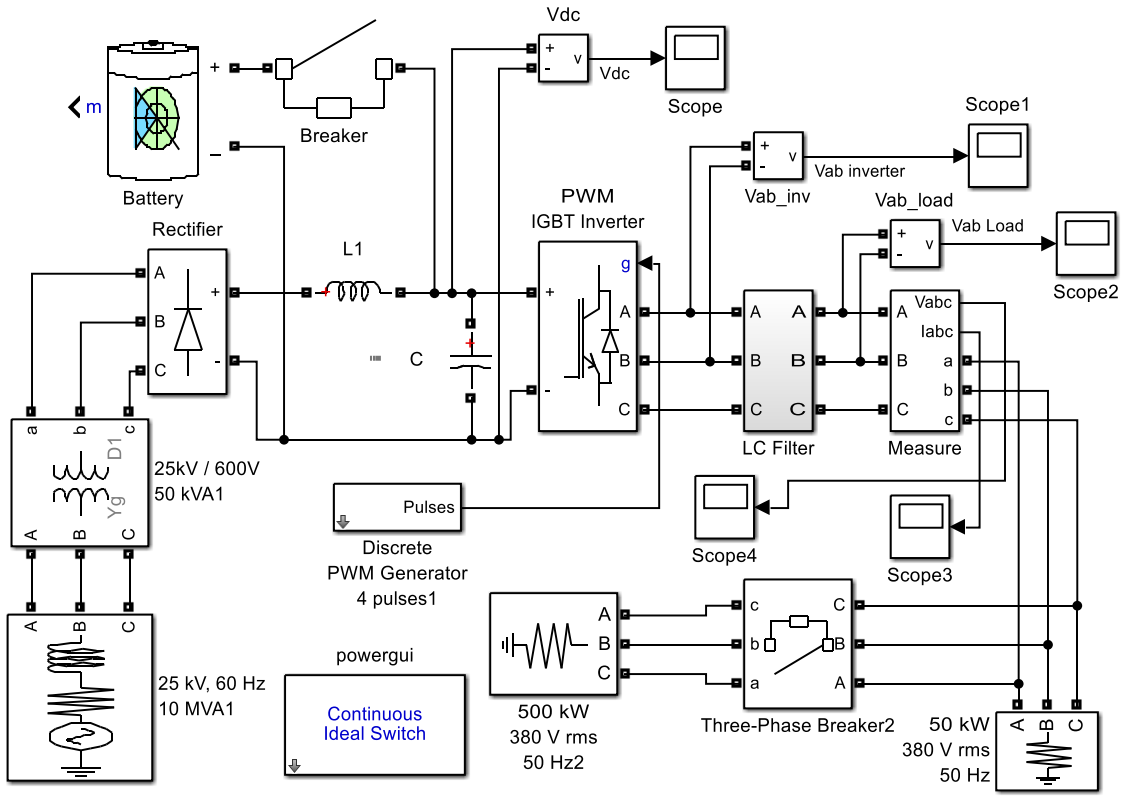

Figure 5.14 Load change diagram

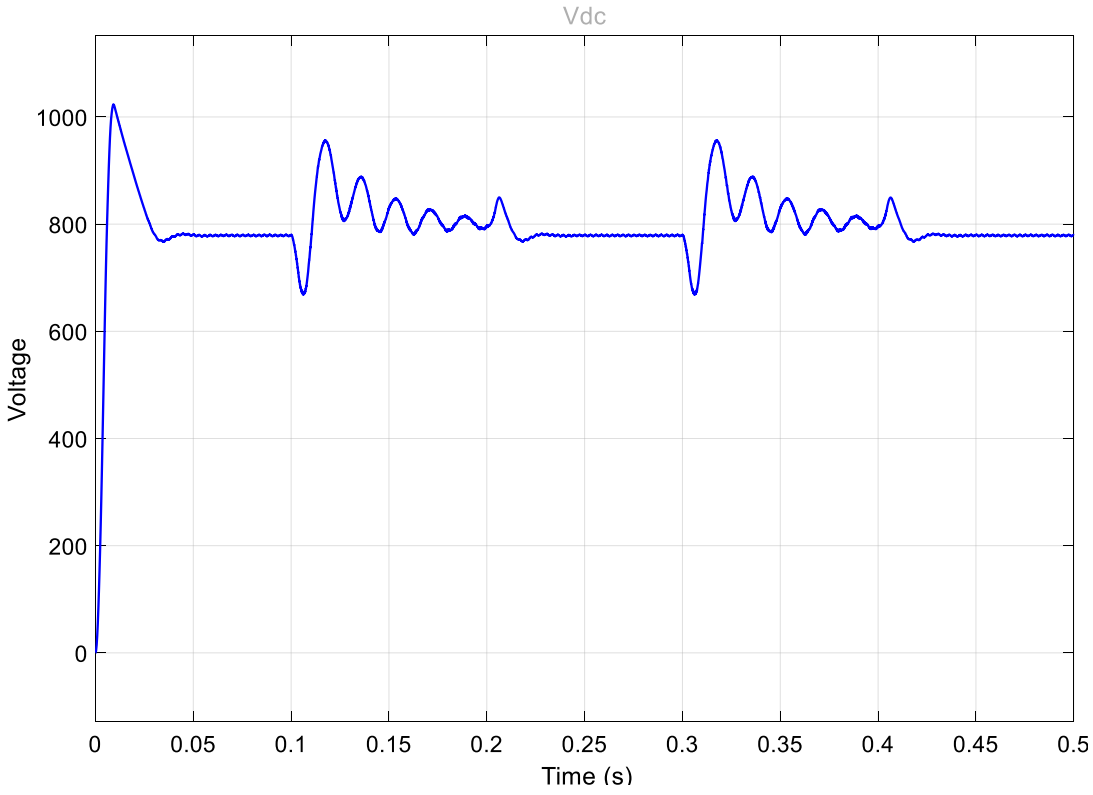

Figure 5.15 Unregulated load change

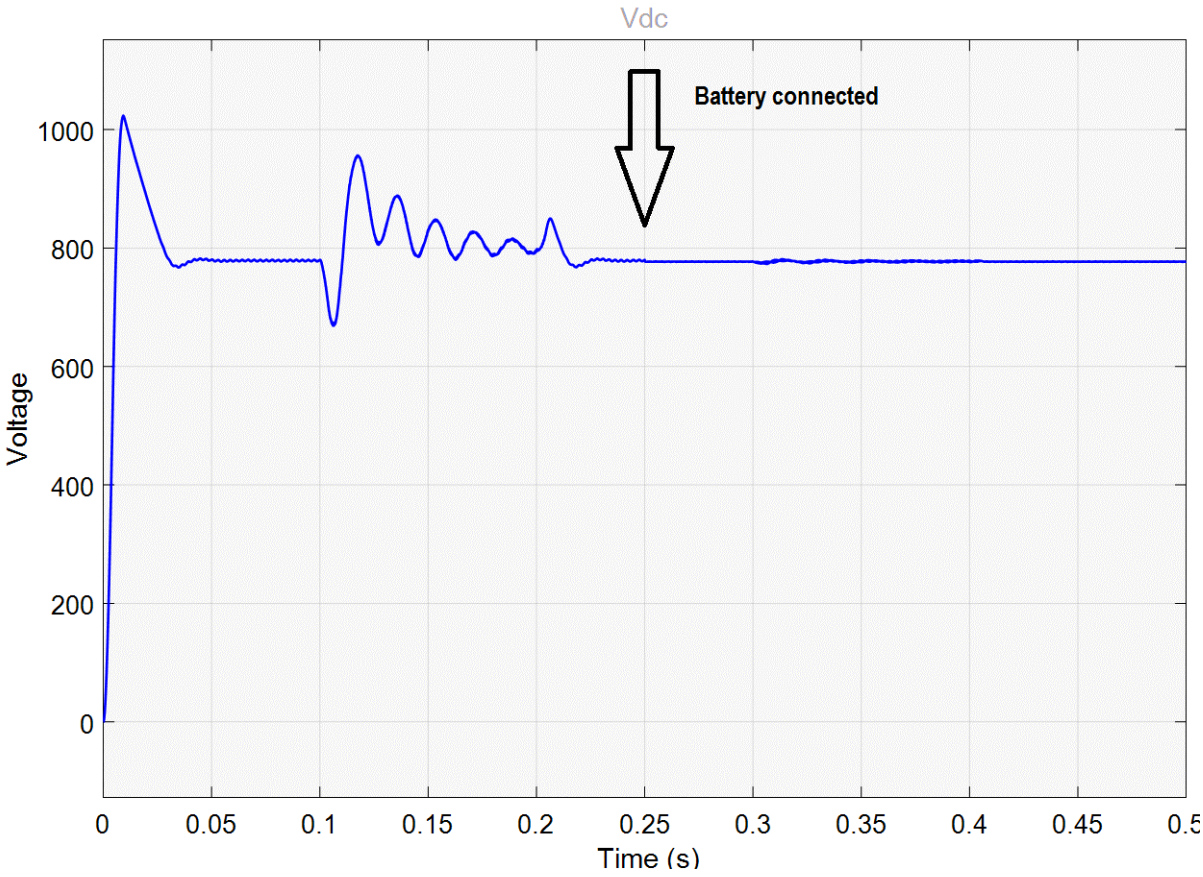

Figure 5.16 Regulated load change

5.2.2 Voltage Source Capacitive Compensator

With the designed capacitor compensator below the starting controllable voltage, source state is on and switches off at 5 seconds as depicted in figure 5.17. The voltage sensor disconnects the load as soon as the ultra-capacitor discharges till it reaches a value below 9.5 voltage. The second controllable voltage source is set as a back-up and switches on at 15 seconds. The ultra-capacitor compensates for the sudden voltage drop.

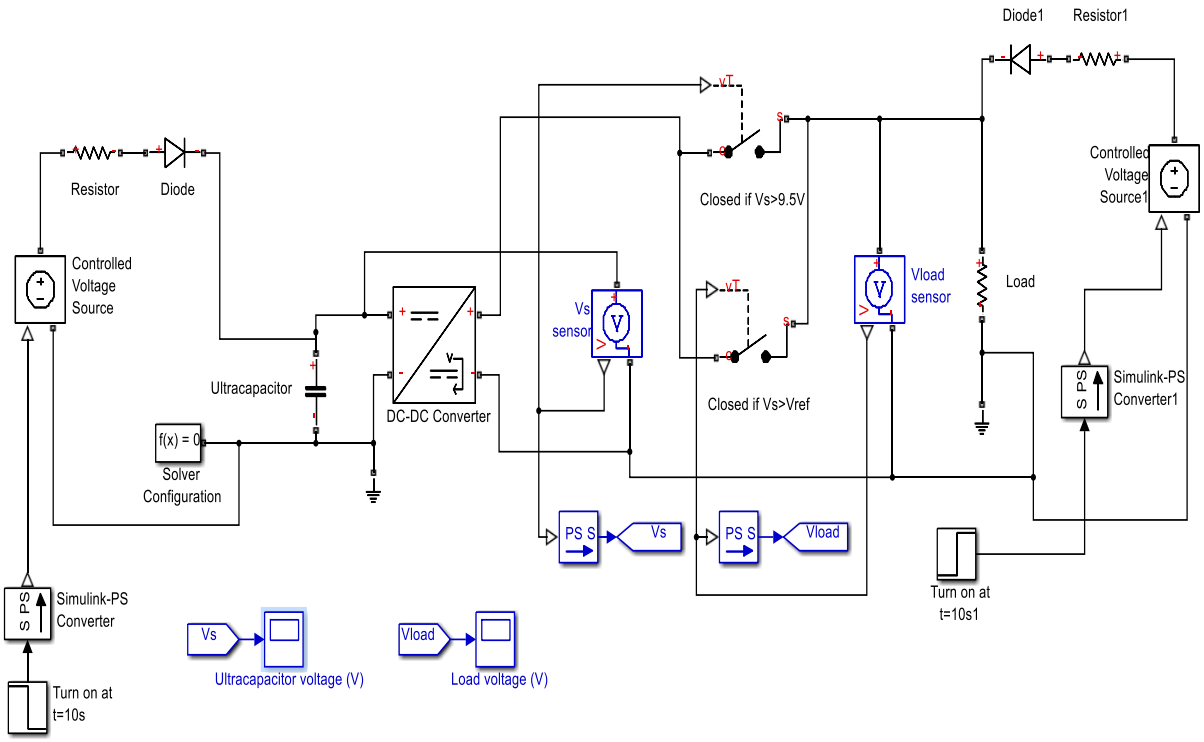

Figure 5.17: Ultra-capacitor with Voltage Compensator

Note that the capacitor charges till 5 seconds when the source is disconnected, then it discharges till the load is disconnected. The capacitor charges again when the back-up source connects at 15 seconds. See figure 5.18.

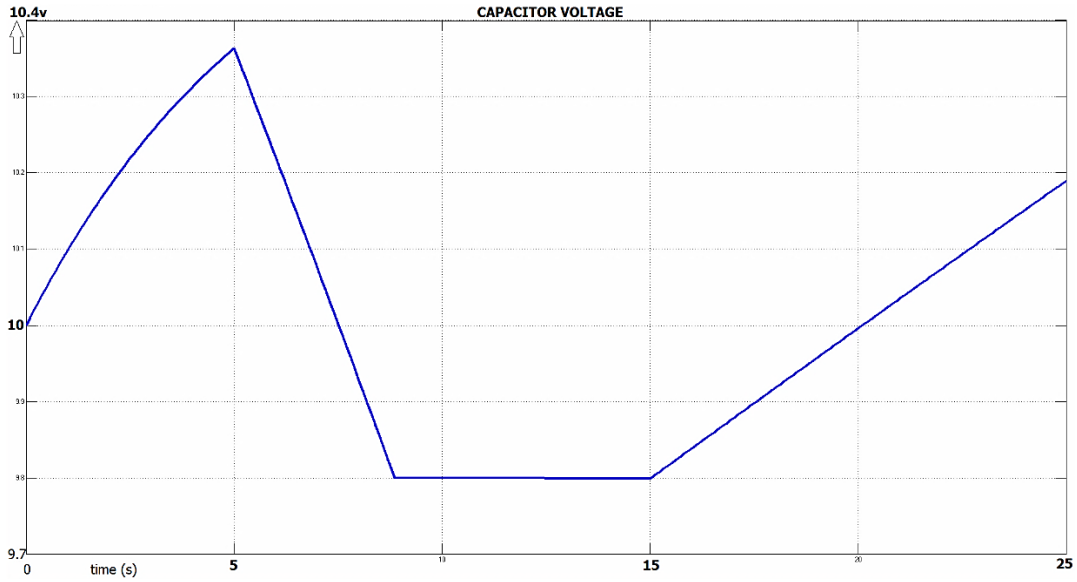

Figure 5.18: Measured Voltage across the Ultra Capacitor

Note in the figure below that the voltage drops across the load as the starting source disconnects after 5 seconds and the back-up source connects at 15 seconds. The trend is shown in figure 5.19 below.

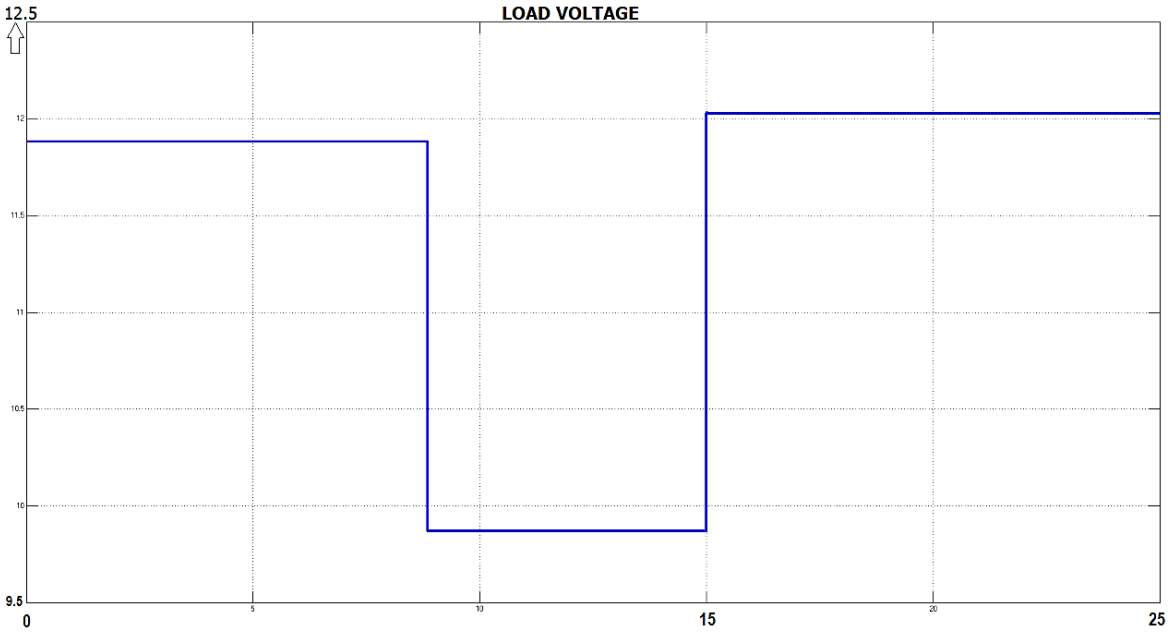

Figure 5.19: Measured Voltage across the Load

Battery life can be improved by incorporating an ultra-capacitor. This hybrid energy storage system features high power density, large energy storage as well as good power performances. Battery life time can be extended through peak shaving by a complementary coupled ultra-capacitor (Shen & Khaligh, Oct 2015) .

CHAPTER 6: CONCLUSION & FUTURE WORK

6.1 Overview

The study was set out to compare efficient control and storage strategies within the renewable energy sector integrated into a microgrid. Renewable energy sources such as the sun and the wind are carbon friendly yet fluctuates continuously and directly effects the power output which causes unwanted transient responses.

Distributed generator operation and control was researched as well as different storage methodologies. Different control concepts were explored and developed while energy storage methods were discussed and incorporated in terms of power conditioning to ensure a smooth power output. Energy storage systems are highly beneficial in stabilizing a microgrid yet at an additional cost.

6.2 Observations and findings

The main empirical findings were discussed in chapter five and which will amalgamate the empirical findings.

Renewable energy grows exponential as the control and storage component of this technology improves faster. Conventional droop control manipulates the voltage and frequency by adapting the field current and speed of the rotor in ac generator. Distributed generators can supplement the main grid with additional power and can improve control with individual control topologies.

Energy storage plays a key role in maintaining a constant power output when the distributed generators fails. It can also be described as an UPS system. An ultra or super capacitor can maintain a stable voltage out for a couple seconds, while a battery bank and pumped storage system can maintain a steady and constant power output for hours if not days; depending on the volumetric capacity of the upper water storage dam and the size of the battery bank.

A plethora of time, money and expertise are spent on developing higher efficient DG's, but the first priority for the producer would be to improve the existing configuration and topologies of the microgrid's components in how it responds to disturbances. Efficient control systems including better storage arrangements would improve the power efficiency vastly.

The drawback in South Africa regarding renewable energy is that in most cases the excess produced cannot be fed back into the grid. The challenge of a microgrid is to synchronize the DG's with each other. Conventional battery back-up is a very costly exercise yet an efficient stabilizer. The trade-off would be reliable energy supply versus the high cost of added reserve capacity.

The limitation of the study was the challenge to compare different microgrid control methods on a universal system with the exact same components, ratings, conditions and time intervals. The different methods could only be analysed separately and the basic concepts rather than the precise simulation results could be compared with each other. This same challenge applied to the energy storage systems.

6.3 Future work

So far in past research, the concept of a heavily loaded car on a railway can use the over supply of electricity to thrusts itself uphill and return energy by coasting downhill. (Pickard, August 2015). Incompressible fluid could also be pumped up a large cylinder which is connected to a raising mass, thus creating and storing potential energy (Shively, et al., Nov 2008). Gravitational energy can also be harvested with a generator that is driven by a suspended object which is connected to a rope on a pulley hence this object needs to be hoisted up for continual usage.

The principles of gravitational energy and methods can be used to supplement a more sufficient method of power generation rather than replacing it. For example, PV panels can be utilized to hoist a weight and thus create potential energy via gravitational force. Wind turbines can be used to wrench an object of mass against gravity to store potential kinetic energy.

This noble kinetic mechanical storage system would be accessible to the lower income class as well. The aim for the proposed design would to make it more scalable and less technical i.e. electrical. The design will aim to be rugged and simple to minimise maintenance and maximise the lifespan of the system to at least 20years of operation.

The design could be implemented, manufactured and patented in South Africa to supplement the national grid. The idea would be to provide training and manuals to train the local installers and system integrators to implement this design alongside the latest available renewable sources at minimal cost and maintenance complexities.

References

Abdullah, M. A., Muttaqi, K. M., Sutanto, D. & Agalgaonkar, A. P., June 2015. An Effective Power Dispatch Control Strategy to Improve Generation Schedulability and Supply Reliability of a Wind Farm Using a Battery Energy Storage System. *IEEE Transactions on Sustainable Energy,* 6(3), pp. 1093 - 1102.

Adhikari , S. & Li, F., April 2014. Coordinated V-f and P-Q Control of Solar Photovoltaic Generators With MPPT and Battery Storage in Microgrids. *IEEE Transactions on Smart Grid,* 5(3), pp. 1270 - 1281.

Ali, M. H., Wu, B. & Dougal, R. A., April 2010. An Overview of SMES Applications in Power and Energy Systems. *IEEE Transactions on Sustainable Energy,* 1(1), pp. 38 - 47.

Alobeidli , K. A., Syed, M. H., El Moursi, M. S. & Zeineldin, H. H., April 2015. Novel Coordinated Voltage Control for Hybrid Micro-Grid With Islanding Capability. *IEEE Transactions on Smart Grid,* 6(3), pp. 1116 - 1127.

Arai, J. et al., 2008. Power electronics and its applications to renewable energy in Japan. *IEEE Circuits and Systems Magazine,* 29 August, 8(3), pp. 52-66.

Arboleya , P. et al., Feb 2015. Efficient Energy Management in Smart Micro-Grids: ZERO Grid Impact Buildings. *IEEE Transactions on Smart Grid ,* 6(2), pp. 1055 - 1063.

Ashabani , S. M. & Mohamed, Y. A., July 2013. General Interface for Power Management of Micro-Grids Using Nonlinear Cooperative Droop Control. *IEEE Transactions on Power Systems,* 28(3), pp. 2929 - 2941.

Bakhoum , E. G., Feb 2009. New mega-farad ultracapacitors. *IEEE Transactions on Ultrasonics, Ferroelectrics, and Frequency Control,* 56(1), pp. 14 - 21.

Baral, L., Aug 2010. *Study of the technology development of harvesting gravitational potential energy for transportation by using CASWAT-G.* Kyoto, IEEE.

Barater , D. et al., Feb 2016. Recent advances in single-phase transformerless photovoltaic inverters. *IET Renewable Power Generation,* 10(2), pp. 260 - 273.

Bascetta , L., Magnani, G., Rocco, P. & Zanchettin, A. M., April 2010. Performance Limitations in Field-Oriented Control for Asynchronous Machines With Low Resolution

Position Sensing. *IEEE Transactions on Control Systems Technology,* 18(3), pp. 559 - 573.

Bayram, I. S., Abdallah, M., Tajer, A. & Qaraqe, K. A., August 2015. A Stochastic Sizing Approach for Sharing-Based Energy Storage Applications. *IEEE Transactions on Smart Grid ,* PP(99), p. 1.

Benavides, N. & Chapman, P., May 2008. Mass-Optimal Design Methodology for DC-DC Converters in Low-Power Portable Fuel Cell Applications. *IEEE Transactions on Power Electronics,* 23(3), pp. 1545 - 1555.

Benda, V., Dec 2015. Photovoltaics towards terawatts – progress in photovoltaic cells and modules. *IET Power Electronics,* 8(12), pp. 2343 - 2351.

Beshr, E., Oct 2013. *Comparative study of adding PV /wind energy systems to autonomus micro grid.* Istanbul, IEEE, pp. 1-6.

Best, R., Kennedy, J., Morrow , D. & Fox, B., Dec 2010. Steady-State and Transient Performance of Biodiesel-Fueled Compression-Ignition-Based Electrical Generation. *IEEE Transactions on Sustainable Energy,* 2(1), pp. 20 - 27.

Bevrani , H. & Shokoohi, S., Aug 2013. An Intelligent Droop Control for Simultaneous Voltage and Frequency Regulation in Islanded Microgrids. *IEEE Transactions on Smart Grid,* 4(3), pp. 1505 - 1513.

Binyu, X., Jiyun, Z. & Jinbin, L., July 2013. *Modeling of an all-vanadium redox flow battery and optimization of flow rates.* Vancouver, BC, IEEE.

Bird, J., 2007. *Engineering Mathematics.* 5 ed. Oxford: Elsevier Ltd..

Bisht , M. S., Oct 2014. *Fuzzy based intelligent frequency control strategy in standalone hybrid AC microgrid.* Juan Les Antibes, IEEE.

Black, M. & Strbac, G., Feb 2007. Value of Bulk Energy Storage for Managing Wind Power Fluctuations. *IEEE Transactions on Energy Conversion,* 22(1), pp. 197 - 205.

Boicea , V. A., Oct 2014. Energy Storage Technologies: The Past and the Present. *Proceedings of the IEEE,* 102(11), pp. 1777 - 1794.

Brett, G. & Barnett, M., Oct 2013. *Utility-scale energy storage: Liquid air a pioneering solution to the problem of energy storage.* London, IET.

Brett, G., June 2015. *Lessons learned developing liquid air energy storage.* London, IET, pp. 1-24.

Brown, P. D., Lopes, J. & Matos, M., April 2008. Optimization of Pumped Storage Capacity in an Isolated Power System With Large Renewable Penetration. *IEEE Transactions on Power Systems,* 23(2), pp. 523 - 531.

Brusco, G. et al., Sept 2014. Energy Management System for an Energy District With Demand Response Availability. *IEEE Transactions on Smart Grid,* 5(5), pp. 2385 - 2393.

Buchmann, I., n.d. *BU-102: Battery Developments.* [Online]
Available at: http://batteryuniversity.com/learn/article/battery_developments
[Accessed 30 July 2015].

Bukhari, S., Maqsood, J. & Baig, M., 2015. *Comparison of Characteristics - Lead Acid, Nickel Based, Lead Crystal and Lithium.* Washington DC, IEEE.

Cai, L.-J. & Erlich, I., June 2015. Doubly Fed Induction Generator Controller Design for the Stable Operation in Weak Grids. *IEEE Transactions on Sustainable Energy,* 6(3), pp. 1078 - 1084.

carbonTRACK, n.d. *carbonTRACK Intelligent Energy Management.* [Online]
Available at: http://www.carbontrack.com.au/
[Accessed 03 10 2016].

Carpinelli, G. et al., May 2013. Optimal Integration of Distributed Energy Storage Devices in Smart Grids. *IEEE Transactions on Smart Grid,* 4(2), pp. 985 - 995.

Carreon-Bautista , S., Erbay, C., Han, A. & Sanchez-Sinencio, . E., Oct 2015. An Inductorless DC–DC Converter for an Energy Aware Power Management Unit Aimed at Microbial Fuel Cell Arrays. *IEEE Journal of Emerging and Selected Topics in Power Electronics,* 3(4), pp. 1109 - 1121.

Carreon-Bautista, S., Erbay, C., Han, A. & Sánchez-Sinencio, E., Feb 2015. Power Management System With Integrated Maximum Power Extraction Algorithm for Microbial Fuel Cells. *IEEE Transactions on Energy Conversion,* 30(1), pp. 262 - 272.

Centre for Energy Economics Research and Policy, Heriot-Watt University, 2015. *BP Statistical Review of World Energy June 2015,* London: BP.

Chen, L. & Mei, S., May 2015. An integrated control and protection system for photovoltaic microgrids. *CSEE Journal of Power and Energy Systems ,* 1(1), pp. 36 - 42.

Chen, Y.-K., Liang, T.-J. & Wu, W.-C., June 2015. *Design and implementation of a photovoltaic grid-connected micro-inverter with power factor correction technology.* Seoul, IEEE, pp. 294 - 300.

Chen, Z. et al., Sept 2015. *A synchronization control method for micro-grid with droop control.* Montreal, QC, IEEE.

Cleary, B. et al., June 2015. Assessing the Economic Benefits of Compressed Air Energy Storage for Mitigating Wind Curtailment. *IEEE Transactions on Sustainable Energy,* 6(3), pp. 1021 - 1028.

Colson, C. M. & Nehrir, M. H., Feb 2011. Evaluating the Benefits of a Hybrid Solid Oxide Fuel Cell Combined Heat and Power Plant for Energy Sustainability and Emissions Avoidance. *IEEE Transactions on Energy Conversion,* 26(1), pp. 140 - 148.

D'Agostino, R., Baumann, L., Damiano, A. & Boggasch, E., May 2015. A Vanadium-Redox-Flow-Battery Model for Evaluation of Distributed Storage Implementation in Residential Energy Systems. *IEEE Transactions on Energy Conversion,* 30(2), pp. 421 - 430.

Daniels, B. & Daniels, A., n.d. *Wind-Turbine.* [Online]
Available at: http://beaudaniels.com/Infographic-pages/Wind-turbine.htm
[Accessed 05 Aug 2015].

Dasgupta, S., Mohan, S. N., Sahoo, S. K. & Panda, S. K., July 2012. A Plug and Play Operational Approach for Implementation of an Autonomous-Micro-Grid System. *IEEE Transactions on Industrial Informatics,* 8(3), pp. 615 - 629.

De Andrade, R. et al., July 2007. Flywheel Energy Storage System Description and Tests. *IEEE Transactions on Applied Superconductivity,* 17(2), pp. 2154 - 2157.

De Brabandere , K. et al., July 2007. A Voltage and Frequency Droop Control Method for Parallel Inverters. *IEEE Transactions on Power Electronics,* 22(4), pp. 1107 - 1115.

De Souza, W. F., Severo-Mendes, M. A. & Lopes, L. A., Aug 2015. Power sharing control strategies for a three-phase microgrid in different operating condition with

droop control and damping factor investigation. *IET Renewable Power Generation,* 9(7), pp. 831 - 839.

Divshali, P. H., Alimardani, A., Hosseinian, S. H. & Abedi, M., Oct 2012. Decentralized Cooperative Control Strategy of Microsources for Stabilizing Autonomous VSC-Based Microgrids. *IEEE Transactions on Power Systems,* 27(4), pp. 1949 - 1959.

Dong, J. et al., March 2016. Storage-Reserve Sizing With Qualified Reliability for Connected High Renewable Penetration Micro-Grid. *IEEE Transactions on Sustainable Energy,* 7(2), pp. 732 - 743.

Dou , C. et al., July 2011. *Hybrid control for micro-grid based on hybrid system theory.* San Diego, CA, IEEE, pp. 408-417.

Eghtedarpour , N. & Farjah, E., Jan 2014. IET Renewable Power Generation. *IET Renewable Power Generation,* 8(1), pp. 45 - 57.

Enalou , H. B. & Soreshjani, E. A., April 2015. A Detailed Governor-Turbine Model for Heavy-Duty Gas Turbines With a Careful Scrutiny of Governor Features. *IEEE Transactions on Power Systems,* 30(3), pp. 1435 - 1441.

Eskom Holdings SOC Ltd, n.d. *Eskom Services.* [Online]
Available at:
http://www.eskom.co.za/Whatweredoing/ElectricityGeneration/PowerStations/Pages/Palmiet_Pumped_Storage_Scheme.aspx
[Accessed 03 10 2016].

Falvo, M. C. et al., Sept 2014. *Micro-grids and Energy Storage Systems.* Trieste, IEEE, pp. 1-5.

Filipescu , S. & Filipescu, A., Oct 2014. *Speed estimators based control of permanent magnet syncronous motor.* Sinaia, IEEE.

Finarelli, D. G. et al., Sept 2012. *Microbial fuel cell electric behaviour.* Hangzhou, IEEE, pp. 1-3.

Fish, A., 2014. *SYNCHRONOUS MACHINES.* Bellville: CPUT.

Fletcher, J. & Yang, J., 2010. Introduction to doubly-fed induction generator for wind power applications Chapter 14. In: *Paths to Sustainable Energy, Dr Artie Ng (Ed.).* University of Strathclyde, Glasgow: Intechopen, pp. 261-279.

Gong, K. et al., April 2016. Application of SMES in the Microgrid Based on Fuzzy Control. *Application of SMES in the Microgrid Based on Fuzzy Control,* 26(3), p. 1.

Gow, J. A. & Manning, C. D., Mar 1999. Developement of a photovoltaic array model for use in power-electronic simulation studies. *IEE Proceedings - Electric Power Applications,* 146(2), pp. 193 - 200.

Grillo, S. et al., Aug 2010. Microturbine Control Modeling to Investigate the Effects of Distributed Generation in Electric Energy Networks. *IEEE Systems Journal,* 4(3), pp. 303 - 312.

Guangzhou HY Energy Technology Limited Corp, 2008-2016. *HY Energy.* [Online] Available at: http://www.hyenergy.com.cn/Technology.asp?id=759 [Accessed 25 July 2015].

Guan, X., Xu , Z. & Jia, Q., July 2010. *Energy efficient buildings facilitated by micro grid.* Minneapolis, MN, IEEE.

Guerrero , J. M., Vásquez, J. C. & Teodorescu, R., Nov 2009. *Hierarchical control of droop-controlled DC and AC microgrids — a general approach towards standardization.* Porto, IEEE.

Gunter, S., Perreault, D. & Afridi, K., May 2013. Optimal Design of Grid-Connected PEV Charging Systems With Integrated Distributed Resources. *IEEE Transactions on Smart Grid,* 4(2), pp. 956 - 967.

Gu, Y. et al., May 2012. *Development of micro-grid coordination and control overview.* Tianjin, IEEE.

Hadjidemetriou, L., Kyriakides, E. & Blaabjerg, F., Nov 2013. A New Hybrid PLL for Interconnecting Renewable Energy Systems to the Grid. *IEEE Transactions on Industry Applications,* 49(6), pp. 2709-2719.

Hallam, C. A. & Contreras, C., March 2015. Evaluation of the Levelized Cost of Energy Method for Analyzing Renewable Energy Systems: A Case Study of System Equivalency Crossover Points Under Varying Analysis Assumptions. *IEEE Systems Journal,* 9(1), pp. 199 - 208.

Hasan, A., Ahmed, M. & Hasan, A., Dec 2013. *Experiment for producing a renewable alternative fuel for Bangladesh from mustard oil.* Dhaka, IEEE.

Hayes, B., Wilson, A., Webster, R. & Djokic, S., March 2016. Comparison of two energy storage options for optimum balancing of wind farm power outputs. *IET Generation, Transmission & Distribution,* 10(3), pp. 832 - 839.

Hebrink, T. J., June 2009. *Infra-red transmissive mirrors for concentrated photovoltaics.* Philadelphia, PA, IEEE.

Hedman , K. & Sheble, G., June 2006. *Comparing Hedging Methods for Wind Power: Using Pumped Storage Hydro Units vs. Options Purchasing.* Stockholm, IEEE.

Highview Power Storage, 2016. *Highview Power Storage.* [Online]
Available at: http://www.highview-power.com/
[Accessed 27 01 2016].

Hiskens, I. A. & Fleming, E. M., June 2008. *Control of inverter-connected sources in autonomous microgrids.* Seattle, WA, IEEE.

Hou, C., Hu, X. & Hui, D., Oct 2010. *Hierarchical control techniques applied in micro-grid.* Hangzhou, IEEE.

Hredzak, B., Agelidis, V. G. & Jang, M., Sept 2013. A Model Predictive Control System for a Hybrid Battery-Ultracapacitor Power Source. *IEEE Transactions on Power Electronics,* 29(3), pp. 1469 - 1479.

Hussein, A., Kutkut, N., Shen, Z. J. & Batarseh, I., June 2012. Distributed Battery Micro-Storage Systems Design and Operation in a Deregulated Electricity Market. *IEEE Transactions on Sustainable Energy,* 3(3), pp. 545 - 556.

IEEE Standards Coordinating Committee 21, April 2009. IEEE Application Guide for IEEE Std 1547™, IEEE Standard for Interconnecting Distributed Resources with Electric Power Systems. *The Institute of Electrical and Electronics Engineers,* pp. 1 - 217.

Islam , M. & Mekhilef, S., March 2016. Efficient Transformerless MOSFET Inverter for a Grid-Tied Photovoltaic System. *IEEE Transactions on Power Electronics,* 31(9), pp. 6305 - 6316.

Jaehong, K. et al., May 2011. Mode adaptive Droop Control with Virtual Output Impedances For an inverter-Based Flexible AC Microgrid. *IEEE Transactions on Power Electronics,* 3(26), pp. 689-701.

Jia, Q.-S., Shen, J.-X., Xu, . Z.-B. & Guan, . X.-H., 15-18 May 2011. *Simulation-based policy improvement for power management in buildings.* Kaohsiung, IEEE.

Jia, Q., Shen, J., Xu, Z. & Guan, X., Dec 2012. Simulation-Based Policy Improvement for Energy Management in Commercial Office Buildings. *IEEE Transactions on Smart Grid,* 3(4), pp. 2211 - 2223.

Jing, W., Xiaohui , W. & Hong, D., Sept 2012. *Research on operation control of micro sources within a microgrid.* Wuhan, IEEE, pp. 1-4.

Ju, F., Deng, W. & Li, J., April 2016. Performance Evaluation of Modularized Global Equalization System for Lithium-Ion Battery Packs. *IEEE Transactions on Automation Science and Engineering,* 13(2), pp. 986 - 996.

Kang, M., May 2007. Generation Cost Assessment of an Isolated Power System With a Fuzzy Wind Power Generation Model. *IEEE Transactions on Energy Conversion,* 22(2), pp. 397 - 404.

Kazmerski, L., April 2011. *Best research solar cell efficiencies NREL,* U.S.: Golden, CO.

Khaled, F., Ondel, O. & Allard, B., May 2015. Optimal Energy Harvesting From Serially Connected Microbial Fuel Cells. *IEEE Transactions on Industrial Electronics,* 62(6), pp. 3508 - 3515.

Kim, J. et al., Nov 2010. Mode Adaptive Droop Control With Virtual Output Impedances for an Inverter-Based Flexible AC Microgrid. *IEEE Transactions on Power Electronics,* 26(3), pp. 689 - 701.

Kıray, V., Şağbanşua , L. & Topal, T., Oct 2013. *Utilization of energy storage systems charged from grid in buildings and comparison with solar systems.* London, IET.

Kohansal, M., Gharehpetian, G. B., Abedi, M. & Sanjari, M. J., March 2012. *Droop Controller Limitation for Voltage Stability in Islanded Microgrid.* Santiago de Compostela, EA4EPQ.

Kohn, W., Zabinsky, Z. & Nerode, A., Oct 2015. A Micro-Grid Distributed Intelligent Control and Management System. *IEEE Transactions on Smart Grid,* 6(6), pp. 2964 - 2974.

Kost, C. et al., Nov 2013. *Levelized Cost of Electricity Renewable Energy Technologies,* Freiburg: Fraunhofer ISE.

Kouro, S., Leon, J. I., Vinnikov, D. & Franquelo, L. G., March 2015. Grid-Connected Photovoltaic Systems: An Overview of Recent Research and Emerging PV Converter Technology. *IEEE Industrial Electronics Magazine,* 9(1), pp. 47 - 61.

Lasseter, R. et al., 23 Dec 2010. CERTS Microgrid Laboratory Test Bed. *IEEE Transactions on Power Delivery,* 26(1), pp. 325 - 332.

Lee, S., Kwon, B. & Lee, . S., Oct 2014. Joint Energy Management System of Electric Supply and Demand in Houses and Buildings. *IEEE Transactions on Power Systems,* 29(6), pp. 2804 - 2812.

Li, N. & Hedman, K. W., June 2015. Economic Assessment of Energy Storage in Systems With High Levels of Renewable Resources. *IEEE Transactions on Sustainable Energy,* 6(3), pp. 1103 - 1111.

Liu, X., Wang, P. & Loh, P. C., May 2011. A Hybrid AC/DC Microgrid and Its Coordination Control. *IEEE Transactions on Smart Grid,* 2(2), pp. 278 - 286.

Lo, C. & Ansari, N., March 2013. Decentralized Controls and Communications for Autonomous Distribution Networks in Smart Grid. *IEEE Transactions on Smart Grid,* 4(1), pp. 66 - 77.

Lu, L. & Chu, C., July 2015. Consensus-Based Droop Control Synthesis for Multiple DICs in Isolated Micro-Grids. *IEEE Transactions on Power Systems,* 30(5), pp. 2243 - 2256.

Lumbreras, C. et al., May 2016. Control of a Small Wind Turbine in the High Wind Speed Region. *IEEE Transactions on Power Electronics,* 31(10), pp. 6980 - 6991.

Lu, S. & Corzine, K., July 2007. Advanced Control and Analysis of Cascaded Multilevel Converters Based on P-Q Compensation. *IEEE Transactions on Power Electronics,* 22(4), pp. 1242 - 1252.

Majumber, R. et al., Jan 2009. *Operation and control of a microgrid containing inertial and non-inertial micro sources.* Singapore, IEEE, pp. 1-6.

Martinez, E. V. & De La O Serna, J. A., Jan 2015. Smart grids Part 1: Instrumentation challenges. *IEEE Instrumentation & Measurement Magazine,* 18(1), pp. 6 - 9.

Matlab, 2012. *Simulink.* Natick U.S.: Mathworks.

Matlab, 2013. *Simulink.* Natick U.S.: Mathworks.

Matlab, 2016. *Simulink.* Natick U.S.: Mathworks.

Mazumdar , P., Enjeti, P. N. & Balog, R. S., July 2014. Analysis and Design of Smart PV Modules. *IEEE Journal of Emerging and Selected Topics in Power Electronics,* 2(3), pp. 451 - 459.

McGowan , D. J., Morrow, D. J. & Fox, B., June 2006. Integrated governor control for a diesel-generating set. *IEEE Transactions on Energy Conversion,* 21(2), pp. 476 - 483.

Mohan, N., Undeland, T. M. & Robbins, W. P., 2003. *Power Electronics Converters, Applications and Design.* 6 ed. Hoboken, USA: John Wiley & Sons, Inc..

Mohod , S. W. & Aware, M. V., Feb 2012. Micro Wind Power Generator With Battery Energy Storage for Critical Load. *IEEE Systems Journal ,* 6(1), pp. 118 - 125.

Morlier, A., Haase, F. & Köntges, M., Oct 2015. Impact of Cracks in Multicrystalline Silicon Solar Cells on PV Module Power—A Simulation Study Based on Field Data. *IEEE Journal of Photovoltaics,* 5(6), pp. 1735 - 1741.

NEC Energy Solutions, 2015. *HIGH PERFORMANCE, LONG LASTING, SAFE.* Westborough: NEC Energy Solutions Inc. .

Ni, J. & Ai, Q., Jan 2016. Economic power transaction using coalitional game strategy in micro-grids. *IET Generation, Transmission & Distribution,* 10(1), pp. 10 - 18.

Niu , Y. & Santoso, S., June 2016. Sizing and Coordinating Fast- and Slow-Response Energy Storage Systems to Mitigate Hourly Wind Power Variations. *IEEE Transactions on Smart Grid,* PP(99), p. 1.

Niu, H., Jiang, M., Zhang, D. & Fletcher, J., Oct 2014. *Autonomous micro-grid operation by employing weak droop control and PQ control.* Perth, WA, IEEE.

Odgaard, P. F. & Stoustrup, J., April 2015. A Benchmark Evaluation of Fault Tolerant Wind Turbine Control Concepts. *IEEE Transactions on Control Systems Technology,* 23(3), pp. 1221 - 1228.

Oh, K. et al., May 2015. A Novel Method and its Field Tests for Monitoring and Diagnosing Blade Health for Wind Turbines. *IEEE Transactions on Instrumentation and Measurement,* 64(6), pp. 1726 - 1733.

Ornelas-Tellez, F., Nov 2014. *Optimal control for a renewable-energy-based micro-grid.* Ixtapa, IEEE.

Pantelimon, R., Adam, M., Andruşcă , M. & Pancu, C., May 2013. *Aspects regarding solar battery charge controllers.* Bucharest, IEEE.

Parker, M. A., Soraghan, C. & Giles, A., April 2016. Comparison of power electronics lifetime between vertical- and horizontal-axis wind turbines. *IET Renewable Power Generation,* 10(5), pp. 679 - 686.

Pastor, L. P., Rodriguez, L. G. & Velez, C. V., Feb 2014. Flywheels Store to Save. *IEEE Electrification Magazine,* 26 February, 1(2), pp. 13-20.

Pei, W., Deng, W., Shen, Z. & Qi, Z., March 2016. Operation of battery energy storage system using extensional information model based on IEC 61850 for micro-grids. *IET Generation, Transmission & Distribution,* 10(4), pp. 849 - 861.

Pickard, W. F., August 2015. Massive Electricity Storage for a Developed Economy of Ten Billion People. *IEEE Access,* Volume 3, pp. 1392 - 1407.

Planas, E. et al., Aug 2013. Design and implementation of a droop control in d-q frame for islanded microgrids. *IET Renewable Power Generation,* 7(5), pp. 458 - 474.

Qian, X., Oct 2010. *Application research of flywheel battery in the wind and solar complementary power generation.* Taiyuan, IEEE, pp. V13-546 - V13-550.

Reddy, K. et al., March 2016. A Three Phase Hybrid cascaded Modular Multilevel Inverter for Renewable Energy Environment. *IEEE Transactions on Power Electronics,* PP(99), p. 1.

Saadat, M. & Li, P. Y., June 2012. *Modeling and control of a novel compressed air energy storage system for offshore wind turbine.* Montreal, QC, IEEE, pp. 3032 - 3037.

Sager, M., 2014. *Renewable Energy Vision 2030,* South Africa: WWF-SA.

Savaghebi, M., Jalilian, A., Vasquez, J. C. & Guerrero, J. M., Dec 2012. Secondary Control for Voltage Quality Enhancement in Microgrids. *IEEE Transactions on Smart Grid,* 3(4), pp. 1893 - 1902.

Sawin, L., 2015. *RENEWABLES 2016 GLOBAL STATUS REPORT,* Paris: RENEWABLES GSR.

Scherer, L. G., Tambara, R. V. & de Camargo, R. F., March 2016. Voltage and frequency regulation of standalone self-excited induction generator for micro-hydro

power generation using discrete-time adaptive control. *IET Renewable Power Generation,* 10(4), pp. 531 - 540.

Schneider Electric Software, LLC, n.d. *Wonderware Sout Africa.* [Online]
Available at: https://www.wonderware.com/hmi-scada/
[Accessed 03 10 2016].

Seitz, C. W., 6. Industrial battery technologies and markets. *IEEE Aerospace and Electronic Systems Magazine*, 2002 August, pp. 10-15.

Shang, W. & Redfern, M. A., 1-4 Sept. 2009. *Control schemes for distributed generators connected to distribution networks.* Glasgow, IEEE, pp. 1-5.

Shen, J. & Khaligh, A., Oct 2015. A Supervisory Energy Management Control Strategy in a Battery/Ultracapacitor Hybrid Energy Storage System. *IEEE Transactions on Transportation Electrification,* 1(3), pp. 223 - 231.

Shively, D., Gardner, J., Haynes, T. & Ferguson, J., Nov 2008. *Energy Storage Methods for Renewable Energy Integration and Grid Support.* Atlanta, GA, IEEE.

Shu, J. et al., March 2009. *Double Fed Induction Wind Generator Model and Its Operation Investigation.* Wuhan, IEEE, pp. 1-5.

Singh, D., Sharma, N. K., Sood, Y. R. & Jarial, R. K., July 2011. *Global status of renewable energy and market: Future prospectus and target.* Chennai, IEEE, pp. 171 - 176.

Solargis, n.d. *Geosun Africa.* [Online]
Available at: http://geosun.co.za/solar-maps/
[Accessed 1 April 2016].

Sudarkasa, M., 2013. *South Africa.* Pretoria, s.n.

Surprenant, M., Hiskens, I. & Venkataramanan, G., Sept 2011. *Phase Locked Loop Control of Inverters in a Microgrid.* Phoenix, AZ, National Science Foundation.

Suvire, G. O. & Mercado, P. E., Sept 2015. *Energy storage for wind power: A comparative analysis considering the type and size of the wind system.* Porto, IEEE, pp. 1 - 6.

Suwan, M., Neumann, T., Feltes, C. & Erlich, I., July 2012. *Educational experimental rig for Doubly-Fed Induction Generator based wind turbine.* San Diego, CA, IEEE, pp. 1 - 8.

Syed, M. H., Zeineldin, H. H. & El Moursi, M. S., March 2014. Hybrid micro-grid operation characterisation based on stability and adherence to grid codes. *IET Generation, Transmission & Distribution ,* 8(3), pp. 563 - 572.

Sygkridou, D., Vitoratos, D., Sygkridou , D. & Stathatos, E., July 2015. *Highly transparent counter electrodes for dye-sensitized solar cells made with advanced nanocomposite materials.* Rome, IEEE.

Tang , X. et al., December 2015. A Novel Frequency and Voltage Control Method for Islanded Microgrid Based on Multienergy Storages. *IEEE Transactions on Smart Grid,* 7(1), pp. 410 - 419.

Tech Mart, 2007. *Solar Power Mart.* [Online]
Available at: http://www.solarpower-mart.com/mppt_controller
[Accessed 08 July 2015].

Tesla Motors, 2016. *Powerwall.* [Online]
Available at: https://www.teslamotors.com/powerwall
[Accessed 04 November 2015].

The Department of Energy, 2015. *State of Renewable Energy in South Africa,* Pretoria: Department of Energy.

The SUSTAINABLE ENERGY RESOURCE HANDBOOK South Africa Volume 6, 2015. ENERGY. *Sustainable and Daylight Design*, p. 122.

Tran, D. & Khambadkone, A. M., August 2013. Energy Management for Lifetime Extension of Energy Storage System in Micro-Grid Applications. *IEEE Transactions on Smart Grid,* 4(3), pp. 1289 - 1296.

Van Vuuren, G., 2006. *An Introduction to process Instrumentation.* 4 ed. Wandsbeck: Quad Technologies.

Vandoorn , T. L. et al., Dec 2013. Microgrids: Hierarchical Control and an Overview of the Control and Reserve Management Strategies. *IEEE Industrial Electronics Magazine,* 7(4), pp. 42 - 55.

Varas , P., Tironi, M., Rudnick, H. & Rodriguez, N., April 2013. Latin America Goes Electric: The Growing Social Challenges of Hydroelectric Development. *IEEE Power and Energy Magazine,* 11(3), pp. 66 - 75.

Victron Eneregy, n.d. *Vidtron Energy Blue Power.* [Online]
Available at: https://www.victronenergy.com/panel-systems-remote-monitoring/color-control
[Accessed 29 09 2016].

Victron Energy B.V., 2016. *VE Configure tools.* Almere Haven: Victron Energy B.V.

Wang, L. & Lin, P., Feb 2009. Analysis of a Commercial Biogas Generation System Using a Gas Engine–Induction Generator Set. *IEEE Transactions on Energy Conversion,* 24(1), pp. 230 - 239.

Wei, C., Fadlullah , Z. M., Kato , N. & Stojmenovic, I., Aug 2014. On Optimally Reducing Power Loss in Micro-grids With Power Storage Devices. *IEEE Journal on Selected Areas in Communications,* 32(7), pp. 1361 - 1370.

Wei, W., Liu, F., Mei, S. & Hou, Y., Dec 2015. Robust Energy and Reserve Dispatch Under Variable Renewable Generation. *IEEE Transactions on Smart Grid ,* 6(1), pp. 369 - 380.

Winelands Solar, 2016. *Fresh Produce Report.* Stellenbosch: s.n.

Wonderware, 2016. *Wonderware South Africa.* [Online]
Available at: http://www.wonderware.co.za/live/index.php
[Accessed 10 Oct 2015].

Xie, Y. et al., Nov 2014. *Simulation on a micro-grid system based on superconducting magnetic energy storage.* Shanghai, IEEE.

Xiu , Y., Xiang, Z., Fei, Y. & Hai-yang, Z., Sep 2011. *A research on droop control strategy and simulation for the micro-grid.* Yichang, IEEE.

Yang, P. & Nehorai, A., June 2014. Joint Optimization of Hybrid Energy Storage and Generation Capacity With Renewable Energy. *IEEE Transactions on Smart Grid ,* 5(4), pp. 1566 - 1574.

Yuan, Y., Sun, Y. & Huang, Y., May 2016. Energy on the fly. *Electronics Letters,* 52(11), p. 890.

Yubing, D., Yulei, G., Qingmin, L. & Hui, W., Oct 2008. *Moddeling and simulation of the micro sources within a microgrid.* Wuhan, IEEE, pp. 2667-2671.

Yukitomo, M., Shigemasa , T. & Kojima, F., 20-23 July 2004. *A two degrees of freedom PID control system, its features and applications.* Melbourne, IEEE.

Zhao , B., Song, Q., Liu, W. & Xiao, Y., May 2013. Next-Generation Multi-Functional Modular Intelligent UPS System for Smart Grid. *IEEE Transactions on Industrial Electronics,* 60(9), pp. 3602 - 3618.

Zheng, F. et al., Feb 2015. Transient Performance Improvement of Microgrid by a Resistive Superconducting Fault Current Limiter. *IEEE Transactions on Applied Superconductivity,* 25(3), p. 1.

Zhong, Q. & Zeng, Q., March 2016. Universal Droop Control of Inverters With Different Types of Output Impedance. *IEEE Access,* Volume 4, pp. 702 - 712.

Zhou , H. et al., May 2011. Composite Energy Storage System Involving Battery and Ultracapacitor With Dynamic Energy Management in Microgrid Applications. *IEEE Transactions on Power Electronics,* 26(3), pp. 923 - 930.

Zubieta, L., May 2016. Are Microgrids the Future of Energy?: DC Microgrids from Concept to Demonstration to Deployment. *IEEE Electrification Magazine,* 30 May, 4(2), pp. 37 - 44.

APPENDICES

Appendix A: DQ Transformation

DQ Transformation derivation

$$\mathrm{X}ab = [au \quad bu \quad cu] \begin{bmatrix} xa \\ xb \\ xc \end{bmatrix} \tag{A-1}$$

$$\mathrm{T} = \frac{2}{3}\begin{bmatrix} \cos(wt) & \cos(wt - \frac{2}{3}\pi) & \cos(wt + \frac{2}{3}\pi) \\ -\sin(wt) & -\sin(wt - \frac{2}{3}\pi) & \sin(wt + \frac{2}{3}\pi) \end{bmatrix} \tag{A-2}$$

$$[\alpha u \quad \beta u \quad ou] = [au \quad bu \quad cu]\begin{bmatrix} 1 & 0 & \frac{1}{2} \\ -\frac{1}{2} & \frac{\sqrt{3}}{2} & \frac{1}{2} \\ -\frac{1}{2} & -\frac{\sqrt{3}}{2} & \frac{1}{2} \end{bmatrix} \tag{A-3}$$

$$[du \quad qu \quad ou] = [\alpha u \quad \beta u \quad ou]\begin{bmatrix} \cos\theta & -\sin\theta & 0 \\ \sin\theta & \cos\theta & 0 \\ 0 & 0 & 1 \end{bmatrix} \tag{A-4}$$

$$[du \quad qu \quad ou] = [au \quad bu \quad cu]\frac{2}{3}\begin{bmatrix} \cos\theta & -\sin\theta & \frac{1}{2} \\ \cos\theta - \frac{2\pi}{3} & \sin\theta - \frac{2\pi}{3} & \frac{1}{2} \\ \cos\theta + \frac{2\pi}{3} & \sin\theta + \frac{2\pi}{3} & \frac{1}{2} \end{bmatrix} \tag{A-5}$$

$\mathrm{X}dq = \mathrm{T}\mathrm{X}abc$

Inverse

$$\mathrm{T}' = \begin{bmatrix} \cos(wt) & -\sin(wt) \\ \cos(wt - \frac{2}{3}\pi) & -\sin(wt - \frac{2}{3}\pi) \\ \cos(wt + \frac{2}{3}\pi) & -\sin(wt + \frac{2}{3}\pi) \end{bmatrix} \tag{A-6}$$

$$\mathrm{X}abc = \mathrm{T}'\mathrm{X}dq \tag{A-7}$$

Appendix B: Levelized Cost of Electricity

$$C(X_t) = C(X_0)\,\frac{X_t}{X_0}^{-b} \qquad \text{A-8}$$

$$LR = 1 - 2^{-b} \qquad \text{A-9}$$

An alternative but basically the same approach can be used in the following equation

t	:	investment expenditures in the year t
Mt	:	operations and maintenance expenditures in the year t
Ft	:	fuel expenditures in the year t
Et	:	electricity generation in the year t
r	:	discount rate
n	:	expected lifetime of system or power station

$$LCOE = \frac{sum\ of\ costs\ over\ lifetime}{sum\ of\ electricity\ produced\ over\ lifetime} \qquad \text{A-10}$$

$$= \frac{\sum_{t=1}^{n} \frac{It+Mt+Ft}{(1+r)^t}}{\sum_{t=1}^{n} \frac{Et}{(1+r)^t}}$$

Appendix C: Victron Microgrid Control Configuration (Adapted from Durand, 2016)